Design and Analysis of Multifunctional Actuators for Assistive Knee Braces

GUO, Hongtao

A Thesis Submitted in Partial Fulfillment

of the Requirements for the Degree of

Doctor of Philosophy

in

Mechanical and Automation Engineering

The Chinese University of Hong Kong

September 2010

Thesis/Assessment Committee

Professor Liu Yunhui （Chair）

Professor Liao Wei-Hsin （Thesis Supervisor）

Professor Men Qinghu （Committee Member）

Professor Sun Dong （External Examiner）

論文評審委員會

劉雲輝教授 （主席）

廖維新教授 （論文導師）

孟慶虎教授 （委員）

孫東教授 （校外委員）

ABSTRACT

In this research, a novel magnetorheological (MR) fluids based multifunctional actuator for assistive knee braces is designed. To decrease the dimension of the actuation device while enhancing its performances, a motor and MR fluids are integrated into a single device. With MR fluids, the actuator possesses multiple functions as motor, clutch, and brake while meeting the requirement of normal human motion as well. In this thesis, design details and operating principle of the actuator are illustrated, and possible configurations of the motor part and clutch/brake part are discussed. Finite element method is utilized to analyze the magnetic circuits, influence of permanent magnet on MR fluids, and magnetic flux distribution. Different clutch/brake parts with various inner coils are compared and analyzed, followed by a design optimization to improve the output torque. Prototypes of the multifunctional actuator are fabricated and tested, and characteristics of each function are investigated. As the actuator has multiple functions, modeling is developed for different functions, and system identification is carried out to determine the parameters. Adaptive control is utilized to control the actuator for torque and speed tracking. A smart joint using such a multifunctional actuator is designed, and its prototype is fabricated and tested. Power consumptions of knee brace using the smart joint are investigated during normal walking cycle. The results show that the developed actuator and smart joint are promising to be used in assistive knee braces.

摘要

在本研究中，作者設計了一種全新的應用于輔助膝架的多功能磁流變驅動器。爲了減小驅動設備的尺寸並同時提高性能，本設計將馬達和磁流變液結合在同一器件。利用磁流變液，該驅動器可以擁有馬達、離合器和制動器等多種功能，從而滿足穿戴者正常運動的需要。在論文中，作者闡述了該驅動器的詳細設計、工作原理，以及馬達部份和離合制動部份可能的結構，並利用有限元法對設計中磁路和永磁體對磁流變液的影響，以及磁通分佈等方面進行了分析。通過對具有不同內置線圈的離合制動部份的比較和分析，文中給出了優化設計從而提高了輸出力矩。在本研究中，作者製造了該驅動器的多個原型，並對這些原型的各種功能進行了實驗測試。由於該驅動器擁有多重功能，因此其建模也根據各功能而分別給出，並通過系統識別得到了該模型相應的參數。自適應控制方法被應用於該驅動器的力矩和速度追蹤。隨後，作者設計了一種應用該驅動器的智能關節並對相應的原型進行了測試。此外，作者在正常行走步態下對應用該智能關節的輔助膝架的能量消耗進行測試，並與只使用馬達的輔助膝架進行了評估和比較。結果顯示，將該驅動器以及智能關節應用於輔助膝架是可行的。

ACKNOWLEDGEMENTS

TABLE OF CONTENTS

LIST OF FIGURES

- xi -

LIST OF TABLES

CHAPTER ONE

INTRODUCTION

This chapter covers background and related literature reviews on assistive knee braces and MR fluids based devices. Motivation and background of the research are provided first. State-of-the-art technologies about lower extremity exoskeletons are reviewed; actuators for these devices are illustrated; gait analysis of human walking is discussed; the basic knowledge and general information about MR fluids and MR fluids based medical devices are introduced. Then the research objectives as well as organization of the thesis are presented.

1.1 Motivation and Background

1.1.1 Mobility Impaired Problems

The population of the elderly people increases rapidly in many countries. In China, the population of elderly, aged 60 years and more is increasing at a rate of 5.96 million per year due to decreasing mortality rates and longer life expectancy. It is estimated that the older population in China will reach 437 million by the year 2051 resulting in China becoming the country with the largest population of elderly in the world [Chinese National Committee of Aging, 2007].

Aging bring various physical deteriorations on their mobility. In general, the muscular strength of elderly people may decrease to be unable to walk or lose their stability during walking. Without appropriate exercise and rehabilitation, their muscle would be further deteriorated and they may become bedridden.

Other patients who suffer from diseases, such as cerebral paralysis, stroke and poliomyelitis, also have problems on the lower extremity due to these symptoms. Stroke is the leading cause of long-term adult disability [Johnson et al., 2005]. It has found that exercise training can increase strength and may improve motor activity in people with cerebral palsy (CP) without adverse effects [Damiano et al., 2000, Dodd

et al., 2002]; also it was demonstrated to increase the strength of affected major muscle groups of stroke survivors [Teixeira-Salmela et al., 1999, Andrews et al., 2003].

Such aged person and patients with mobility troubles would be at worst bedridden all day long. The most effective method to relieve these problems and support them for realizing the daily activities is to provide a way for them to be able to continue walking.

1.1.2   Lower Extremity Exoskeletons

In biology, exoskeleton is the exterior protective or supporting structure or shell of animals including bony or horny parts such as nails or scales. In this research the term of exoskeleton means the powered mobile machine consisting primarily of an exoskeleton-like framework worn by a person and a power supply that supplies at least part of the activation-energy for movement. Generally, it can be classified as lower extremity exoskeleton, upper extremity exoskeleton or full body exoskeletons.

Assistive knee brace is a species of wearable lower extremity exoskeletons. Such assistive equipment can enhance people's strength and provide desired locomotion and have advantages over wheelchairs which are commonly used for patients with

mobility disorder. For example, assistive knee braces could help the wearer walk on his or her own legs as a normal person does and therefore exercise their own lower bodies. Moreover, it is possible to use this kind of lower extremity exoskeletons to assist elderly or disabled people in improving their mobility so as to solve many daily life problems, like going up and down stairs and over obstacles.

The first wearable exoskeleton was developed in early 1960s, when the US Defense Department expressed interest in the development of a man-amplifier, which would augment soldiers' capabilities of lifting and carrying load. From 1960 to 1971, General Electric developed and tested a prototype called Hardiman (Human Augmentation Research and Development Investigation), which was a set of overlapping exoskeleton worn by a human operator [General Electric Co., 1969]. It weighted three-quarters of a ton and only one arm had been made to work. Although it could help wearer lift 341 kg, the studies found difficulties in human sensing and system complexity kept it from walking.

The Berkeley Lower Extremity Exoskeleton (BLEEX) was developed to support a human's walking while carrying heavy load on the back [Kazerooni et al., 2006]. BLEEX was first unveiled in 2004, at UC Berkeley's Human Engineering and Robotics Laboratory. It is comprised of two powered anthropomorphic legs, a power

unit, and a backpack-like frame on which heavy loads can be mounted. The device provides the wearer with the ability to carry significant loads with minimal effort over any type of terrain. The wearer could comfortably squat, bend, swing, twist and walking on ascending and descending slopes as well as stepping over obstructions.

Pratt et al. developed a one degree of freedom exoskeleton called RoboKnee for adding power at the knee to assist in squatting [Pratt. et al., 2004]. This exoskeleton system could provide assistance for wearer to climb stairs and perform deep knee bends while carrying a significant load in a backpack. Low impedance was achieved by using series elastic actuators (SEA) coupling the upper and the lower portions of a knee brace.

The MIT exoskeleton developed by the Biomechantronics Group at the MIT Media Laboratory, relies on the controlled release of energy stored in springs during walking gait, instead of using any actuators for adding power at joints [Walsh et al., 2007]. The prototype weights about 11.8 kg and is powered by a 48 V battery pack.

At the university of Tsukuba in Japan, Sankai et al. developed the Hybrid Assistive Limb (HAL) [Kawamoto et al., 2002, 2003, Lee et al., 2002, 2003]. The device can help people walk, climb stairs, and carry things around. HAL utilizes skin-surface

electromyographic (EMG) electrodes placed below the hip and above the knee, joint angle sensors and ground reaction force sensors to detect human intention and motion information. In distinction to BLEEX and MIT exoskeleton, the HAL does not transfer a load to the ground surface, but simply augments joint torques at the hip, knee, and ankle.

Honda developed a kind of walking assist device support bodyweight and reduce the load on wearer's legs while walking, climbing stairs, and in a semi-crouching position. The device has ability of controlling the torque in concert with the movement of legs and makes it possible to provide natural assistance in various postures and motions [HONDA, 2008].

Argo Medical Technologies in Israel developed a robotic ambulation system for wheel chair users, named as ReWalk [Bogue, 2009]. Utilizing sophisticated algorithms, upper-body motions are analyzed and used to trigger and maintain walking patterns such as going up and down stairs. The crutches are also used for stability and safety as well as guiding the motion of legs.

Wearable Walking Helper (WWH) developed by Kosuge et al. could support the weight of the wearer during walking by reducing loads of user's antigravity muscles

[Nakamura et al., 2005]. Another wearable assistive leg, Walking Power Assist Leg (WPAL) [Chen et al., 2007], for elderly or disabled people was designed to augment human power during walking based on human-robot interaction.

1.1.3   Actuators in Lower Extremity Exoskeletons

The actuators in lower extremity exoskeletons should not only provide desired torque, but also have the ability of agile and accurate control in various conditions. Meanwhile, in order to assist the wearer in various postures and prevent knee braces from exceeding the restricted motion, actuators should function as brake/clutch with the ability of safety interlock. Furthermore, power consumption in the actuation devices is another consideration in lengthening the working time of batteries after fully charged. Therefore, well designed actuators would be the key component for assistive knee braces in terms of performance and safety.

Generally, actuators in lower extremity exoskeletons can be classified as active and semi-active actuators. The most widely used active actuators are electric DC motors in form of rotary or linear ones.

The actuation system in HAL is called power unit including DC motor with harmonic drive. Each leg of HAL powers the flexion/extension motion at the hip and knee in the

sagittal plane. Honda's walking assist device, ReWalk and WPAL all use rotary DC motors as actuators to support bodyweight and reduce the load on wearer's legs while walking. WWH utilizes a linear actuator by a DC motor and a power screw to translate force to the user's knee joint. The device could support the weight of the wearer during walking by reducing loads of user's antigravity muscles.

RoboKnee uses SEA as actuator which comprises a spring intentionally placed between the motor and the load. In principle, the SEA is similar to any motion actuator with a load sensor and closed loop control system, and it has benefits of shock tolerance, lower reflected inertia, more accurate and stable force control, less damage to the environment, and energy storage [Pratt et al., 1995].

Besides electric motors, hydraulic and pneumatic actuators are another active actuators used in assistive knee braces and exoskeletons. BLEEX is actuated via bidirectional linear hydraulic cylinders mounted in a triangular configuration with the rotary joints, resulting in an effective moment arm that varies with joint angle. The device consumes an average of 1143 W of hydraulic power during level walking, as well as 200 W of electrical power for the electronics and control. It was found in their further study that the electric motor with harmonic drive would significantly decrease

power consumption during level walking in comparison to hydraulic actuation [Zoss and Kazerooni, 2006].

Nurse-Assisting Exoskeleton [Yamamoto et al., 2002] equipped DC pneumatic rotary actuators for the flexion/extension of the hips and knees. The purpose of the power assisting suit is to assist nurses during patient transfer.

For active actuators, especially for electric DC motors, brake function would consume large power to maintain any posture and might cause safety problems. For example, RoboKnee can only work 30-60 minutes of heavy use with 4kg of nickel-metal-hydride batteries. HAL-5 could operate around 160 minutes after fully charged.

In order to overcome the power consumption problems, some researchers adopted smart fluids in actuation mechanisms as semi-active actuators. For instance, a rehabilitative knee orthosis equipped electro-rheological (ER) fluids based actuators into knee braces [Nikitczuk et al., 2005]. An orthopedic active knee brace using magneto-rheological (MR) fluids based shear damper was developed to make the knee brace have controllable resistance [Ahmadkhanlou et al., 2007]. In the MIT exoskeleton, the knee consists of a MR damper with a spring (motion in the

flexion/extension direction), which is controlled to dissipate energy at appropriate levels throughout the gait cycle. By carrying current in the electromagnet, the magnetic field was controlled within the magnetic circuit and thus the level of knee damping.

MR fluids are a kind of smart fluids that comprise micro scale ferromagnetic particulates dispersed in an organic or aqueous carrier liquid. When a magnetic field is applied to this fluids, the dispersed magnetic particles become magnetized and behave like tiny magnets then the suspensions change their magnetic, electric, thermal, acoustic and optical properties and in particular the rheological behavior. It happened because the magnetic interactions between these particles line up the magnetic particles along the direction of the magnetic field. The yield stress of the MR fluids increases as the applied magnetic field increases. It has advantages over ER fluid, like higher yield stress, faster response and better safety.

Some researchers have also applied MR fluids to medical applications such as prosthetic or rehabilitation devices. Carlson et al. designed a portable controllable MR fluid device for rehabilitation of injured limbs appendages and joints [Carlson, 1998] and a smart prosthetics using a controllable MR damper [Carlson et al., 2001]. The resistance force of the device can be adjusted and controlled, and thus make them

adaptable to the patient.

Herr and his associates developed a prosthetic knee with an MR brake. Using local sensing information of force, torque and position, the smart prosthetic knee can automatically adapt damping to the gait of the amputee [Herr et al., 2003, Deffenbaugh et al., 2004].

Dong et al. developed a rehabilitation device using MR damper [Dong et al., 2006]. This device is in the form of rotating joint arm mounted on an adjustable seat that provides passive resistance during strength training for muscles. The MR damper is controlled based on the prescription of the therapist such that it can provide both isometric and isokinetic strength training for several human joints.

Li et al. developed a prosthetic ankle joint to help walk more naturally and smoothly. The ankle joint is controlled by a specially designed linear MR brake [Li et al., 2006]. The prosthetic ankle joint has been evaluated with walking experiments and it was proved that the device can improve the patient's walk.

Gait analysis also gives evidence that such smart fluid based actuators have advantages to be used in assistive knee braces. Gait analysis is usually adopted when designing and selecting actuators for lower extremity exoskeletons. A large amount of data available from laboratories that specialized in analysing human motion was collected. This Clinical Gait Analysis (CGA) data is collected via video motion capture equipment along with force plates to measure ground reaction forces [Winter, 2005]. Research groups in developing lower extremity exoskeletons also relay on CGA data to acquire information of human walking and determine the expected motions for exoskeletons so as to implement the accurate control algorithms.
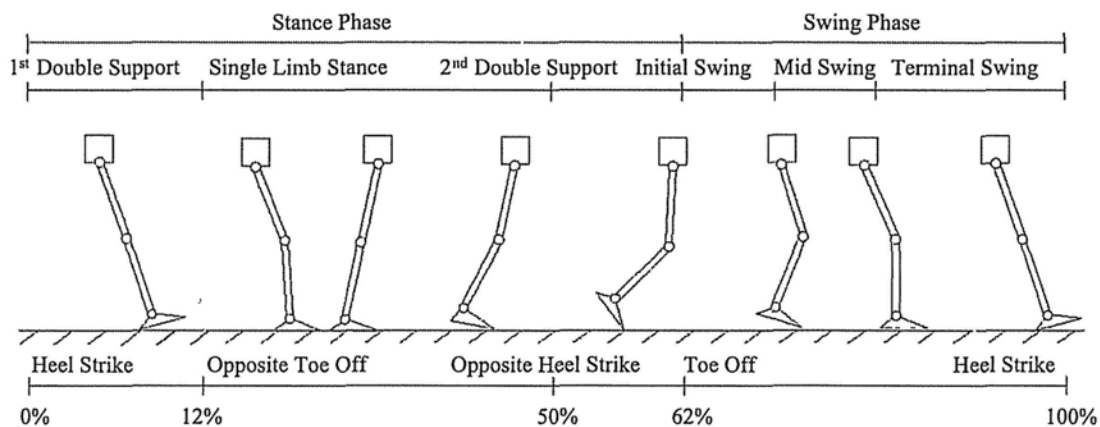
Figure 1.1-1 Gait cycle and walking states
adopted from [Wikenfeld and Herr, 2003]

Figure 1.1-1 is the gait information which is used in developing MIT exoskeleton. The figure shows a person moving through a normal gait cycle and the location of each walking mode [Wikenfeld and Herr, 2003]. During walking each leg alternates between a stance and swing mode. Stance mode is the state when the foot is contacting the ground and the leg supports partial or all of the person's body weight and can propel the person forward. During swing the foot is in the air and moving forward for the next stance mode. The leg switches from swing to stance mode at heel strike and then switches back to swing at toe off.
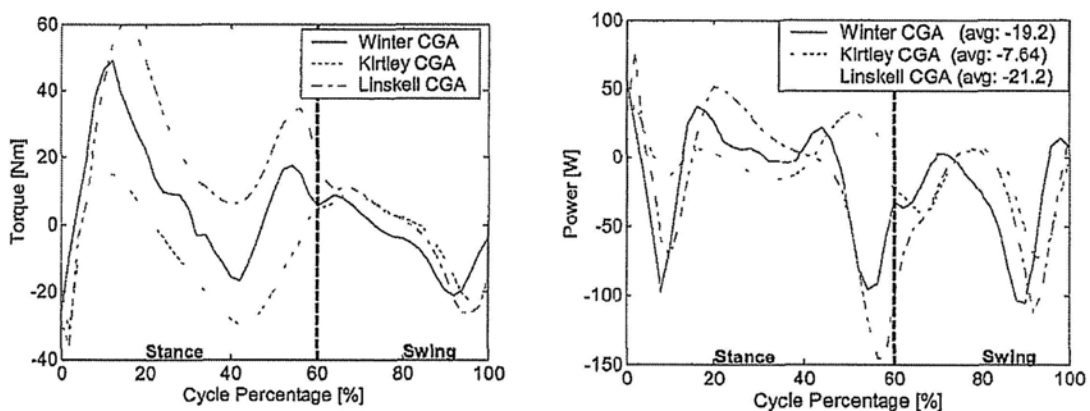
Figure 1.1-2 CGA data of knee angle and knee power during level ground walking
[Zoss and Kazerooni, 2006]

Figure 1.1-2 shows the CGA data of human knees movement utilized in developing BLEEX [Zoss and Kazerooni, 2006]. It can be found that the knee torque can be positive or negative, which indicates the need for a bi-directional actuator. The highest peak torque is extension in early stance (up to 60 Nm). From the figure, it can

- 13 -

also be found that the average power is negative which means the knee joint is usually dissipating power during walking. Hence, the knee joint dynamics could closely be matched by a controlled energy dissipative device, for example the MR fluids based actuators.

The developed knee braces using smart fluids could provide controllable torque as assistive devices in passive and semi-active means while consuming little power. However, in some situations for the wearer going upstairs or stepping over obstacles, such knee braces would not help in active ways.

To combine the advantages of active and semi-active actuation devices, like electric motors and smart fluids based actuators, a hybrid assistive knee brace by integrating MR actuator with electric motor was developed [Chen and Liao, 2010]. The MR actuator can function as brake when adjustable torque is preferred while little power is consumed; or work as clutch to transfer torque from motor to the brace. With adaptive control, the actuation system worked well and could provide desired torque with better safety and energy efficiency. However, the actuator seemed a bit bulky to be used on human body and could not fulfill the tasks of bi-directional rotation. Therefore, designing a more compact, multifunctional actuator is desired for assistive knee braces.

1.2 Research Objective

In the above discussions, actuators used in assistive knee braces are desired to provide large assistive torque and integrate multiple functions while being compact and lightweight. In order to increase the working time for this kind of wearable mobile assistive devices, power consumption should be low. Meanwhile, the actuator is also expected to ensure safety in the case of excessive output occurrence.

According to CGA data for normal human walking, the knee power is mainly passive, where usually happens during the bending of the knee joint; active power occurs during the extending of the knee. Therefore, energy dissipation devices like MR fluids based actuators takes the advantage over electric DC motors. However, in conditions where the active power is required, the energy dissipation actuators would not do much help.

The objective of this research is aimed to develop a novel actuator with multiple functions as motor, clutch, and brake for assistive knee braces. Meanwhile, the actuator could be able to rotate bi-directionally. To integrate the advantages of electric motor and MR fluids while decreasing the dimension, MR fluids are filled inside the motor part with an inner clutch/brake part. The multiple functions can be achieved by applying currents on inner and/or outer coils. Furthermore, using MR fluids the

actuator's brake function consumes less power than conventional electric motors to fulfill the same task. In this research, design details of the actuator will be considered. To analyze the magnetic circuit and performances of the actuator, finite element analysis will be performed. Prototypes will be fabricated and tested to investigate the multiple functions. In order to control the actuator, modeling and control algorithm will be developed. Finally, a mechanism using the multifunctional actuator will be implemented on the knee brace.

1.3 Thesis Organization

This thesis consists of seven chapters. Chapter One is an overview of the background and literatures related to the research on lower extremity exoskeletons and their actuators. Properties and applications of MR fluids are discussed and research objectives are presented. In Chapter Two, design considerations of multifunctional actuators are proposed. Design constraints as well as possible design configurations for the multifunctional actuator are illustrated. In Chapter Three, design details of the actuator are provided for each motor part and clutch/brake part. Magnetic circuit and influence of permanent magnets on MR fluids as well as the dynamic sealing are analyzed using finite element method. The prototypes with different clutch/brake parts are fabricated and characteristics of each function are investigated. Chapter Four covers the design optimization and analysis of the actuator. Models with different inner coils are analyzed and compared. The optimized prototype is fabricated and each function of the actuator is tested. Chapter Five provides modeling and system identification of the actuator. Adaptive control algorithms are proposed for torque and speed tracking. Chapter Six presents a smart joint using the optimized multifunctional actuator. The prototype is assembled and characteristics of each function are tested. Power consumption of the knee brace using the smart joint is investigated and compared with that using an electric motor. In Chapter Seven, conclusion and future work are summarized.

CHAPTER TWO

DESIGN CONSIDERATIONS

In this chapter, fundamental principles of designing the multifunctional actuator are explained in details. As the actuator is used in assistive knee braces, several design constraints for the multifunctional actuator are described. Then, the operating principle of the actuator is presented. Characteristics and configurations of the motor part and clutch/brake part are discussed. Brushless permanent magnet DC motors as well as the configurations of clutch/brake part are introduced. Possible combinations of the motor part and clutch/brake part of the actuator are discussed. Materials used in designing the actuator, such as MR fluids, high magnetic permeable and non-magnetic materials are considered.

2.1 Design Constraints

It is aimed to use the actuator in assistive knee braces. Therefore, several factors should be considered before designing a desired actuator for assistive knee braces, such as dimension, weight, input/output power and speed, stiffness, appearance, cooling, sealing, noise, and so on. Among them, the output torque and compactness are the most important design considerations.

According to the CGA data on human walking, the average walking speed is about 1.3 m per second and the knee on one leg rotates 40 degrees in this period [Lafortune et al., 1992]. The average peak torque during extension in isometric exercises is 172 Nm for healthy men and 112 Nm for healthy women [Neder et al., 1999]. For knee torques which is much smaller than these peak torques, is around output 50 Nm to move the body [Deffenbaugh et al., 2004]. The objective of the assistive knee braces is to provide assistive support to wearer. Therefore, the aim of the output torque and speed of the actuation system in assistive knee braces are set to 25 Nm and 8 rpm, accordingly. It is presumed that the transmission mechanism will be utilized into the system.

To meet the requirement of compactness, in this research, the diameter of the actuator limited in 100 mm and the width no larger than 40 mm would be desirable. Besides

these geometric constraints, other factors like mechanical and electromagnetic design considerations are illustrated in the following chapters for each of the motor part and clutch/brake part, and then the desired specification of the actuator is listed in Table 2.1-1.

Table 2.1-1 Desired specifications of multifunctional actuator

Parameters	Values
Width	30-40 (mm)
Diameter	80-100 (mm)
Weight	1-2 (kg)
Rated voltage	24 (V)
Range of output torque	0.25-1.0 (Nm)
Range of output speed	800-1000 (rpm)
Maximal input power	100-200 (W)

2.2 Operating Principle

In order to design a novel actuator with multiple functions as motor, clutch and brake, the actuator is comprised of two parts, motor part and clutch/brake part. Motor part is based on brushless permanent magnet DC motors with an adjusted internal structure. The motor part converts electric power into mechanical power to provide active torque. Clutch/brake part is the component that is placed inside of the motor part integrating with the MR fluids. Utilizing MR fluids, the clutch/brake part could transfer the torque generated from motor part to outside as clutch or provide controllable semi-active torque as brake with less power consumption than conventional electric motors. Therefore, the actuator is compact while providing multiple functions

The multiple functions of the actuator can be operated by applying current to different coils. When the current is applied to the outer coil of the motor part, the induced electromagnetic field would drive the rotor to rotate and then provide active torque. If the current is applied to both the outer and inner coils, simultaneously, the MR fluids would produce shear stress under the electromagnetic field induced from the inner coil. As a result, the clutch/brake part could transfer the torque from the motor part to outside as clutch. By adjusting the current, the actuator could produce controllable torque via the clutch. In another operation, when the current is applied only on the

inner coil, the actuator functions as brake. In this situation, with no current applied on the stator coil, the rotor will not rotate because of the magnetic interaction force between stator and permanent magnets. The advantage of this design is that it can deal with the tradeoff between the brake function and bi-directional rotation.

Therefore, for normal human walking, when passive assistive torque is required, the actuator in assistive knee braces acts as a brake by applying currents only on inner coil. When active assistive torque is required, the currents are applied on both inner and outer coils so as to make the actuator transfer torque from motor part. If no torque is needed, the actuator just work as a freely rotating knee joint and there is no current applied on any coil.

2.3 Configurations of Motor Part

2.3.1 BLPM DC Motors

A brushless permanent magnet (BLPM) DC motor is a kind of synchronous electric motor powered by DC electricity and having an electronic commutation system instead of a mechanical commutator or brushes.

The BLPM DC motor is essentially configured as a stator around which windings are wound and a rotor with permanent magnets. The windings provide an electromagnetic field to drive the permanent magnets fixed on the rotor. In this respect it is equivalent to an inverted brushed DC motor.

Limitations of brushed DC motors include lower efficiency and susceptibility of the brushes to mechanical wear and consequent need for servicing, and more complex and expensive control electronics. For BLDC motors, the electromagnets do not move whereas the permanent magnets rotate and the stator remains static. This solves the problem of how to transfer current to a moving armature. In order to do this, the brush is replaced by an electronic controller using a circuit rather than a commutator.

Figure 2.3-1 shows a basic structure of a BLPM DC motor. It comprises of three parts

as stator, rotor, and permanent magnets. The stator is generally made of high permeable material in form of lamination to provide magnetic field and improve the effect of eddy currents generated in the stator. The coil comprises a plurality of turns of wire wound on the stator so that it is effective for establishing an electromagnetic field when supplied with electrical currents. A number of permanent magnets are distributed in a circular pattern fixed on the iron core and form a rotor together with the iron core. The magnetic direction of permanent magnets is aligned with N and S alternately on the iron core, which is made of high magnetic permeable material.

BLPM DC motors have come to dominate many applications such as computer hard drives, CD/DVD players, and PC cooling fans. Low speed, low power ones are used
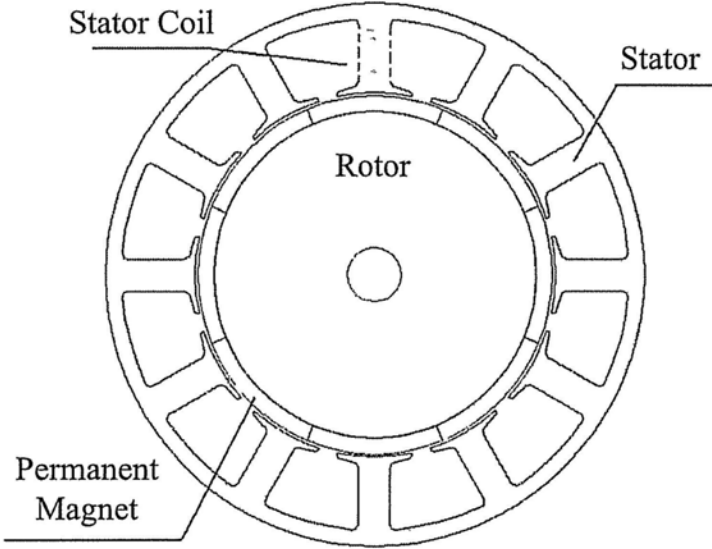
Figure 2.3-1 Basic structure of a BLPM DC motor
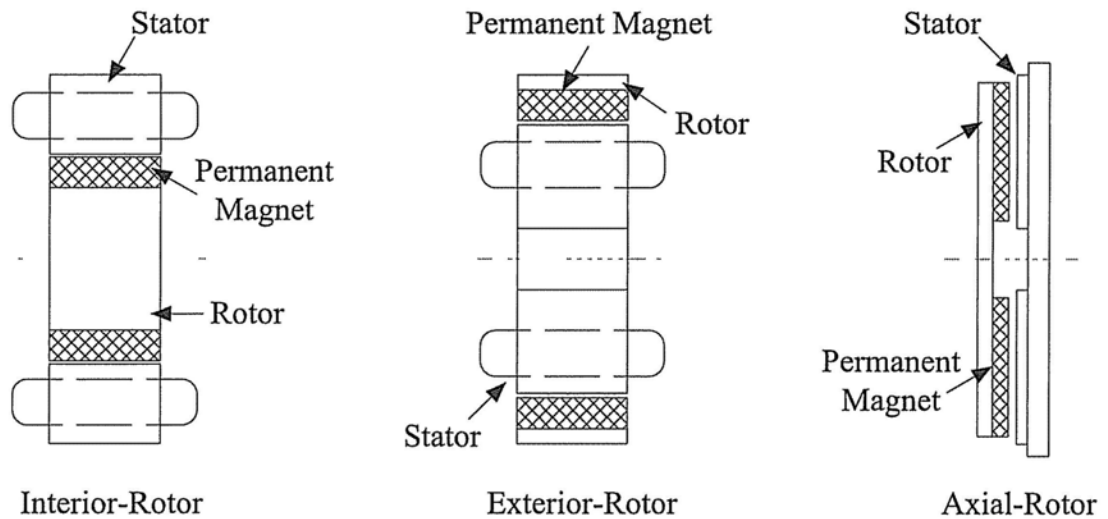
Figure 2.3-2 Three basic BLPM DC motor configurations

in direct-drive turntables for audio records. High power ones are found in electric vehicles, hybrid vehicles and some industrial machinery. A number of electric bicycles use BLPM DC motors as the wheel hub.

2.3.2   Basic Configurations

There are various configurations of BLPM DC motors can be adjusted as motor part in designing the multifunctional actuator. Generally, BLPM DC motors are constructed in three different physical configurations as shown in Figure 2.3-2, interior-rotor, exterior-rotor and axial-rotor.

The interior-rotor BLPM DC motor has similar configuration to that of the AC induction motor. If a high torque, low speed machine is required, then an interior-rotor design would be appropriate using rare earth magnets and a high pole count. Such motors can be made with a large hole through the center of the rotor, which provides valuable space for other parts of mechanisms [Hendershot et al., 1994]. Thus, for assistive knee braces, motor part of the actuator with interior-rotor configuration is an appropriate choice as high torque with low speed is needed.

2.4 Configurations of Clutch/brake Part

As illustrated in Chapter one, the majority power provided by human knees during normal walking is passive. In such conditions, using motor will consume large power to fulfill the task of dissipating energy and bring complexity to control algorithms. It is more appropriate to utilize energy dissipating actuators, such as MR fluids based devices to provide passive power when energy dissipation is required. In this research, MR fluids are filled inside of the motor part to provide clutch or brake torque while making a compact design. The motor part is operating in rotation, thus the MR fluids are working in shear mode. Therefore, clutch/brake part is placed inside the motor along with the MR fluids to produce the torque.

The inner clutch/brake part of the actuator may be implemented in form of inner armature with slots and shoes. In this case, inner coils are wound on each shoe of the inner armature. An example of such a clutch/brake element is illustrated in Figure 2.4-1. As shown, the clutch/brake part comprises an inner coil, an inner armature and a shaft. A plurality of turns of wire is wound on the inner armature, which is made of high magnetic permeable material in form of lamination with shoes and slots. The shaft is fixed into the inner armature to transfer torque. An additional guide layer made of high magnetic permeable material may be utilized to guide the magnetic flux produced by the inner coil through the MR fluids.
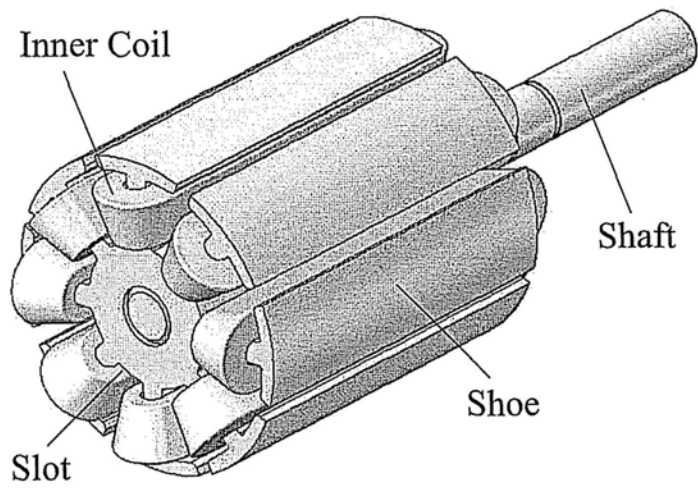
Figure 2.4-1 Clutch/brake part in form of inner armature
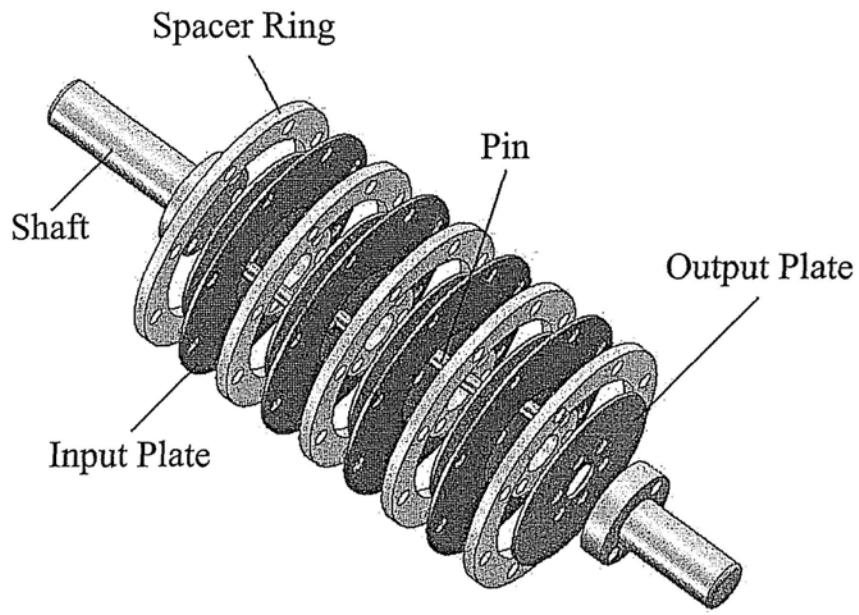
Figure 2.4-2 Clutch/brake part in form of input/output plates

Alternatively, the clutch/brake part can also be implemented in form of a plurality of input/output plates spaced apart by nonmagnetic spacer rings forming gaps therebetween to carry MR fluids. The output plates and spacer rings may be clamped by shafts with flanges. An example of such a clutch/brake part is illustrated in Figure 2.4-2. As shown, the clutch/brake part includes a set of input plates and a set of output plates which are separated by input spacer rings and output spacer rings. Two shafts are used to fix these plates and transfer torque.

Interior Inner Coil   Exterior Inner Coil

(a)   (b)

Axial Inner Coil

(c)

Figure 2.4-3 Three basic forms of inner coil in clutch/brake part

Table 2.4-1 Combinations of motor part and clutch/brake part

		Motor part		
		Interior-rotor	Exterior-rotor	Axial-rotor
Clutch/brake part	Inner armature	+	+	+
	Input/output plates (with interior coil)	+	+	+
	Input/output plates (with exterior coil)	+	+	+
	Input/output plates (with axial coil)	+	+	+

In this configuration of clutch/brake part, the inner coil can be implemented in form of interior coil, exterior coil or axial coil. For the interior inner coil (as shown in Figure 2.4-3 a), the coil is wound on a core in a cavity formed by shafts to provide electromagnetic field. For the exterior inner coil (as shown in Figure 2.4-3 b), the coil is wound on a nonmagnetic bobbin outside of the input/output plates instead of the inside core. For axial inner coil (as shown in Figure 2.4-3 c), the coil comprises two sets of axial coils which are in circular pattern around the flanges. Each set of the coils provides opposite electromagnetic directions.

Based on the above discussions, three main configurations of BLPM DC motor are possible to be used as motor part. Considering that there exist three different inner

coil configurations for clutch/brake part which is in form of input/output plates, the clutch/brake part can be implemented in four forms. Therefore, there are various combinations of motor part and inner clutch/brake part for designing the multifunctional actuator. Table 2.4-1 shows the possible combinations.

Appendix A shows some configurations listed in Table 2.4-1. Although all the above configurations can be implemented in designing the multifunctional actuator, as described in Section 2.3, the motor part with interior-rotor configuration is an appropriated option to be used in assistive knee braces. In the following chapters, only this form of motor part is to be covered. Similarly, the various configurations of clutch/brake part are different in providing clutch and brake torque. In Chapter Four, the analysis and comparison between the presented clutch/brake parts are conducted, and the configuration with interior inner coil is the final choice.

2.5 Materials Used in Design

MR fluids have the following advantages: (1) High yield stress - normally, MR fluid has a highest shear stress of nearly 100 kPa; (2) Temperature stability - MR fluids is relative stable between -40 and +150 $°C$; (3) Low voltage supply - the voltage for MR fluids is about several volts, which makes MR devices safe for applications.

To implement MR fluids into applications, there are three basic operation modes: flow mode (valve mode), shear mode (clutch mode) and squeeze mode (compression mode), as shown in Figure 2.5-1 [Carlson and Jolly, 2000].
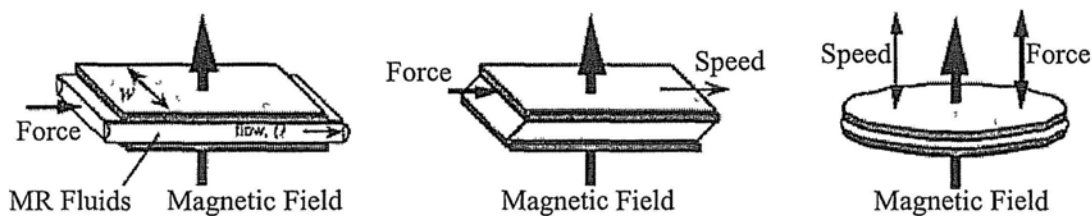
Figure 2.5-1 Basic operation modes for MR fluids
adopted from [Carlson and Jolly, 2000]

MR devices using flow mode include servo-valves, dampers, shock absorbers, etc; examples using shear mode include clutches, brakes, chucking and locking devices, etc; and the applications utilizing squeeze mode are usually for small amplitude vibration and impact dampers. Among them, vibration control and torque transfer are the most important applications for MR fluids.

The Lord Corporation has manufactured commercial MR fluid devices for applications including passenger protection of vehicles, knob & detent of automobiles, clutches of vehicles, vehicle seat suspensions, seismic protection, cable-stayed bridges, noise and vibration suppression of washing machines, smart prosthetic joints. Delphi and Cadillac developed commercial MR fluid based MagneRide™ semi-active suspension systems.

MR fluids have also been used in train suspensions [Liao and Wang, 2003, Lau and Liao, 2005], dissipative passive haptic displays [Swanson and Book, 2003, An and Kwon, 2009], hydraulic power actuation systems [Yoo and Wereley, 2002, 2004], MR fluid isolators [Oh, 2004], and high precision finishing [Kordonski and Golini, 1999, Shimada et al., 2002], etc.

The MR fluids used in this research are a kind of hydrocarbon-based MR fluids, MRF-132DG, which is commercially available in Lord Cooperation. Compared to the other MR fluids, MRF-132DG presents relative large yield stress under magnetic field while shows relative low yield stress without magnetic field. It has the benefits of fast response time, broad dynamic yield strength, wide operating temperature, low hard settling and non-abrasive. Figure 2.5-2 to Figure 2.5-4 show the properties of MRF-132DG when no magnetic field applied at 40 $°C$.
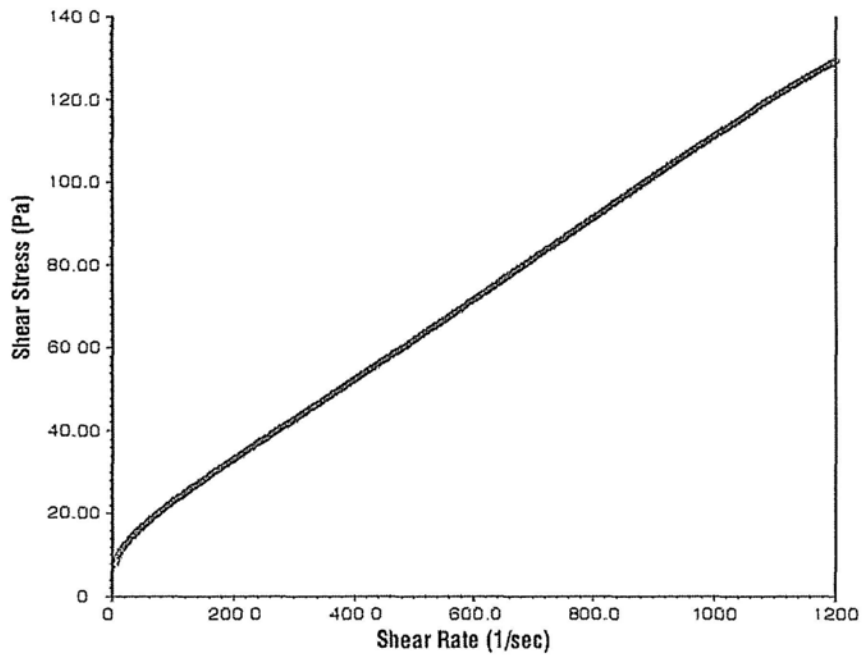
Figure 2.5-2 Relationship between shear stress and shear rate

[data from http://www.lordfulfillment.com]
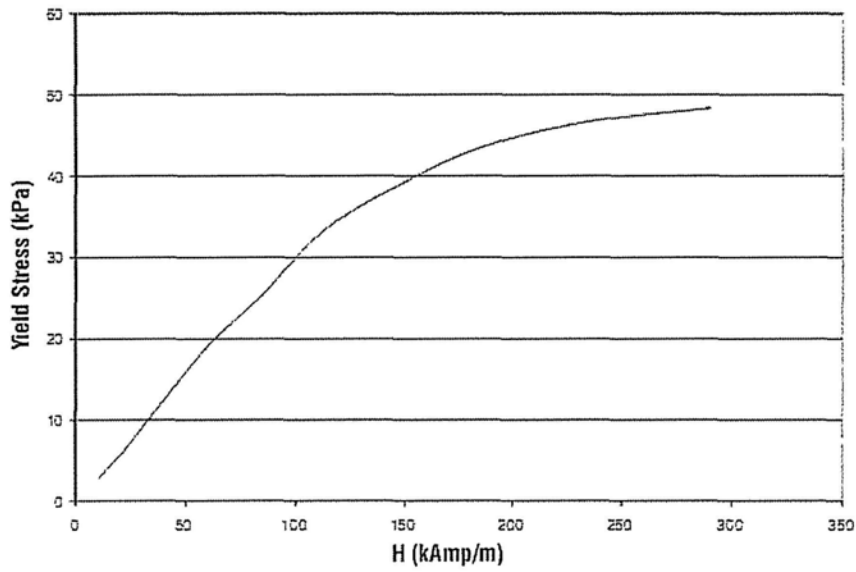
Figure 2.5-3 Yield stress vs. magnetic field strength

[data from http://www.lordfulfillment.com]

- 34 -
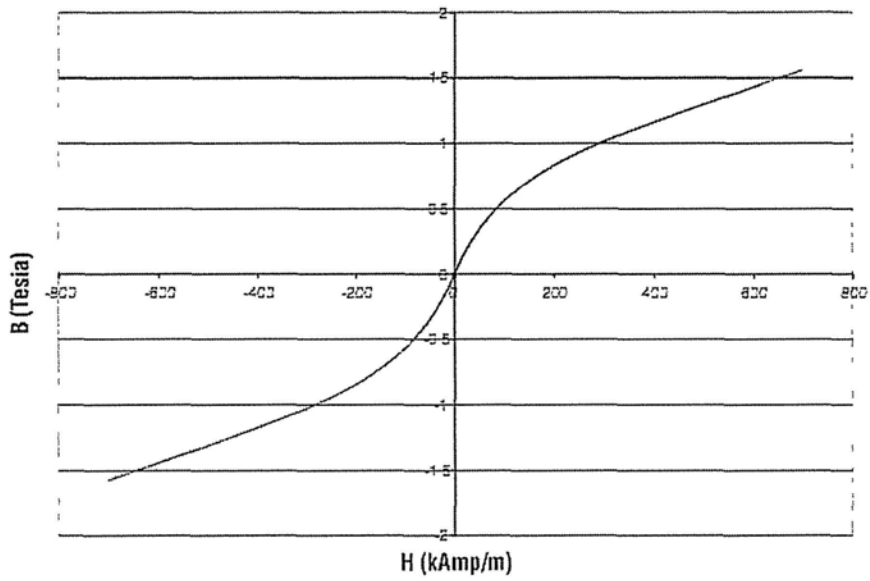
Figure 2.5-4 Typical magnetic properties

[data from http://www.lordfulfillment.com]
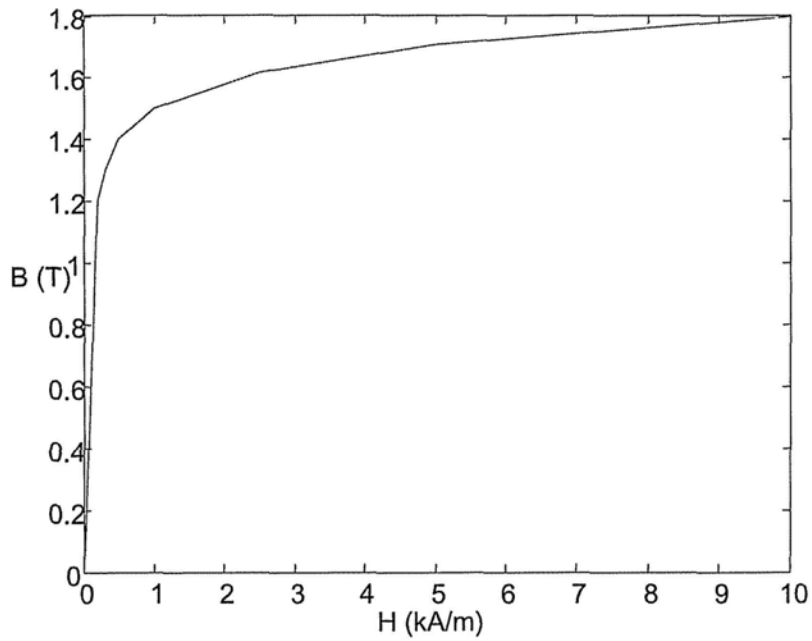
Figure 2.5-5 Magnetic properties of pure iron (DT4C)

[Data from http://www.atmcn.com]

High magnetic permeable materials used in this research are pure iron and silicon steel. Pure iron is a kind of economical soft magnetic material and easy to be machined. It has relatively high magnetic permeability and magnetic flux density. The pure iron used in this research is DT4C. Figure 2.5-5 shows the magnetic properties of this material.

Silicon steel is commonly used in fabricating laminations of generators, motors, and transformers, as it has lower hysteresis loss and high permeability. In this research, non-oriented silicon steel, 5A1300, is adopted to make the stator, inner armature or input/output plates. Figure 2.5-6 shows the B-H curve of this kind of silicon steel.
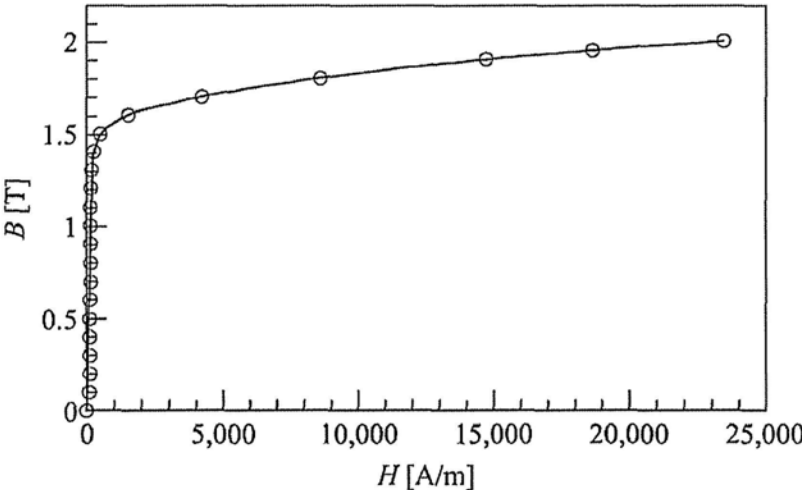
Figure 2.5-6 Magnetic properties of silicon steel (50A1300)
[Takahashi et al., 2005]
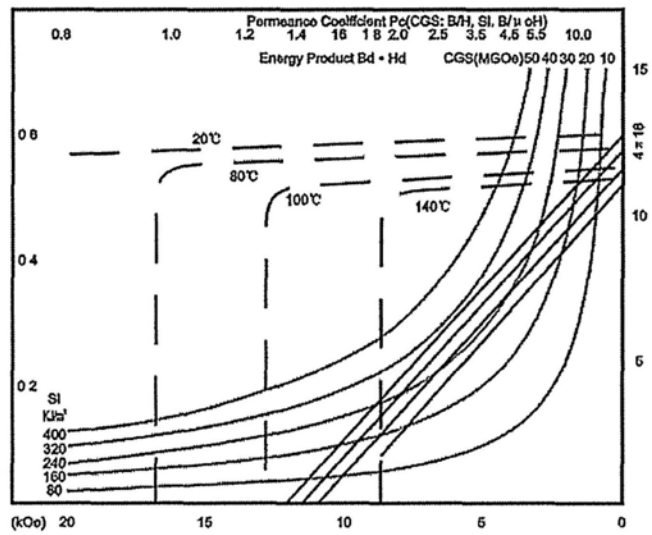
Figure 2.5-7 Magnetic properties of NdFeB permanent magnets (N38SH)

[data from http://www.zy-magnetics.com]

Permanent magnet is the main source of magnetic flux. The rare-earth magnets are the strongest permanent magnets made from alloys of rare earth elements. In this research, a kind of neodymium magnet, NdFeB-N38SH, is utilized as permanent magnets in motor part. Figure 2.5-7 shows the magnetic properties of the N28SH.

Non-magnetic materials are used to reduce or insulate magnetic flux so as to confine the flux into the desired magnetic circuit. The non-magnetic materials used in this research are aluminum (Al6061) and stainless steel (1Cr18Mn8Ni5N). The relative permeability of these materials is equal to constant 1.

2.6 Chapter Summary

This chapter covers the principles of designing the multifunctional actuator utilizing MR fluids. In order to be used in assistive knee braces, desired specifications of the actuator are provided to meet the requirement of design constraints. The actuator is comprised of a motor part and a clutch/brake part with outer and inner windings. The multiple functions can be operated by applying current on different coils. In this research, BLPM DC motors are modified to be used for motor part. Various configurations of the motor part as well as different forms of clutch/brake part are presented. Then, possible combinations of two parts are discussed. At the end of this chapter, materials to be used in designing the actuator are considered.

CHAPTER THREE

DESIGN AND ANALYSIS OF MULTIFUNCTIONAL

ACTUATORS

In this chapter, design and analysis of the multifunctional actuator is discussed. Design details of motor part and clutch/brake part are illustrated, respectively. Two different forms of clutch/brake part, inner armature and input/output plates, are presented. Then, finite element method is utilized to model and analyze the magnetic circuit, the influence of permanent magnet on MR fluids and dynamic sealing as well. Two prototypes with inner armatures and input/output plates are fabricated and their characteristics are investigated and compared. Each function including motor function, clutch function and brake function, are tested. The properties such as torque-current relationship and dynamic torque response are measured.

3.1 Motor Part Design

Various types of conventional motors could be used for the design of the motor part. As illustrated in the Section 2.3, for assistive knee braces, high torque with low speed is required. Therefore, an interior-rotor configuration would be an appropriate option which can be made with a large hole through the center of the rotor, so as to provide space for inner clutch/brake part along with the MR fluids.

To design a motor part that produce sufficient torque while having good performance, there are several design factors should be considered. The number of stator slots and magnet poles is one of the considerations in motor part design. The number of poles is inversely proportional to the maximum speed of rotation. By increasing the number of poles, the overall diameter then can be reduced.

Cogging force is a kind of magnetic force between the stator and permanent magnets which usually causes oscillation during rotation. For conventional motor design, lots of efforts have been made to reduce the cogging force. However, in this design, the magnetic force between the stator and permanent magnets has its special function. When there is no current applied on stator coils, this magnetic interaction force would hold the rotor still so as to play an important role in operating as brake.

Table 3.1-1 Slot/Pole ratios for BLPM DC motors for minimizing cogging torque [Janocha, 2004]

0.75		1.125		1.5	
Slots	**Poles**	**Slots**	**Poles**	**Slots**	**Poles**
3	4	9	8	3	2
6	8	18	16	6	4
9	12	36	32	9	6
12	16			12	8
15	20			15	10
18	24			18	12
21	28			21	14
24	32			24	16
2.25		**3**		**3.75**	
9	4	6	2	15	4
18	8	12	4	30	8
27	12	18	6	45	12
		24	8		
		30	10		
		36	12		
4.5		**5.25**		**6**	
9	2	21	4	12	2
18	4	42	8	24	4
27	6			36	6
36	8			48	8

Increasing the cogging force would improve the brake function but at the same time impair the dynamic performance of motor function. Hence it is a trade-off to determine a suitable magnetic force between the stator and permanent magnets. Some studies [Zhu et al., 2000, Wang et al., 2003] have been carried out on the reduction of cogging force, such as increasing air gap, using fractional slots/poles combination, skewing stator slots or magnets, varying the magnetization of the poles and using bifurcated teeth, and so on. In this design, fractional slots/poles are adopted to minimize the cogging force while keeping appropriate magnetic force between stator and permanent magnets. Some of the most popular slot and pole combinations for BLPM DC motors, which have been categorized in terms of slot/pole ratios, were given in Table 3.1-1. In this design, a motor part with 12 stator slots and 8 poles permanent magnets is adopted.

In order to design a compact actuator used in assistive knee braces, hall sensor that is used in the conventional motors is removed here. The indirect rotor position sensing can be obtained through a position estimation method using back EMF detection in an unexcited phase winding.

In order to provide sufficient active torque, the motor part needs to produce as large electromagnetic torque as possible. There are some factors affecting the value of the

torque, such as grade of the permanent magnet, permeability of magnetic materials, windings of the coil, and air gap. In motor part, magnetic flux passes between the stator and permanent magnets through the air gap. The output torque or the electromagnetic torque is proportional to the flux in it. The electromagnetic torque provided by the motor part could be calculated with the following equation

$$T_M = C_T \Phi_M I_M \qquad (3.1)$$

where C_T is the torque constant relating to the windings, I is the current applied on the outer coils, Φ is the magnetic flux in the air gap, the subscript $(_M)$ represent the first prototype and the motor part, respectively.

According to the Ampere's law, there is

$$\oint_L H \cdot dl = \sum i \qquad (3.2)$$

which can be simplified as

$$HL = nI = F \qquad (3.3)$$

where H is the magnetic field intensity, L is the length of the magnetic circuit, n is the turns of coil, and F is the magnetomotive force (MMF). Also,

$$\Phi = \int_A B \cdot da = BA \qquad (3.4)$$

$$B = \mu H \qquad (3.5)$$

where B is the magnetic flux density, A is the cross-sectional area, and μ is the magnetic permeability. Using the above equations in the motor part, it can be derived that

$$F_M = nI_M = \sum_{i=1}^{l} \Phi_i \frac{l_i}{\mu_i A_i} = \sum_{i=1}^{l} \Phi_i R_i \qquad (3.6)$$

where subscript ($_i$) represents each component within the magnetic circuit. R is magnetic reluctance and l is length of the magnetic circuit in the motor part which includes the air gap.

As each component in magnetic circuit is connected in series, the magnetic flux can be the same in every component including the air gap. Hence, Equation (3.6) can be rewritten as

$$nI = \Phi_M \sum_{i=1}^{j} R_i = \Phi_M (\sum_{i=1}^{k} \frac{l_i}{\mu_i A_i} + \frac{g}{\mu A_g}) \qquad (3.7)$$

where g is the air gap, μ is the permeable of the air, and A_g is the contacting area of the gap. Hence, with the given turns of coil and current, the magnetic flux is inversely proportional to the magnetic reluctance. According to Equation (3.1), at the steady-state, decreasing the air gap would decrease the magnetic reluctance and increase the air gap flux so as to increase the output torque. From the practical point of view, for small motors, the air gap is usually 0.1 mm to 0.25 mm; and for medium size motors, 0.3 mm to 0.5 mm would be appropriate. In this design, the air gap is set to 0.5 mm.

Three phases' windings of the outer coil in form of *wye* are adopted in this design. Based on the desired specification and parameters achieved above, the maximum outer coil current or the demagnetizing line current can be calculated by the following equation,

$$I_{demag} = [\frac{1000}{4\pi \times 39.37}] \times \frac{2(L_{PM} + g_M)H_d}{z_M / 2p_M} \times a_M = 2.02 \times \frac{4p_M a_M (L_{PM} + g_M)H_d}{z_M} \qquad (3.8)$$

where L_{PM} and H_d are the length and coercive force of the permanent magnets; g is the

air gap; z is the total number of conductors actually carrying current; p is the number

of pole-pairs, q is the number of parallel paths in the winding, and a is the number of

parallel paths in the winding. When the current is larger than this value, the permanent

magnet will be demagnetized so as to impair the performance of the motor part.

3.2 Clutch/brake Part Design

3.2.1   Form of Inner Armature

Two main forms of clutch/brake parts are discussed in Section 2.4, inner armature and

input/output plates with three different inner coils. As shown in Figure 2.4-1, the inner

armature is inside the cavity of the motor part. In particular, the cavity is defined by

the rotor, an insulation layer, a housing cover and a guide layer. The inner armature is

made of high magnetic permeable material in form of lamination with slots and shoes.

The inner coil comprising a plurality of turns of wire is wound on the armature. MR

fluids are filled inside the cavity through which the electromagnetic flux produced by

the inner coil penetrated. To confine MR fluids between the gap defined by guide

layer and inner armature, epoxy is used to seal the inner coil and inner armature for

forming a shell. A shaft with a hole is supported by bearings and the hole is used to

extend wires outside.

To reduce the influence of the permanent magnets on MR fluids, a sandwich layer

including rotor, insulation layer and guide layer, is adopted in this design. The rotor is

used to guide the magnetic flux form permanent magnets. The insulation layer is

made of non-magnetic material and is fixed inside the rotor to insulate the magnetic

field from permanent magnets, while the guide layer is made of a high magnetic

permeable material guides the magnetic flux caused by the inner coil that wound on inner armature. Figure 3.2-1 shows the configuration of the sandwich layer.
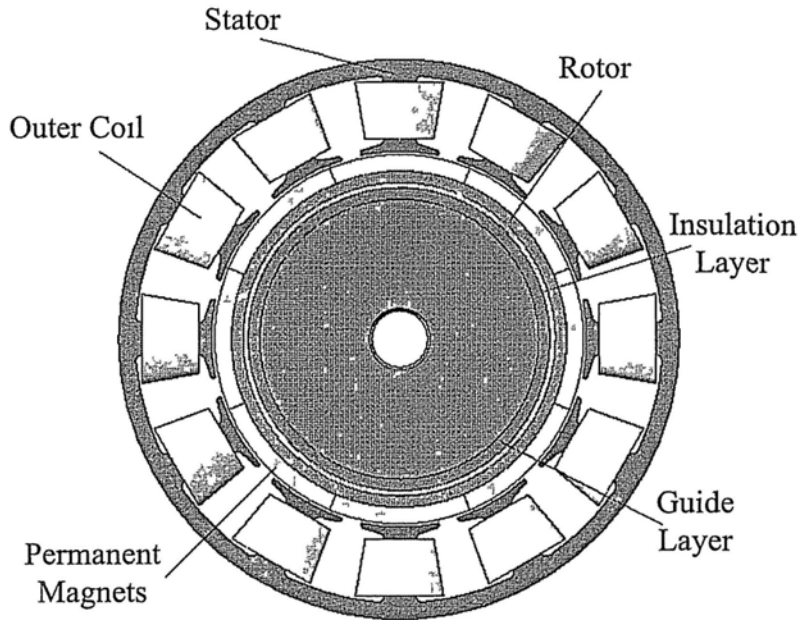
Figure 3.2-1 Configuration of the sandwich layer

A well designed magnetic circuit could produce maximum magnetic flux so as to provide maximum yield torque in clutch/brake part. As shown in Figure 3.2-2, the magnetic circuit in the clutch/brake part consists of the armature shoes, MR fluids, armature core, and guide layer. The inner coil is wound on the armature core, where currents in the windings are opposite to that of the adjacent ones so as to produce the opposite electromagnetic field between each of the adjacent shoes. Therefore, the magnetic flux Φ start form the armature core along the shoe which displays N field,

then penetrate the MR fluids and pass through the guide layer, and finally return to the adjacent shoe which displays S field. When the clutch/brake part begins rotating, under the magnetic field produced by inner coil, the relative rotation between armature shoes and the guide layer make the MR fluids operating in a shear mode.
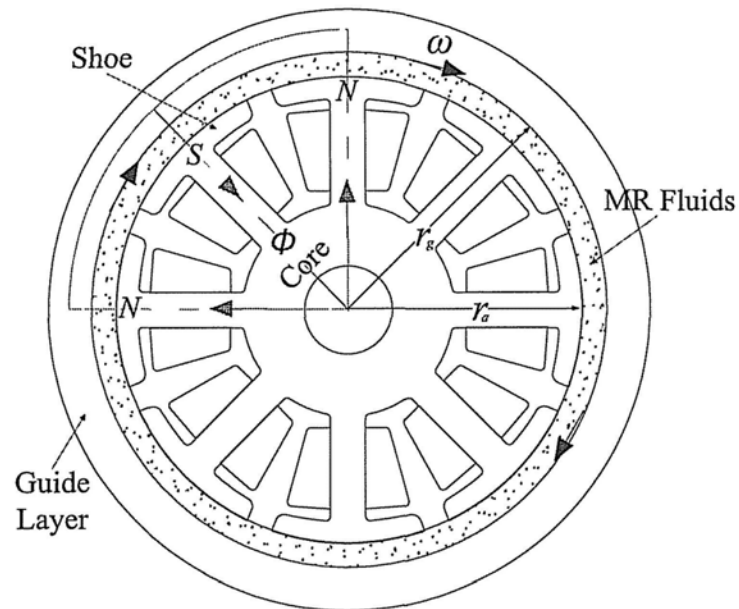
Figure 3.2-2 Magnetic circuit and working principle of the clutch/brake part

According to Ampere's law, the MMF in clutch/brake part depends on the turns of the inner coil and the applied current. Therefore, the magnetic flux within MR fluids in clutch/brake can be obtained as

$$\Phi_{mr} = \frac{n_{mr}I_{mr} - \sum \Phi_i R_i}{R_{mr}} = \frac{n_{mr}I_{mr} - \Phi_{shoe}R_{shoe} - \Phi_{core}R_{core} - \Phi_{guide}R_{guide}}{R_{mr}} \qquad (3.9)$$

where n is turns of the inner coil, R_{shoe}, R_{core}, and R_{guide} are magnetic reluctance of armature shoes, armature core, and guide layer, respectively. The subscript ($_{mr}$) represents MR fluids.

Hence, on the basis of Equation (3.6), by properly selecting the materials (i.e. μ) for the circuit components and their geometry (l and A), the magnetic flux in MR fluids will be increased so as to enlarge the yield torque.

The torque generated by the inner armature can be calculated as follows

$$T_{CB} = \tau_{mr} A_{CB} r_{CB} \tag{3.10}$$

where τ is the shear stress of MR fluids, and A is the contact area of inner armature with MR fluids, and r is the radius of the inner armature. The subscript ($_{CB}$) represents the clutch/brake part.

The contact area is the surface on the inner armature where the MR fluids are activated by applied magnetic field intensity. As shown in Figure 3.2-2, the contact area can be calculated by

$$A_{CB} = 2\pi r_{CB} L_{CB} \tag{3.11}$$

where L is the length of the armature.

The characteristics of the MR fluids can be described using the Bingham plastic model [Phillips, 1969], the shear stress τ is

$$\tau_{mr} = \tau_y + \eta\dot{\gamma} \qquad (3.12)$$

where τ_y is the yield stress due to applied magnetic field, and it could be obtained from the specifications of the MRF-132DG fluids as shown in Section 2.5. It is proportional to the magnetic flux in MR fluids, which can be represented by Equation (3.9) η is the off-field plastic viscosity of the MR fluids, and $\dot{\gamma}$ is the shear rate. The shear rate can also be written as

$$\dot{\gamma} = \frac{\omega r_g}{g_{mr}} = \frac{\omega r_g}{r_g - r_{CB}} \qquad (3.13)$$

where ω is the angular velocity, and g_{mr} is the gap (also the thickness of the MR fluids), which is the difference between the radius of the armature and guide layer, r_g. Similar to the air gap in motor part, to achieve large yield stress in MR fluids, the gap between the armature shoes and the guide layer is the smaller the better. According to Equation (3.9), the magnetic flux in the gap increases sharply with decreasing the gap

(or the length l). Practical gaps typically range from 0.25 to 2 mm for ease of manufacture and assembly [Yoo et al., 2002]. In this design, the gap in the clutch/brake part is set to 0.5 mm.

Therefore, the torque produced by the inner clutch/brake part of the actuator can be obtained as follows

$$T_{CB} = 2L_{CB}\pi[\frac{\tau_y(r_g^3 - r_a^3)}{3} + \frac{\eta\omega(r_g^3 + r_g^2 r_a + r_a r_g^2 + r_a^3)}{4}]$$ (3.14)

According to Equation (3.9), the applied current density on inner coil is proportional to the magnetic flux in MR fluids. However, the current density is limited by the cross-sectional area of the coil, coil material and the saturation flux densities of the magnetic materials used in the clutch/brake part.

The assembly of the motor part and inner armature is shown in Figure 3.2-3. The actuator includes a stationary laminated stator that advantageously includes outer coil. The stator is generally made of high permeable material in form of lamination to provide expected magnetic field and improve the effect of eddy current. The outer coil comprises a plurality of turns of wire wound on the stator and is effective for establishing an electromagnetic field when supplied with electrical current. Housing

and shafts are held and supported by bearings. A pair of seals mounted on shafts provides dynamic sealing to prevent MR fluids leaking from cavity while not reducing the actuator's rotary movement.

A number of axial openings are distributed in a circular pattern around the housing cover, so that circulating air can pass the axial openings to expel heat, which is commonly generated by the outer coil. The magnetic direction of each permanent magnet is aligned with N and S alternately on the rotor, which is made of high magnetic permeable material. A hall sensor with control circuit is used to sense changes in magnetic direction of the permanent magnets during rotation and then adjust voltage on the outer coil to produce desired magnetic field for driving the permanent magnets to rotate continuously.

The inner armature is arranged in a cavity defined inside the motor part. MR fluids are filled inside the cavity and carry the electromagnetic flux produced by the inner coil between a gap defined by the guide layer and the armature shoes which is covered by the epoxy shell.

The actuator can work as motor when currents are applied to the outer coil to produce electromagnetic field driving the permanent magnets. If currents are applied to the

motor part and inner armature simultaneously, then the actuator works with dual

functions, motor and clutch, to transfer torque from the motor part to outside. And if

the currents are applied to the inner coil but not the outer coil, the actuator then works

as brake.
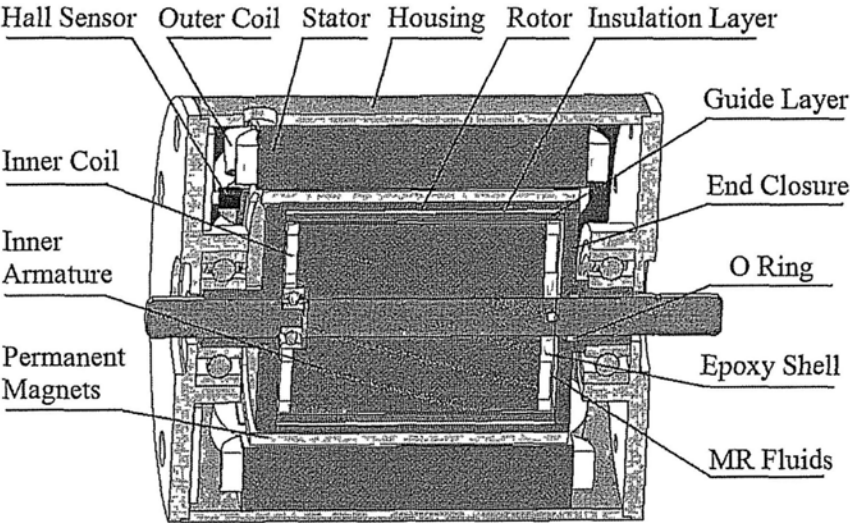
Figure 3.2-3 Assembly of the multifunctional actuator with inner armature

3.2.2   Form of Input/output Plates

In this design, the clutch/brake part is comprised of two sets of input/output plates,

which are separated by spacer rings forming space for MR fluids as shown in Figure

2.4-2. The plates are made of high magnetic permeable materials to form a magnetic

circuit carrying electromagnetic flux produced by the inner coil. MR fluids are filled

inside the cavity through which the electromagnetic flux penetrated. With the electromagnetic field produced by the inner coil, the relative rotation between the two sets of plates would yield shear stress in MR fluids. The gap between every pair of input/output plates is set to 0.5 mm. The copper wires with diameter of 0.45 mm are chosen as inner coils and maximum applied current goes up to 2.4 A.

Therefore, the torque generated by the clutch/brake part of the second prototype can be calculated as follows

$$T_{CB} = \int_A \tau_{mr} r_{CB} dA_{CB} \tag{3.15}$$

where τ_{mr} is the yield shear stress of MR fluids, and A is the overlapping surface, and r is the radius of the inner armature.

The overlapping surface on the shear plates where the MR fluids are activated by applied magnetic field intensity, which can be calculated by

$$A_{mr} = 2n\pi \int_{r_i}^{r_o} r_{mr} dr_{mr} = 2n\pi (r_o^2 - r_i^2) \tag{3.16}$$

where n is number of the surfaces of the plates in contact with MR fluids, r_i and r_o are

radiuses of the input/output plates.

Referring to the Equation (3.12) and Equation (3.13), the torque produced by the clutch/brake part can be obtained as follows

$$T_{CB} = n_{CB} \int_{r_i}^{r_o} (\tau_y + \eta\dot{\gamma})r_{CB}(2\pi r_{CB})dr_{CB} = \frac{2n_{CB}\pi\tau_y}{3}(r_o^3 - r_i^3) + \frac{n_{CB}\pi\omega\,\eta}{2g_{CB}}(r_o^4 - r_i^4) \qquad (3.17)$$

where g is the thickness of the MR fluids which is the gap between every pair of an input and output plate.

If the angular velocity is slow when the torque caused by the fluid viscosity is negligible, the torque produced by clutch/brake part can be rewritten as

$$T_{CB} = n_{CB} \int_{r_i}^{r_o} \tau_y r_{CB}(2\pi r_{CB})dr_{CB} = \frac{2n_{CB}\pi\tau_y}{3}(r_o^3 - r_i^3) \qquad (3.18)$$

As discussed in Section 2.4, there are three forms of inner coils can be used into input/output plates. In this chapter, the exterior inner coil is adopted in the design. To reduce the influence of permanent magnets on the MR fluids while providing electromagnetic field for clutch/brake part, a bobbin that is made of nonmagnetic

material wound with inner coils are fixed underneath the rotor. The inner coils could

provide electromagnetic field as well as weaken the magnetic field induced by the

permanent magnets. Moreover, as end closure and rotor are all made of high magnetic

permeable materials, they form a high permeable container to shield the magnetic flux.

Therefore, the influence of the permanent magnets on MR fluids inside would be

reduced. Figure 3.2-4 shows the assembly of the multifunctional actuator with the

input/output plates with exterior inner coil.
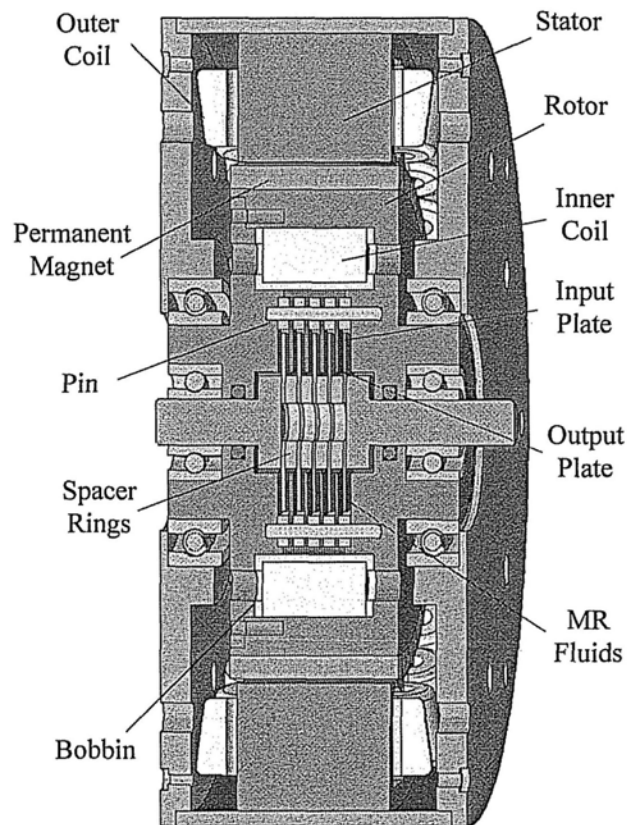
Figure 3.2-4 Assembly of the multifunctional actuator with input/output plates

3.3 Analysis of the Actuator

3.3.1 Finite Element Method

Finite element method (FEM) is a numerical technique for finding approximate solutions of partial differential equations (PDE) as well as of integral equations. It can be used to model and analyze all kinds of mechanical disciplines, such as thermal, electromagnetic, fluid, and structural working environments. In this research the motor part and the inner clutch/brake part are analyzed by FEM.

Commercial FEM software ANSYS® is used in this research. The following governing magnetostatic equations derived from Maxwell's equations are used in this software

$$\nabla^2 A - \mu\varepsilon \frac{\partial^2 A}{\partial t^2} = -\mu J \qquad (3.19)$$

$$\nabla^2 \phi - \mu\varepsilon \frac{\partial^2 \phi}{\partial t^2} = -\frac{\rho}{\varepsilon} \qquad (3.20)$$

where A and ϕ are the magnetic vector potential and magnetic scalar potential, respectively; μ and ε are the permeability and permittivity of a given medium,

respectively; J is the current density, ρ is the electric charge volume density and ∇^2 is Laplace operator which is denoted as

$$\nabla^2 = (\frac{\partial^2}{\partial x^2} + \frac{\partial^2}{\partial y^2} + \frac{\partial^2}{\partial z^2})$$
(3.21)

The magnetic vector potential and magnetic scalar potential can be denoted as

$$B = \nabla \times A$$
(3.22)

$$E = -\nabla \cdot \phi$$
(3.23)

where B is the magnetic flux density and E is the electric field; $\nabla \times$ and $\nabla \cdot$ are divergence operator and curl operator, respectively.

As the actuator is axis-symmetric, 2D axis-symmetric models are built to analyze the interaction magnetic torque between the stator and permanent magnets in motor part and estimate the electromagnetic torque when currents are applied on the outer coil. 2D models can also be used to analyze the interference of the permanent magnets on MR fluids as well as the magnetic flux distribution and the yield stress produced in the inner clutch/brake part. In order to analyze the dynamic sealing in the clutch/brake

part, 2D model cannot provide sufficient information; therefore, 3D model is built and utilized in this kind of analysis.

3.3.2   Finite Element Analysis of the Actuator

In this section, the motor part and clutch/brake part in different forms are analyzed, respectively. The interaction magnetic force between stator and permanent magnets is investigated for motor part. The influence of permanent magnets on MR fluids, magnetic flux distribution and dynamic sealing are analyzed, and the shear stress provided by the inner clutch/brake part is simulated as well.

The actuator with inner armature is analyzed first. To implement the electromagnetic analysis for the motor part, there are some materials should be modeled. They are air in the air gap, silicon steel for stator and inner armature, permanent magnets, pure iron for rotor and guide layer; copper for outer and inner coils, aluminum for insulation layer and MR fluids. The relative permeability of copper, aluminum and air are treated as constant 1. The permeability of silicon steel, permanent magnets, pure iron and MR fluids are given as *B-H* curves which are shown in Section 2.5.

To find a solution of removing or reducing the influence of permanent magnets on MR fluids, two 2D models are built. Figure 3.3-1 is the model without insulation layer
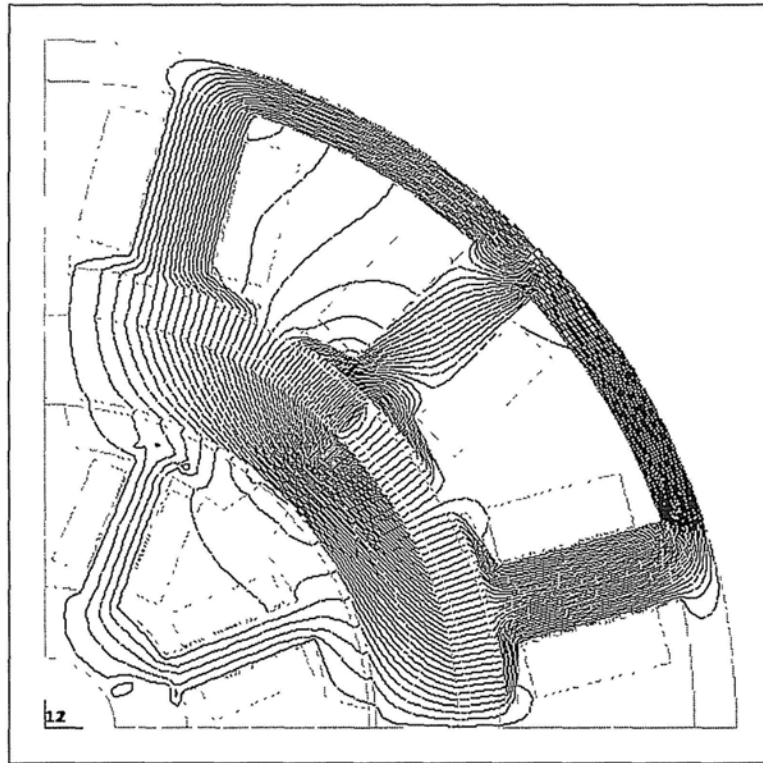
Figure 3.3-1 Interference analysis for the model without insulation layer

and Figure 3.3-2 is the model with a sandwich layer including a rotor, an insulation layer and a guide layer. As shown in Figure 3.3-1, the permanent magnets are fixed on a thick cylinder made of pure iron. Although the cylinder is thick enough, it is obvious to see that the magnetic flux of permanent magnets passed through the MR fluids. Therefore, the performance of clutch and brake functions will be significantly affected by permanent magnets.

The other one shown in Figure 3.3-2 is a model having an insulation layer and a guide layer. The insulation layer is made of aluminum that could weaken the magnetic field.
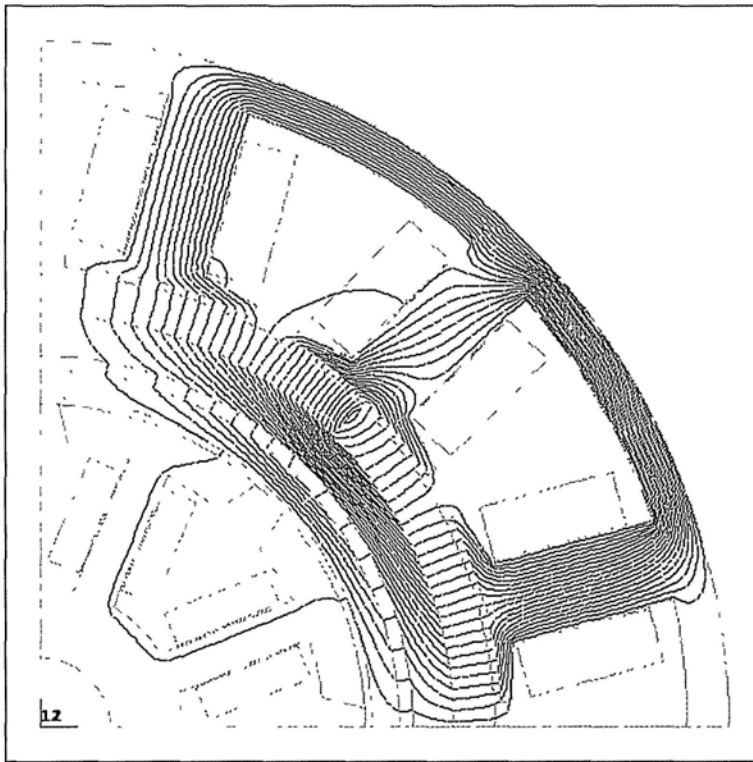
Figure 3.3-2 Interference analysis for the model having a sandwich layer

The guide layer is made of pure iron, which could guide the magnetic flux from inner coil across MR fluids and shield the magnetic flux from permanent magnets. From the analysis, it can be found that the sandwich layer could significantly reduce the effect of permanent magnets on MR fluids as the most of the magnetic flux from permanent magnets pass through the rotor and guide layer.

Analysis for the clutch/brake part is to check whether the magnetic flux in MR fluids is perpendicular to the surface of inner armature so that the maximum shear stress could be produced. It was illustrated that the maximum stress occurred when the

direction of the magnetic field is perpendicular to the shear motion of the MR fluids [Kordonsky et al., 1990]. As shown in Figure 3.3-3, it can be found that the direction of magnetic flux in MR fluids is along the normal direction of the contacting surface of the armature and the guide layer as the result that the shear stress reaches the maximum value.
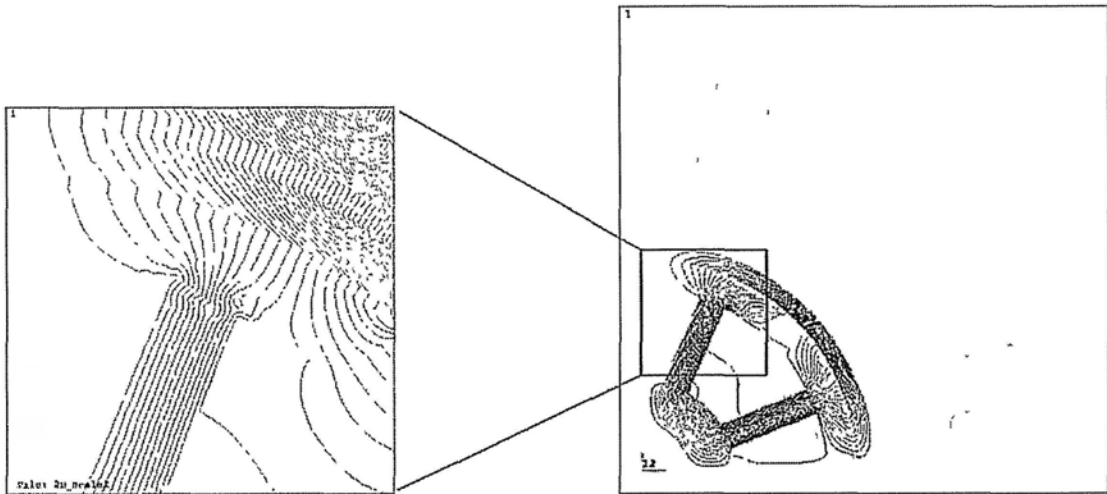
Figure 3.3-3 Magnetic flux in MR fluids

Besides simulation for magnetic flux and yield torque, FEM can also be used to analyze sealing of the actuator. Sealing is an important research issue for preventing MR fluids from flowing outside while not affecting the rotation. In this research, rubbery O ring is used as part of dynamic sealing. However, MR fluids may be still possible to leak from the edge of the end closure. As one solution, a high magnetic permeable material like pure iron is chosen for the end closure. Then, the cylinder and

end closure will form a high permeable container to shield the magnetic flux. A 3D model is built for analyzing the dynamic sealing. Figure 3.3-4 shows the simulation result of the 3D model. The magnetic flux in the end closure is in radial direction, which is perpendicular to the leaking flow. Therefore, under the magnetic field, the MR fluids are confined inside of the cylinder.
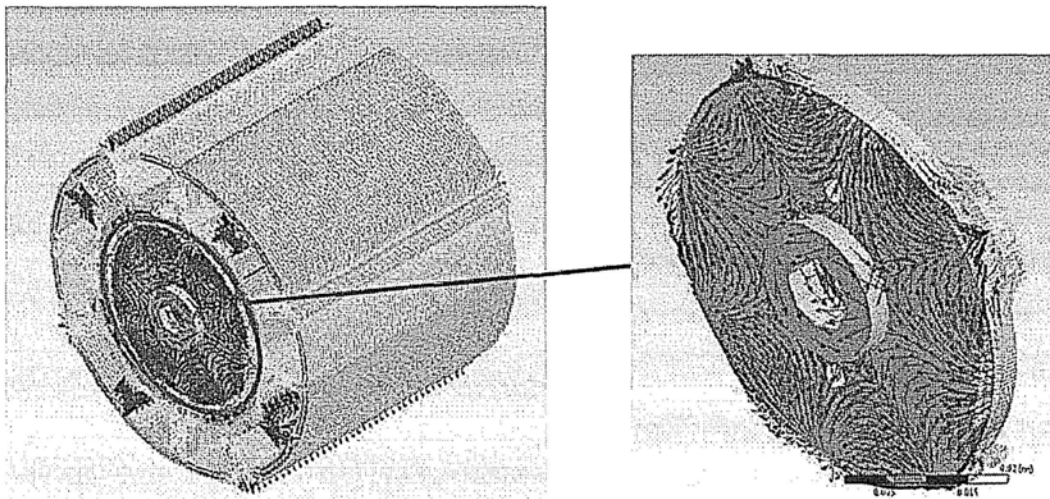
Figure 3.3-4 Sealing analysis of the actuator

For the clutch/brake part with input/output plates, the analysis is similar to the one with inner armature, where FEM is used to model and analyze each of the motor part and the clutch/brake part. 3D models are built to analyze the influence of permanent magnets on MR fluids and the magnetic torque between the stator and the permanent magnets in the motor part. 2D models are built to analyze the electromagnetic flux from the inner coil in MR fluids and the yield stress produced in the clutch/brake part.

Figure 3.3-5 shows the contour plot of the magnetic flux density in motor part when no current applied on outer coil. The torque between the stator and permanent magnets can be calculated based on this flux density distribution. The result of the simulation is about 0.733 Nm. This magnetic interaction torque between stator and permanent magnets can be used to hold rotor statically and then play a role in operating as brake.
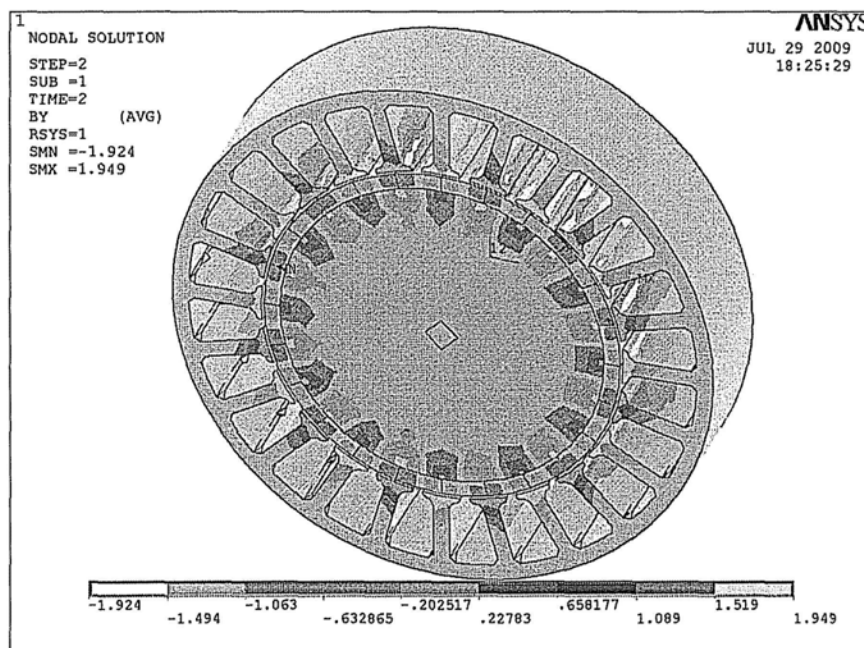
Figure 3.3-5 Contour plot of the magnetic flux density in motor part

3D FEM models is used to analyze whether the flux of permanent magnets get into the MR fluids or not. 3D model with exterior inner coil as shown in Figure 3.3-6 is built. The figure shows the distribution of magnetic flux in the rotor. It can be

observed that the magnetic flux from permanent magnets also does not enter the

inside of the rotor. Therefore, the MR fluids will not be affected by the permanent

magnets in both models.
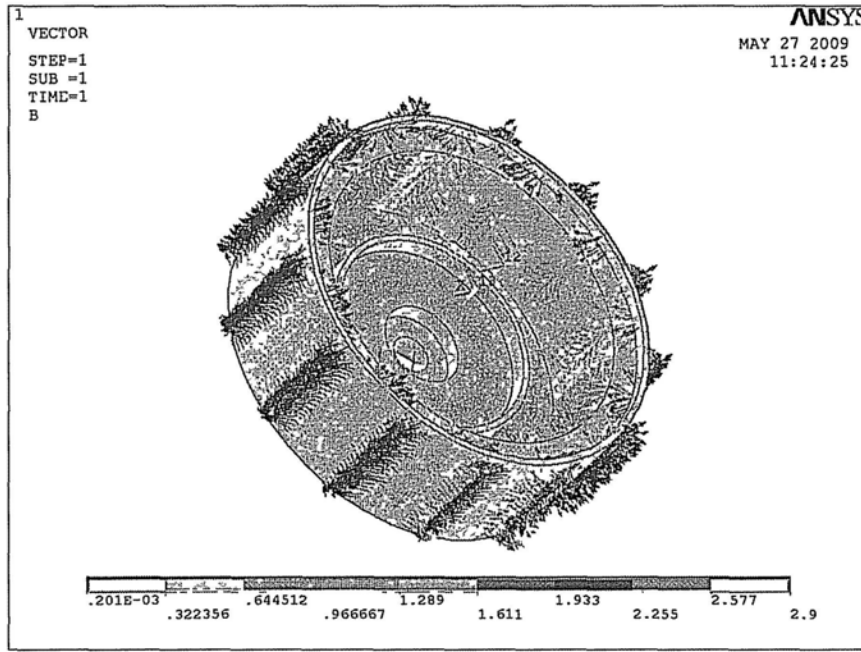
Figure 3.3-6 Magnetic flux in the rotor

Similar to the analysis shown in Figure 3.3.3, the magnetic flux in MR fluids is

analyzed to check whether the flux is perpendicular to the input/output plates so as to

produce the maximum shear stress. As shown in Figure 3.3-7, it can be discovered

that the direction of the magnetic flux in MR fluids are along the normal direction of

the input/output plates with the result that the yield shear stress reaches the maximum

value in both models.

ANSYS 10.0
JUN 10 2009
11:36:04
NODAL SOLUTION
STEP=2
SUB =1
TIME=2
AZ
RSYS=0
SMX =.412E-04
.412E-06
.206E-05
.371E-05
.536E-05
.700E-05
.948E-05
.111E-04
.128E-04
.144E-04
.169E-04
.185E-04
.202E-04
.218E-04
.235E-04
.260E-04
.276E-04
.293E-04
.309E-04
.334E-04
.350E-04
.367E-04
.383E-04
.408E-04

File: FEA_03
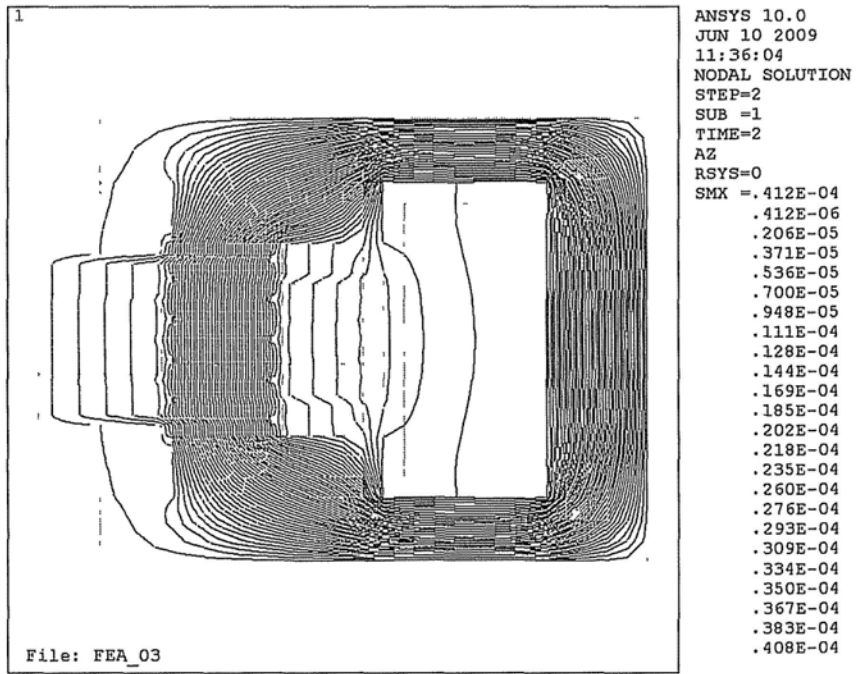
Figure 3.3-7 Magnetic flux in the clutch/brake part

3.4 Fabrication of the Prototypes

Similar to the analysis for two different clutch/brake parts in the former section, two prototypes with inner armature and input/output plates are fabricated, respectively. In order to evaluate torque associated with the number of slots of inner armature, two kinds of inner clutch/brake part are fabricated for comparison, one has eight slots and the other has twelve. Both of them have the identical dimension and contact area. Similar to conventional motors, the stator and inner armature are assembled by pieces of silicon laminates which are fabricated by wire electrical discharge machining method. AWG 40 gauge copper wire is used as the outer and inner coils. The outer coil comprises winding of 10 turns per slot with the resistance of 0.5. Two different inner armatures are fabricated for comparison. The one with eight slots has 70 turns/slot and resistance of 14.2 Ω, named as Inner-I. The other one with twelve slots has 45 turns/slot and resistance of 14.5 Ω, named as Inner-II.

To prevent leakage of MR fluid, the Teflon O-rings are used on the shaft for sealing. Besides O-rings, more means are used to secure the seal. For sealing the hole where MR fluids are injected in, Loctite[®] epoxy is chosen as the sealant and the epoxy is also used to seal the inner armature.

Totally about 3.2 ml MR fluid is filled to the MR actuator and the weight of the MR actuator (filled with MR fluid) is about 2.93 kg. Figure 3.4-1 shows pictures of the first prototype of the multifunctional actuator with Inner-II. Experiments are conducted to investigate the characteristics of prototypes of the actuator.
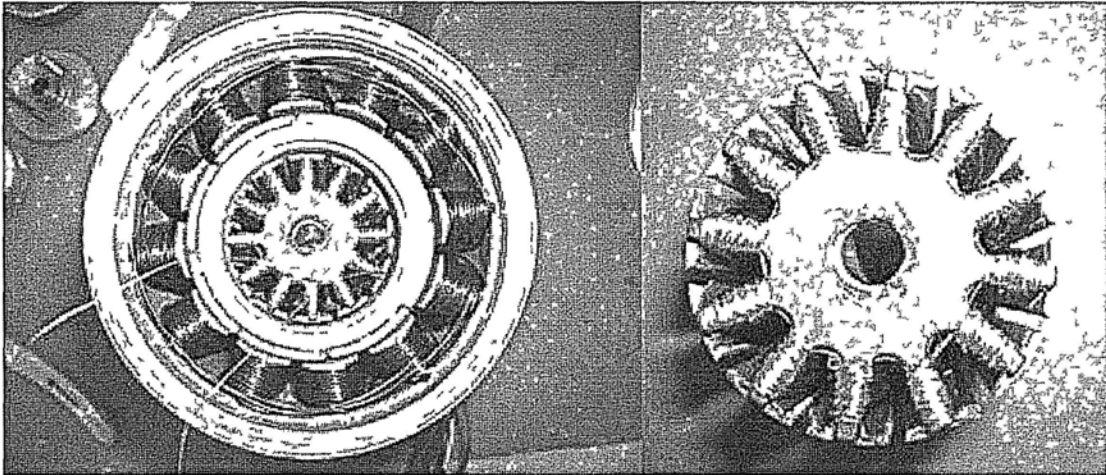
Figure 3.4-1 The first prototype of the actuator with Inner-II

Similarly, for the prototype with input/output plates, the stator is assembled by pieces of silicon laminations which are fabricated by wire electrical discharge machining method. AWG 40 gauge copper wire is used as the outer and inner coils. The outer coil comprises 15 turns winding with the resistance of 10.8 Ω and the windings for exterior inner coils is 350 turns. To prevent leakage of MR fluid, the Teflon O-rings are used on the clutch/brake part for sealing. Figure 3.4-2 shows the parts and assembly of the second prototype.
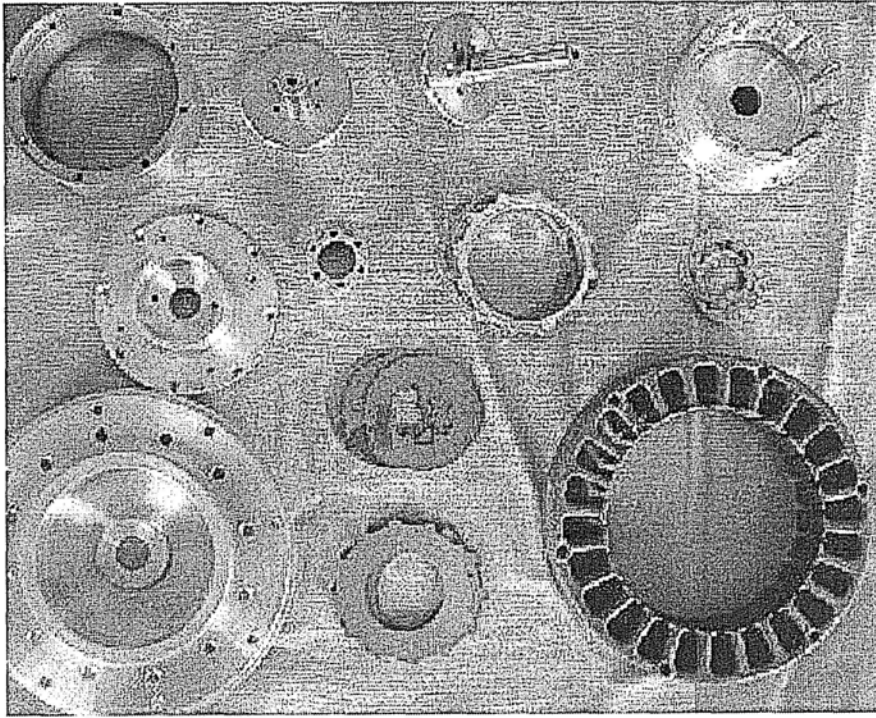
(a) Components of the second prototype
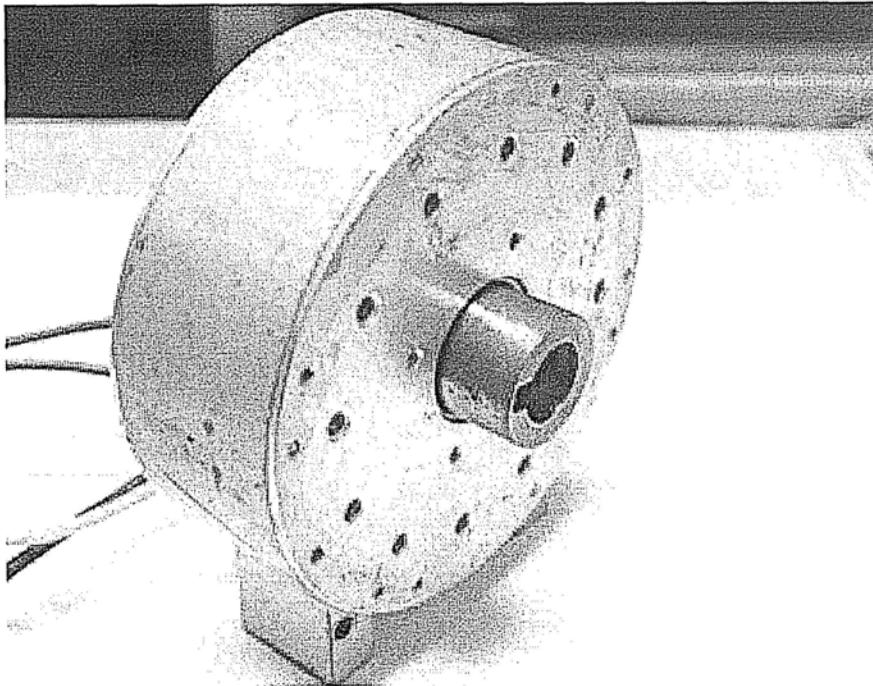
(b) Assembly of the second prototype

Figure 3.4-2 The second prototype of the multifuntional actuator

3.5 Testing of the Prototypes

3.5.1 Testing of the First Prototype

The experimental setup for the first prototype is shown in Figure 3.5-1. The housing of the actuator is fixed while leaving two shafts rotating freely, and the shaft fixed on the inner armature is connected to the torque sensor (Model RST-C4-5-2-A from RSTSensor Inc.) via a coupling. The actuator rotates at a constant speed of 500 rpm while the output torque is measured by the torque sensor under a step input current of 0 - 2 A. The torque signal is conditioned by a signal conditioner (442A101, PCB Piezotronics Inc.), then is acquired by the dSPACE system (DS 1104, dSPACE Inc.), which also commands suitable control voltage signal to the actuator. The dSPACE system allows user to create a control block diagram of the system using the dSPACE Real-Time Interface in Simulink of MATLAB. When the model is built in Simulink, it will be written to the hardware of dSPACE. The hardware of dSPACE includes DS 1104 R&D Controller Board (which is mounted in a PC) and Connector and LED Panel. ControlDesk is a software that can manage and instrument real-time Simulink experiments. In the testing experiments, ControlDesk is used to build the interface that displays the experimental data and input control signals.
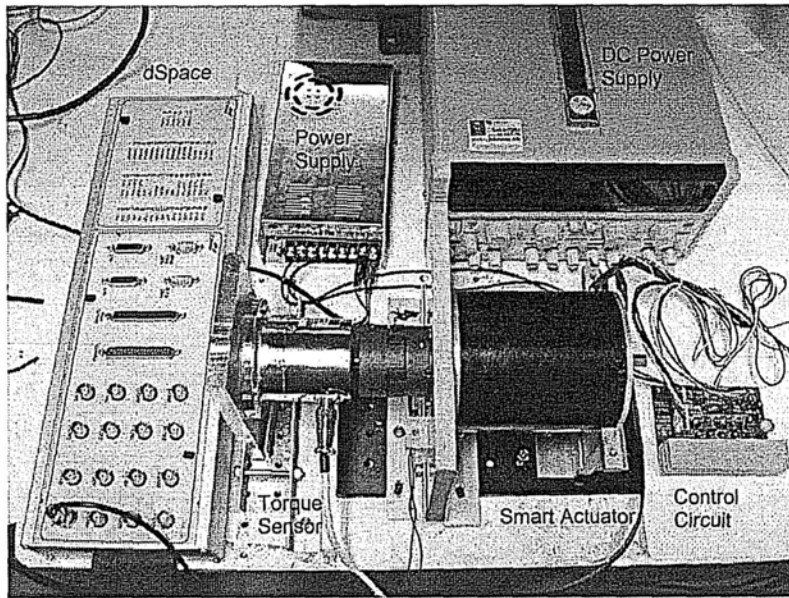
Figure 3.5-1 Experimental setup for testing the first prototype
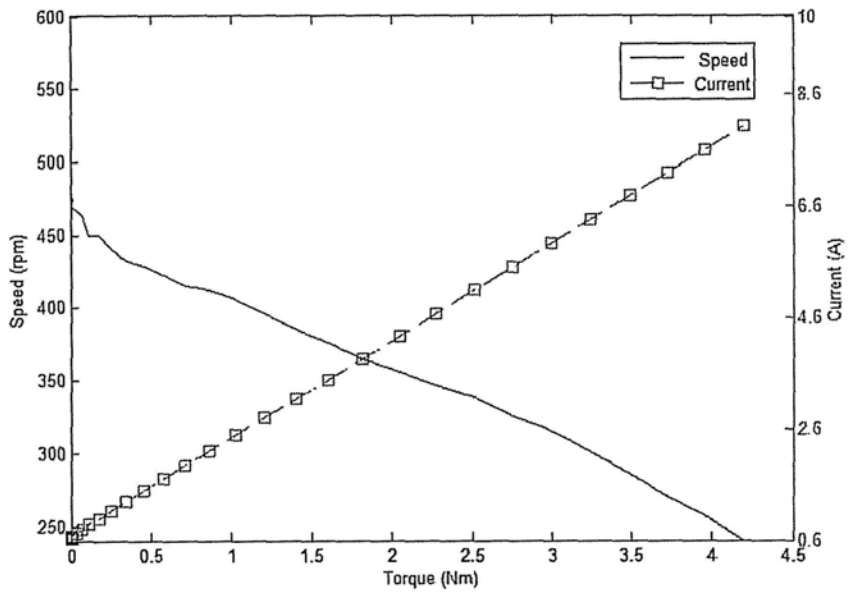
Figure 3.5-2 Torque vs. current and torque vs. speed in motor function of the first prototype
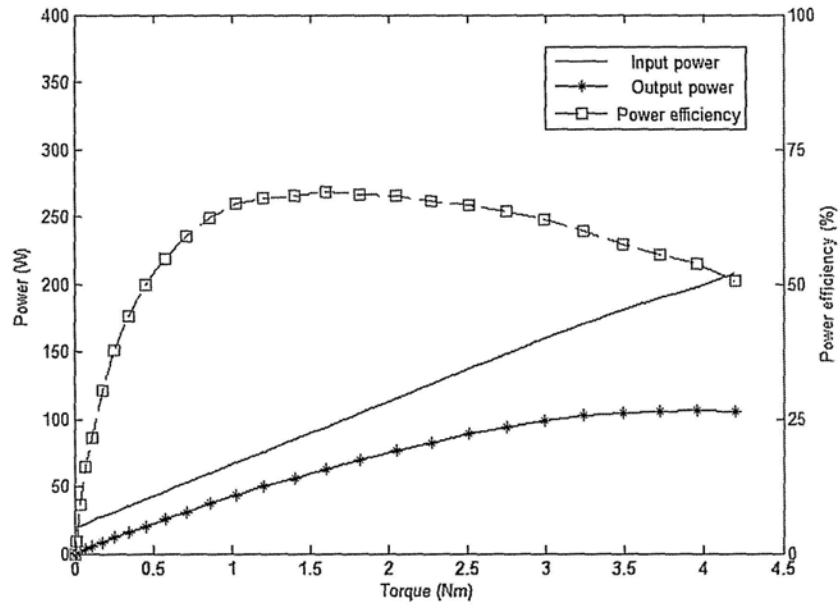
Figure 3.5-3 Input/output power and power efficiency in motor function of the first prototype
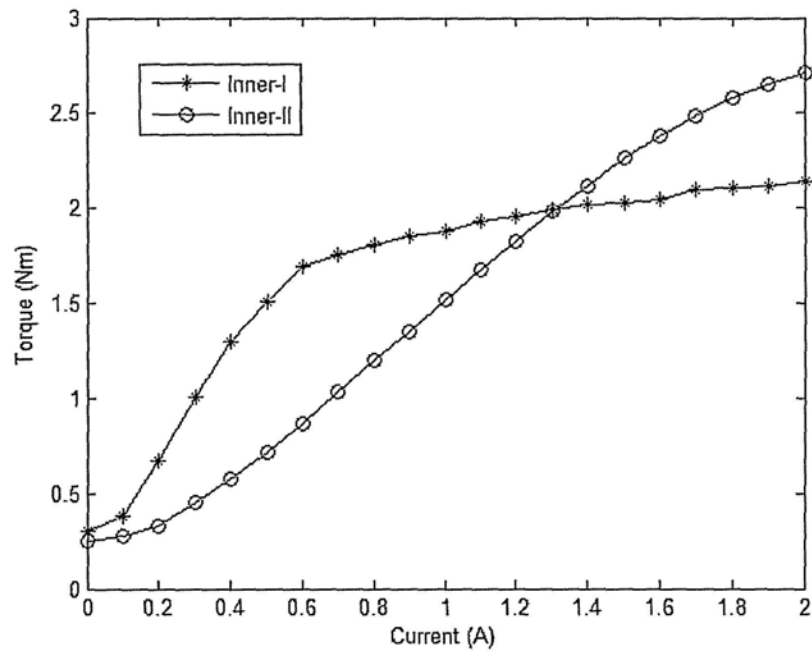
Figure 3.5-4 Torque in brake function for the actuator with two different inner armatures

For motor function, the output torque versus applied stator current, and the output torque versus output speed are the most important characteristics. Figure 3.5-2 and Figure 3.5-3 show the relationship of torque versus applied different currents, torque versus measured speed, and input power, output power and power efficiency.

For brake function, Figure 3.5-4 shows torques versus applied currents produced by the first prototype with Inner-I and Inner-II, respectively. The maximum and minimum values of the torques produced by the first prototype with Inner-I are 2.146 Nm and 0.3 Nm. And it can be found that the torque increases with the increase of the input current. The torques by the prototype with Inner-II has the similar trend as Inner-I with the maximum value of 2.714 Nm and minimum value of 0.25 Nm.

Comparing the torques between the prototype with Inner-I and Inner-II, it can be found that when input current applied to inner armature is smaller than 1.28 A, the torque produced by actuator with Inner-I is larger than that with Inner-II. When the current is larger than 1.28 A, the actuator with Inner-II would produce larger torque than that with Inner-I.

3.5.2   Testing of the Second Prototype

The experimental setup for the second prototype is shown in Figure 3.5-5. Different from the setup for testing the first one, a dynamic torque sensor (Model RST-C4A-30-1-A from RSTSensor Inc.) is utilized to measure the output torque produced by this prototype. The first prototype is adopted as a payload as it could provide controlled output load. By changing the output torque of the payload, for motor function, the output torque versus applied stator current, and the output torque versus output speed then can be investigated. If the output torque of the payload is kept in constant, the rotor is driven by the motor part in a constant speed. Therefore, by changing the current on inner coil, the output torque of the brake function is measured. In this case, if the current in inner coil is input as step signals, the response of the clutch function then is tested. In the experiments, the signals are processed by the dSPACE system (DS 1104, dSPACE Inc.), which also commands suitable control voltage signal to the actuator.

For motor function, the output torque versus applied stator current, and the output torque versus output speed are the most important characteristics. Figure 3.5-6 shows the measured torque at different currents and speeds. The torque/current as well as torque/speed curves are nearly straight lines.
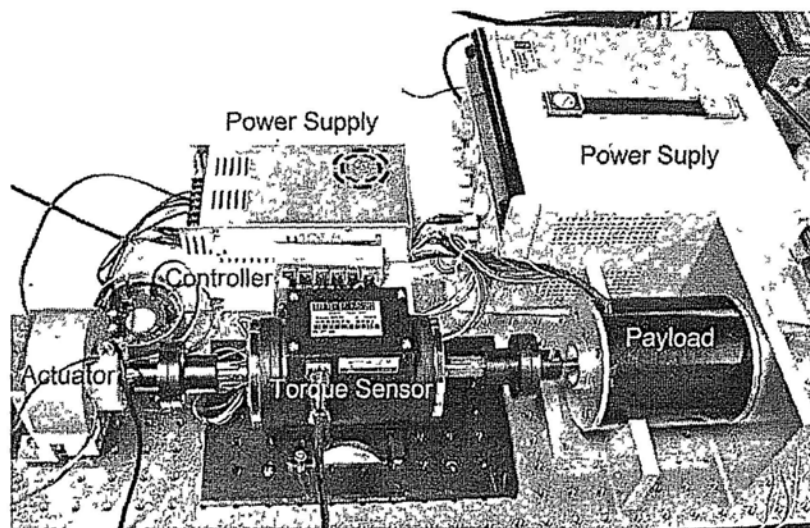
Figure 3.5-5 Experimental setup for testing the second prototype
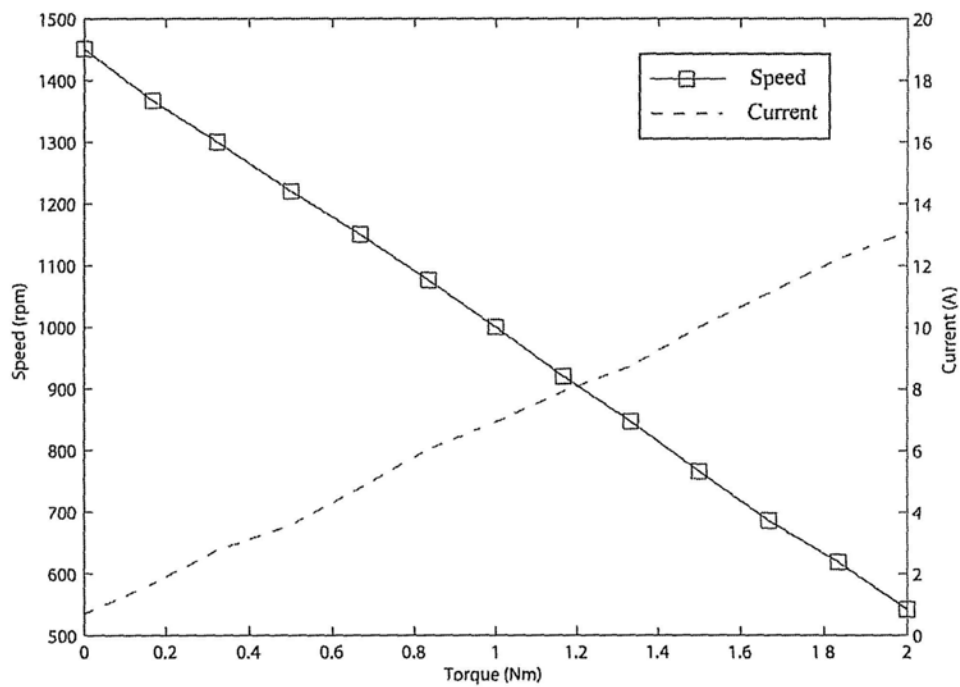
Figure 3.5-6 Torque vs. current and torque vs. speed in motor function of the second prototype
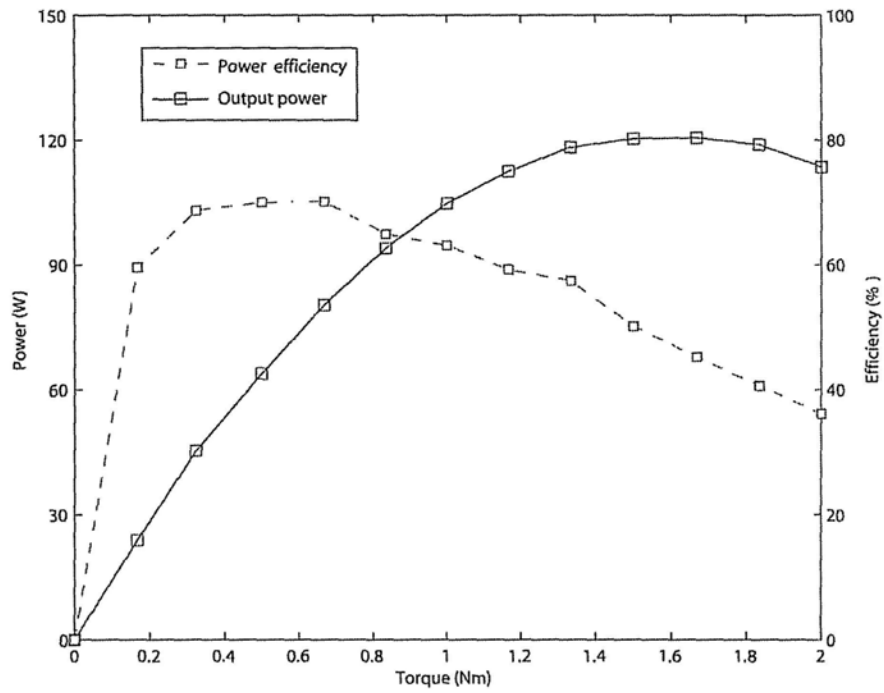
Figure 3.5-7 Output power and power efficiency in motor function of the second prototype
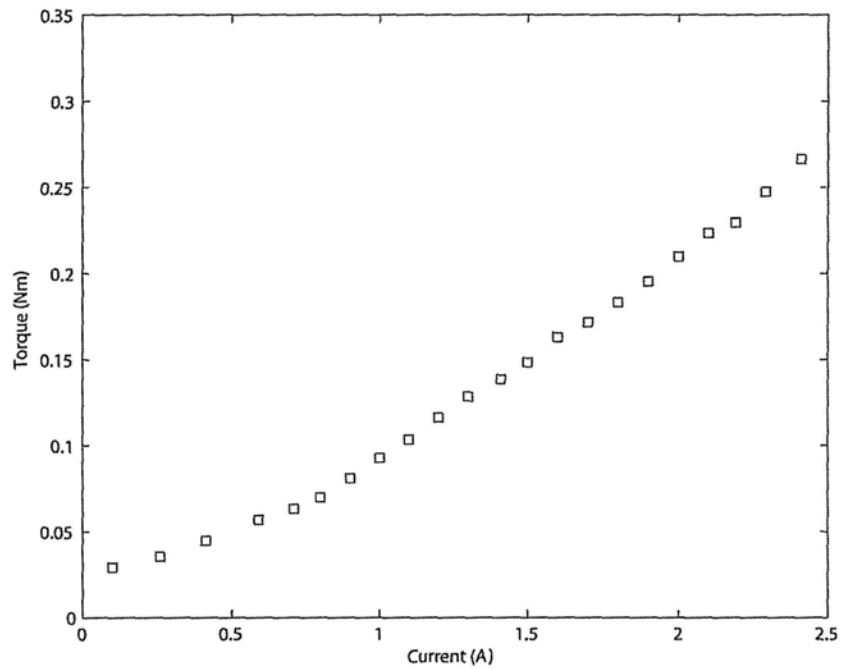
Figure 3.5-8 Measured torque vs. applied current in brake function of the second prototype

For brake function, the torque generated from the clutch/brake part with exterior inner coil is shown in Figure 3.5-8. The relationship between the measured torque and applied current is almost linear. Although the measured output torque is not high, by adding a transmission mechanism such as gearbox or harmonic drive, the torque will be significantly increased while the speed is reduced and therefore it is promising for providing enough torque for assistive knee braces.

For clutch function, the response is investigated. Figure 3.5-9 shows the response of the clutch/brake part under pulse signals. Compared with the reaction time of normal human (0.15 to 0.4 second), the response time of the clutch/brake part is about 0.1 second, so it is capable of providing safety for stopping the torque transfer from the motor to the assistive knee brace in case of emergency.

In order to produce desired electromagnetic field, the length of the inner armature in the first prototype has to be increased with the result that the dimension of the actuator as well as the weight is increased accordingly. The results showed that the first prototype of the multifunctional actuator is promising for assistive knee braces; however, compactness is still an issue. The second prototype that has same multiple functions is more compact than the first one, while the output torque is smaller, accordingly.
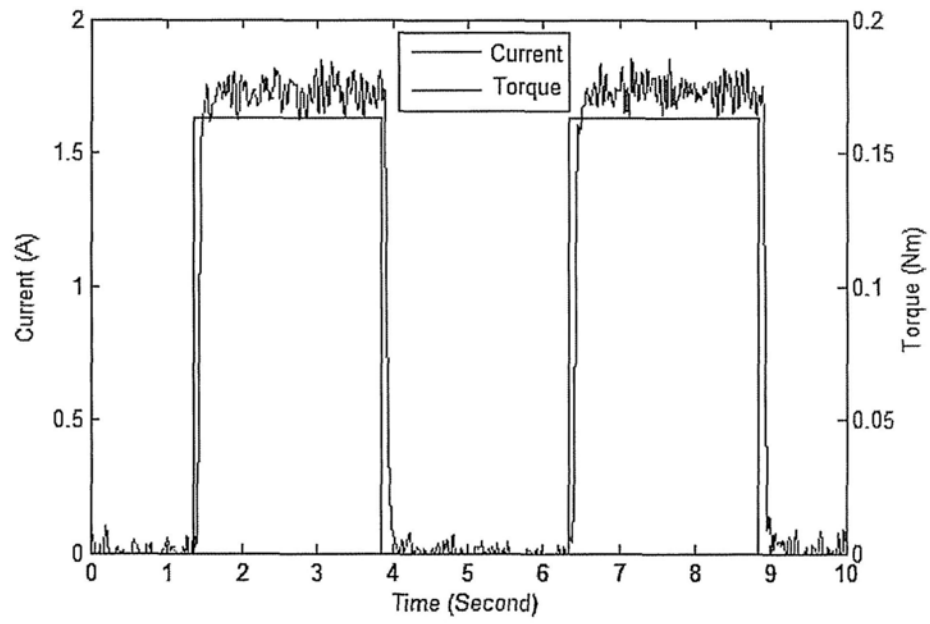
Figure 3.5-9 Response time in clutch function of the second prototype

3.6 Chapter Summary

In this chapter, design details for each motor part and clutch/brake part of the multifunctional actuator are illustrated first. In the design of the clutch/brake part, two different forms, inner armature and input/output plates, are presented and corresponding magnetic circuits are analyzed. Equations on output torque produced from two different clutch/brake parts are derived, respectively. Then, the finite element analysis is introduced. The finite element method is utilized to model and analyze the magnetic circuit, influence of the permanent magnets on MR fluids, magnetic interaction torque, flux distribution, and dynamic sealing of the actuator.

Finally, two prototypes with inner armature and input/output plates are fabricated and tested. Experimental setups are built and described. Each function of the prototypes is investigated. Experimental results show that the torque produced by the clutch/brake part with inner armature is larger than that with input/output plates, which is in form of exterior inner coil. However, the compactness is still an issue. The response time of the actuator is acceptable for application to human body. Though, the measured torques provided by both prototypes are not high, by adding transmission mechanisms, the torque will be increased while the speed is reduced. Therefore, the prototypes are promising to be used in assistive knee braces.

CHAPTER FOUR

OPTIMIZATION OF THE CLUTCH/BRAKE PART

According to the experimental results shown in the previous chapter, the output torque in brake function needs to be increased in order to provide adequate support torque. To investigate the influence of the forms of inner coil on output torque, three simplified clutch/brake models with different configurations of inner coils are built, analyzed, and compared. According to the simulation results, the one with interior inner coil is the best choice. Then, the optimization is carried out to find the optimal value of the geometric parameters. Under the conditions of several constraints, random search method is utilized to solve the optimization problem. To verify the optimized design, finite element method is used to analyze the optimal model. A prototype based on the optimum parameters is fabricated, then its characteristics are investigated and multiple functions are tested as well. The results show that the output torque in brake function produced from the optimized design has been significantly improved.

4.1 Magnetic Circuits Comparison

As illustrated in Section 2.4, the inner coil of the clutch/brake part, which in form of input/output plates, can be classified as interior coil, exterior coil or axial coil as shown in Figure 2.4-3. With various inner coils, the magnetic circuit will be different.
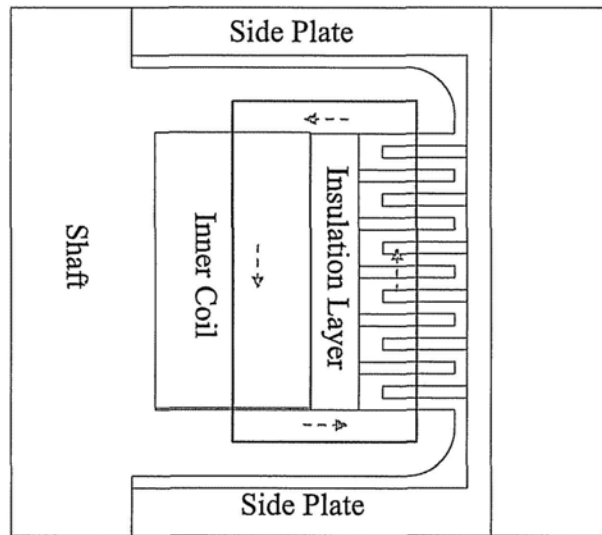
Figure 4.1-1 Magnetic circuit in the clutch/brake part with interior inner coil

Figure 4.1-1 shows the magnetic circuit for the clutch/brake part with interior inner coil. The magnetic circuit is comprised of shaft, inner coil, MR fluids and input/output plates. To confine the electromagnetic flux in the circuit, the materials used in the clutch/brake part should be selected appropriately. The shaft is made of pure iron which has high magnetic permeability. The side plates, insulation ring and spacer rings are all made of non-magnetic materials.
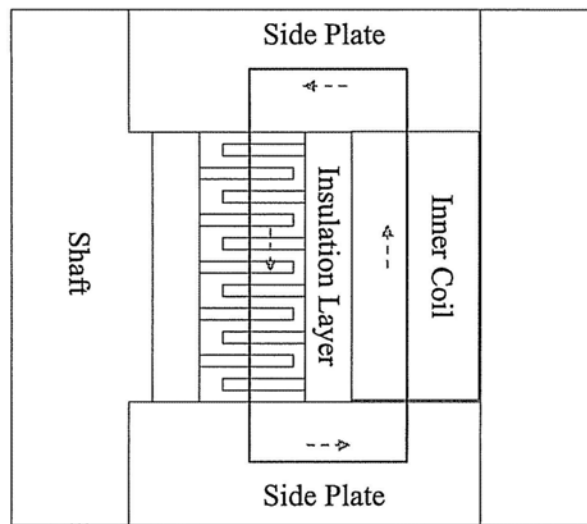
Figure 4.1-2 Magnetic circuit in the clutch/brake part with exterior inner coil
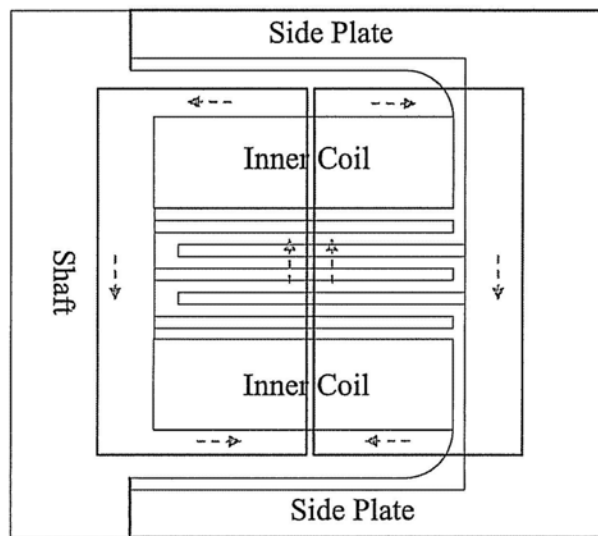
Figure 4.1-3 Magnetic circuit in the clutch/brake part with axial inner coil

Figure 4.1-2 shows the magnetic circuit with exterior inner coil, where the shaft, bobbin and insulation ring are made of non-magnetic materials while side plates are made of pure iron, which make the electromagnetic flux penetrating the MR fluids.

If the inner coil is in form of axial coil as shown in Figure 4.1-3, the coil comprises two sets of axial windings which are in circular pattern around the shaft flanges and each set of the windings provides opposite magnetic directions. To confine the electromagnetic flux in the desired circuit, the shafts with flanges are made of pure iron and housing is made of non-magnetic material.

Although these three basic configurations can all be possibly adopted in designing the clutch/brake part, the electromagnetic flux produced by these magnetic circuits could be much different. To compare the difference, three simplified models in same dimensions are given in Figure 4.1-4, Figure 4.1-5 and Figure 4.1-6, respectively.

The geometry parameters are defined as, L is length, W is width, T is the thickness of the side plate and H is the thickness of the top plate; R is the radius of the shaft, D is the diameter of the coil winding, n_1 and n_2 are turns in axial and radial directions. Here, n_2 is the unknown parameter while n_1 can be obtained by the geometry conditions. The values of these parameters are listed in Table 4.1-1. It is assumed that

the electromagnetic flux passes through the centric line of each circuit member and the section area of side plates are in shape of circles. MR fluids (μ_{mr}), magnetic (μ_{mag}) and non-magnetic (μ_{nmag}) materials are used in the models. Neglect the flux leakage at the corners.

Table 4.1-1 Parameter values in the simplified models

Parameters	Values
L	50
W	30
T	3
H	3
R	5
D	0.4
I	1
μ_{mag}	2000
μ_{mr}	10
μ_{nmag}	1
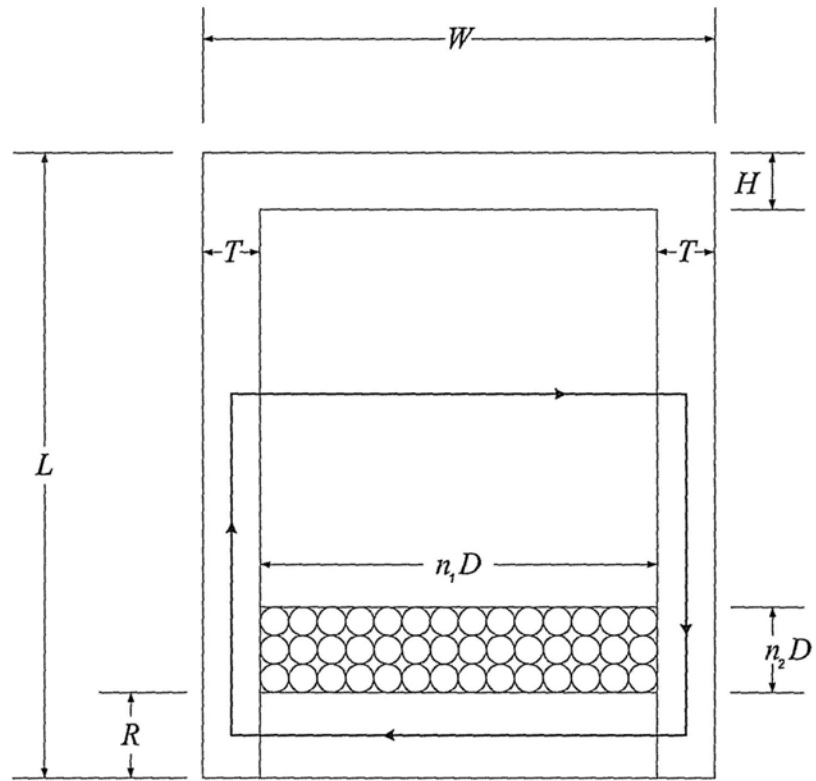
Figure 4.1-4 Simplified model with interior inner coil

According to Equation (3.6), the magnetomotive force provided by interior inner coil can be calculated as follows,

$$F_1 = N_{coil}I = \sum_{i=1}^{j} \Phi_i \frac{l_i}{\mu_i A_i} = \sum_{i=1}^{j} \Phi_i R_i \qquad (4.1)$$

$$N_{coil} = n_1 n_2 \qquad (4.2)$$

$$n_1 = \frac{W - 2T}{D} \qquad (4.3)$$

where R is the magnetic reluctance; μ, l and A are the magnetic permeability and geometry parameters of the circuit components, such as shaft, side plates and MR fluids. The magnetic reluctance of the circuit components can be obtained as

$$R_{shaft} = \frac{W - 2T}{\mu_{mag}\pi R^2} \qquad (4.4)$$

$$R_{sideplates} = \frac{L + n_2 D - H}{\mu_{mag}\pi T^2} \qquad (4.5)$$

$$R_{mr} = \frac{W - 2T}{\mu_{mr}\pi[(L-H)^2 - (R + n_2 D)^2]} \qquad (4.6)$$

Since the magnetic circuit members are connected in series, the magnetic flux is the same in the circuit, let $\Phi = \Phi_i$. Therefore, the overall magnetic reluctance can be obtained as follows

$$R_{overall} = \frac{W - 2T}{\mu_{mag}\pi R^2} + \frac{L + n_2 D - H}{\mu_{mag}\pi T^2} + \frac{W - 2T}{\mu_{mr}\pi[(L-H)^2 - (R + n_2 D)^2]} \qquad (4.7)$$

Based on Equation (4.1), the MMF in this model can be presented as

$$F_1 = \frac{W - 2T}{D} n_2 I = \Phi R_{overall} \qquad (4.8)$$

Similar to Equation (3.17), the torque produced in this simplified model with interior inner coil can be calculated as

$$T_1 = N_{plates} \tau_y A_{mr} R_{arm} \approx N_{plates} K \Phi R_{arm} \qquad (4.9)$$

where N_{plates} is the number of input/output plates, here it can be represented as the thickness of MR fluids (W-$2T$); K is the constant coefficient that simplifies the relationship between the yield stress of MR fluids and the flux density. R_{arm} is the force arm of the output plate which can be obtained as

$$R_{arm} = \frac{L + R + n_2 D - H}{2} \qquad (4.10)$$

As illustrated in Section 2.6, the yield stress of MR fluids is proportional to the magnetic flux density. According to Equation (3.6) and substitute the parameter values listed in Table 4.1-1 into Equation (4.9), therefore, the torque produced in this model can be denoted as

$$T_1 \approx 407203200 K \frac{n_2 (130 + n_2)^2 (n_2 - 105)}{10 n_2^{3} + 1641 n_2^{2} - 101725 n_2 - 25737150} \qquad (4.11)$$
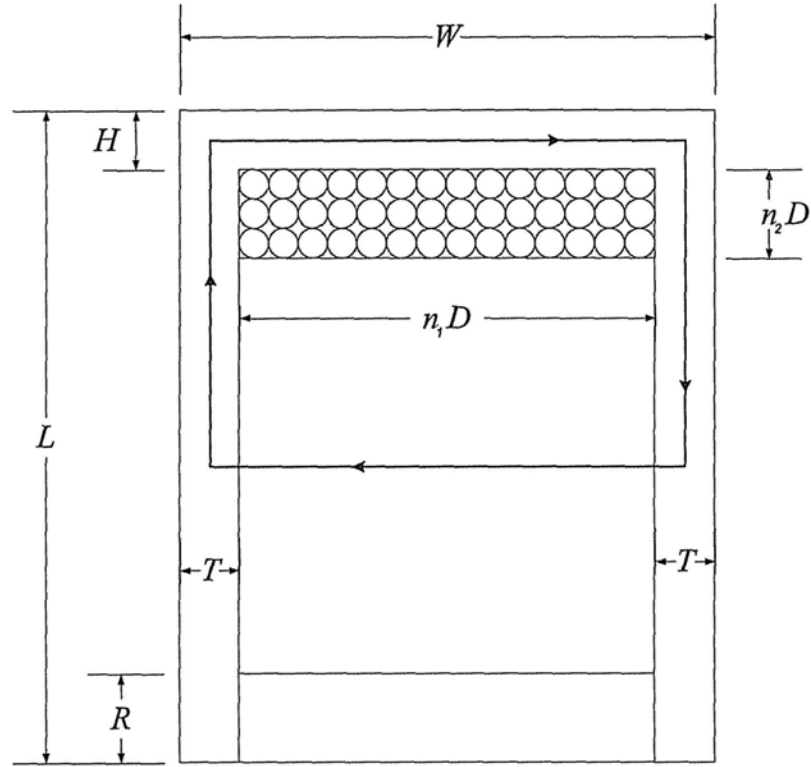
Figure 4.1-5 Simplified model with exterior inner coil

Different from model with interior inner coil, in the model with exterior inner coil as shown in Figure 4.1-5, the magnetic reluctance of the circuit components can be obtained as

$$R_{top} = \frac{W - 2T}{\mu_{mag} \pi H^2} \tag{4.12}$$

$$R_{sides} = \frac{L + n_2 D - R}{\mu_{mag} \pi T^2} \tag{4.13}$$

$$R_{mr} = \frac{W - 2T}{\mu_{mr}\pi[(L - n_2 D - H)^2 - R^2]} \qquad (4.14)$$

Therefore, the overall magnetic reluctance can be obtained as follows

$$R_{overall} = \frac{W - 2T}{\mu_{mag}\pi H^2} + \frac{L + n_2 D - R}{\mu_{mag}\pi T^2} + \frac{W - 2T}{\mu_{mr}\pi[(L - n_2 D - H)^2 - R^2]} \qquad (4.15)$$

The force arm in this model is also different from that of the last model, and it can be denoted as

$$R_{arm} = \frac{L + R - n_2 D - H}{2} \qquad (4.16)$$

Using similar derivation process in the last model and substituting parameter values into the equations, the torque produced in this model can be derived as

$$T_2 \approx -81440640K \frac{n_2(n_2 - 130)^2(n_2 - 105)}{2n_2^3 - 125n_2^2 - 53775n_2 + 6059250} \qquad (4.17)$$

As the n_2 cannot be increased infinitely, it is confined as follows,

$$n_2 \leq \frac{L - R - H}{D} = 105 \qquad (4.18)$$
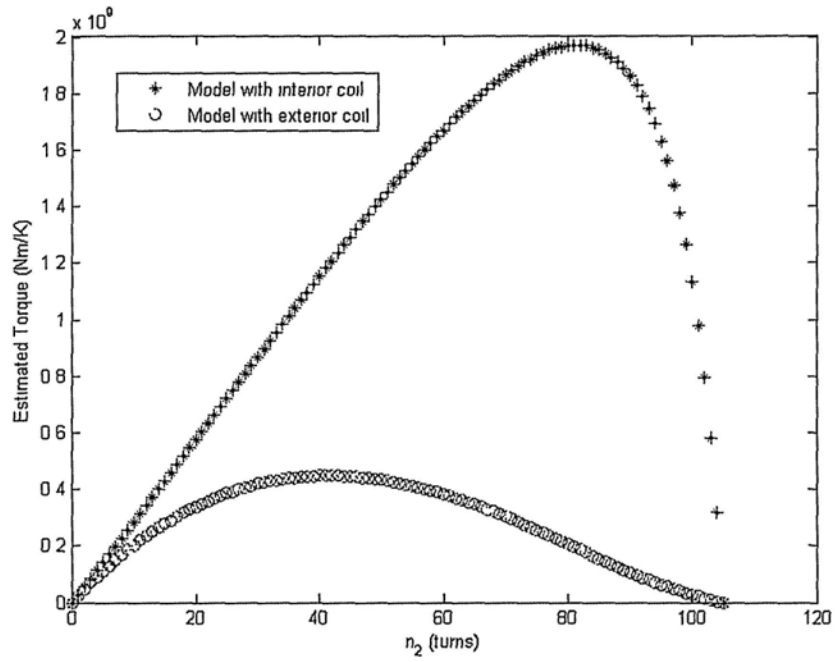
Figure 4.1-6 Torque comparison of the models with interior and exterior inner coil

Figure 4.1-6 shows the comparison of the estimated torque produced from two models.

It can be found that with the same dimension, the torque produced from the model

with interior inner coil is much larger than that from the model with exterior inner
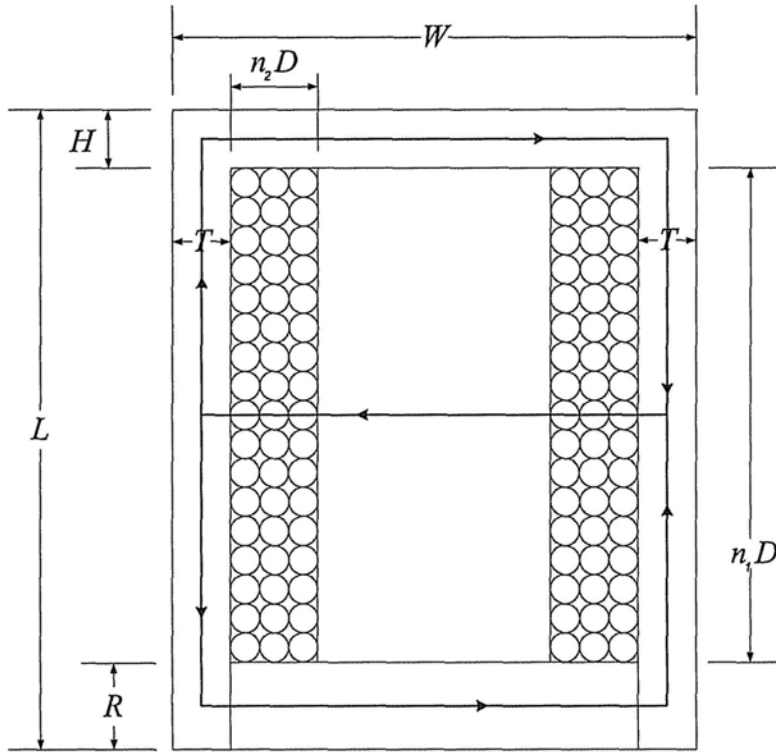
coil.

Figure 4.1-7 Simplified model with axial inner coil

For the model with axial inner coil, the magnetic circuit is different from the above two models. To confine the magnetic flux in MR fluids, the materials used in shaft, and top plate are non-magnetic materials. The definition of n_1 and n_2 are exchanged, where n_2 is the turns in axial direction while n_1 is the turns in radial directions, leaving n_2 to be the unknown parameter. As shown in Figure 4.1-7, the magnetic reluctance of the circuit components can be obtained as

$$R_{shaft} = \frac{W - 2T}{\mu_{nmag} \pi R^2} \tag{4.19}$$

$$R_{top} = \frac{W - 2T}{\mu_{nmag}\pi H^2} \tag{4.20}$$

$$R_{side1} = \frac{L - H}{\mu_{mag}\pi T^2} \tag{4.21}$$

$$R_{side2} = \frac{L - R}{\mu_{mag}\pi T^2} \tag{4.22}$$

$$R_{mr} = \frac{W - 2T - 2n_2 D}{\mu_{mr}\pi[(L - H)^2 - (L - R)^2]} \tag{4.23}$$

As the magnetic circuit is connected in parallel, hence the overall magnetic reluctance can be calculated as

$$R_{overall} = \frac{1}{\dfrac{1}{(R_{shaft} + R_{sideplates1} + R_{mr})} + \dfrac{1}{(R_{topplate} + R_{sideplates2} + R_{mr})}} \tag{4.24}$$

The MMF in this model can be presented as

$$F_3 = \frac{2(L - R - H)}{D} n_2 I = \Phi R_{overall} \tag{4.25}$$

The number of input/output plates is represented as the thickness of MR fluids (W-$2T$-$2n_2D$) and the force arm in this model is also different from the above two models, and it can be denoted as

$$R_{arm} = \frac{L - H + R}{2} \qquad (4.26)$$

Using similar derivation process in the last model and substituting parameter values into the equations, the torque produced in this model with axial inner coil can be obtained as

$$T_3 \approx 7821559066K \frac{n_2(n_2 - 30)(80n_2 - 803207)}{(160n_2 - 853823)(32n_2 - 471801)} \qquad (4.27)$$

As the n_2 has its limitations which can be calculated by the following equation

$$n_2 \leq \frac{W - 2T}{2D} = 30 \qquad (4.28)$$

Figure 4.1-8 shows the estimated torque produced from this model with axial inner coil. From the figure, it can be found the torque it produced is much less than those from the above two models. Therefore, in this research, the axial inner coil design is

eliminated from the options. To improve the output torque of the clutch/brake part,

the configuration of interior inner coil is the best selection.
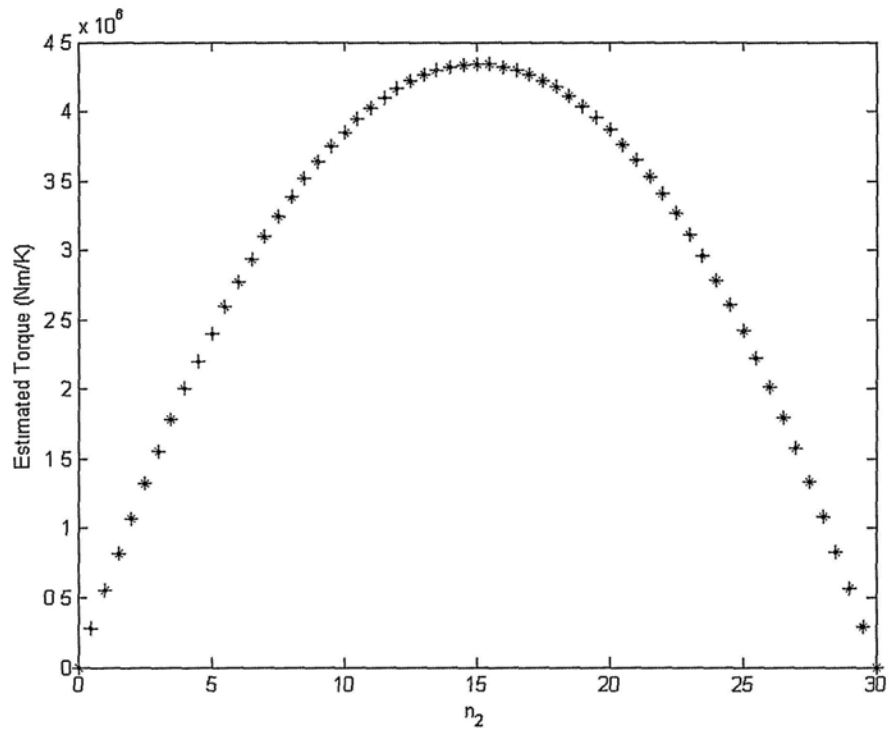
Figure 4.1-8 Estimated torque produced by model with axial inner coil

4.2 Design Optimization

As illustrated in the former section, the clutch/brake part with interior inner coil is the best choice for providing the maximum torque. The model in Figure 4.1-4 is a simplified one. Figure 4.2-1 shows a schematic graph of the magnetic circuit in this design. In order to optimize the magnetic circuit and get optimum values of the radius of the shaft core and the turns of the inner coil, the saturation of pure iron. According to *B-H* curves in Figure 2.6-4, the saturated flux density of pure iron is about 1.8 T. in Figures 2.6-2 and 2.6-3, the yield stress of MR fluids will saturate when the external field is larger than 300 kA/m, where the flux density is around 1 T.
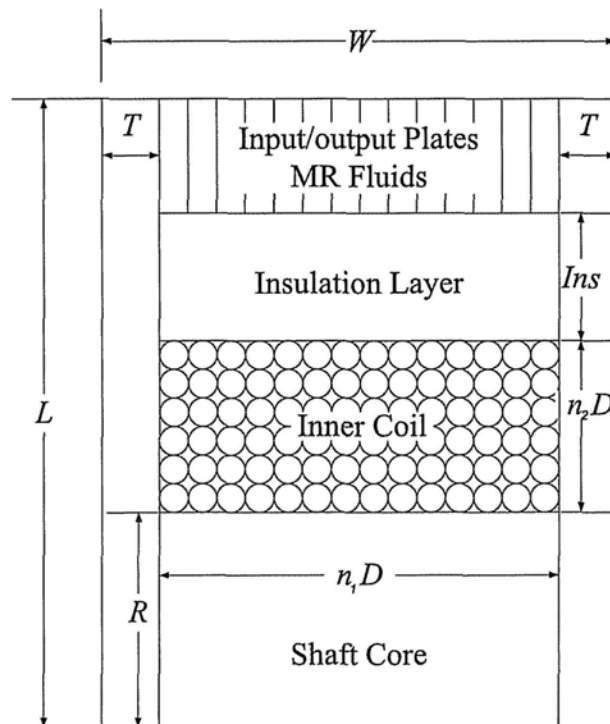
Figure 4.2-1 Geometry of the clutch/brake part for design optimization

In the magnetic circuit, the flux density will not always increase with the coil current.

When one circuit component is saturated, the flux density will not be increased further.

Hence, the actual maximum magnetic flux is

$$\phi_{max} = \min(B_{shaft}A_{shaft}, B_{sideplate}A_{sideplate}, B_{clutchplate}A_{clutchplate}B_{mr}A_{mr}) \qquad (4.29)$$

where B, A are saturated flux density and cross-sectional area of different circuit

components, respectively.

Table 4.2-1 Parameter values in the design

Parameter	Description	Lower limit	Upper limit
L	Radius of the inner clutch/brake part	-	25
W	Width of the inner clutch/brake part	-	18
T	Thickness of the side plates	2	4
Ins	Thickness of the insulation layer	3	5
R	Radius of the shaft	2	10
D	Diameter of the wire	-	0.4
n_1	Turns of the inner coil in axial direction	-	$(W-2T)/D$
n_2	Turns of the inner coil in radial direction	10	-
N_{coil}	Total turns of the inner coil	-	$n_1 \times n_2$
N_{plates}	The thickness of MR fluids	-	$W-2T$
μ_{mag}	Permeability of the magnetic materials	-	~2000
μ_{mr}	Permeability of the MR fluids	-	~10

Therefore, considering the both limits and geometric constraints (shown in Table 4.2-1), the optimization problem of the inner clutch/brake part can be expressed as

Maximize: $\qquad\qquad\qquad T_{inner}(R, n_2, T, Ins)$ $\qquad\qquad$ (4.30)

Subject to: $\qquad\qquad\qquad B_{MRF} = 1T$ when $B_{iron} = 1.8T$ $\qquad\qquad$ (4.31)

$\qquad\qquad 2 \le T \le 4, \; 3 \le Ins \le 5, \; 2 \le R \le 10 \; \text{and} \; 10 \le n_2 \le 12$ $\qquad$ (4.32)

According to the saturation constraints, the relationship between the turns of the coil in radial direction and the radius of the shaft can be represented as

$$n_2 = \frac{\sqrt{L^2 - 1.8R^2} - R - Ins}{D}$$ $\qquad\qquad$ (4.33)

Regarding the geometry constraints, the other parameters can be obtained as

$$R_{shaft} = \frac{W - 2T}{\mu_{mag}\pi R^2}$$ $\qquad\qquad$ (4.34)

$$R_{sideplates} = \frac{L + n_2 D + Ins}{\mu_{mag}\pi T^2}$$ $\qquad\qquad$ (4.35)

$$R_{mr} = \frac{W - 2T}{\mu_{mr}\pi[L^2 - (R + n_2 D + Ins)^2]} \quad (4.36)$$

$$R_{overall} = \frac{W - 2T}{\mu_{mag}\pi R^2} + \frac{L + n_2 D + Ins}{\mu_{mag}\pi T^2} + \frac{W - 2T}{\mu_{mr}\pi[L^2 - (R + n_2 D + Ins)^2]} \quad (4.37)$$

$$R_{arm} = \frac{L + R + n_2 D + Ins}{2} \quad (4.38)$$

$$T_{inner} = N_{coil}\tau_y A_{mr} R_{arm} \quad (4.39)$$

Substitute Equation (4.33) to Equations (4.38) into Equation (4.39), the optimization problem can be rewritten as

Maximize:

$$T_{inner}(R, T, Ins)$$
$$= \frac{45000\pi(T - 9)^2 R^2 T^2\left(5R + 5Ins - \sqrt{15625 - 45R^2}\right)\left(125 + \sqrt{15625 - 45R^2}\right)}{-90810T^2 + 10090T^3 - 1125R^2 - 9R^2\sqrt{15625 - 45R^2} + 45R^3} \quad (4.40)$$

Subject to: $2 \le T \le 4$, $3 \le Ins \le 5$ and $2 \le R \le 10$ (4.41)

Therefore, this is a problem of single objective optimization. Random search method

- 99 -

is used to find out the maximum torque produced by the clutch/brake part with

interior inner coil. Figure 4.2-2 shows the optimization process.
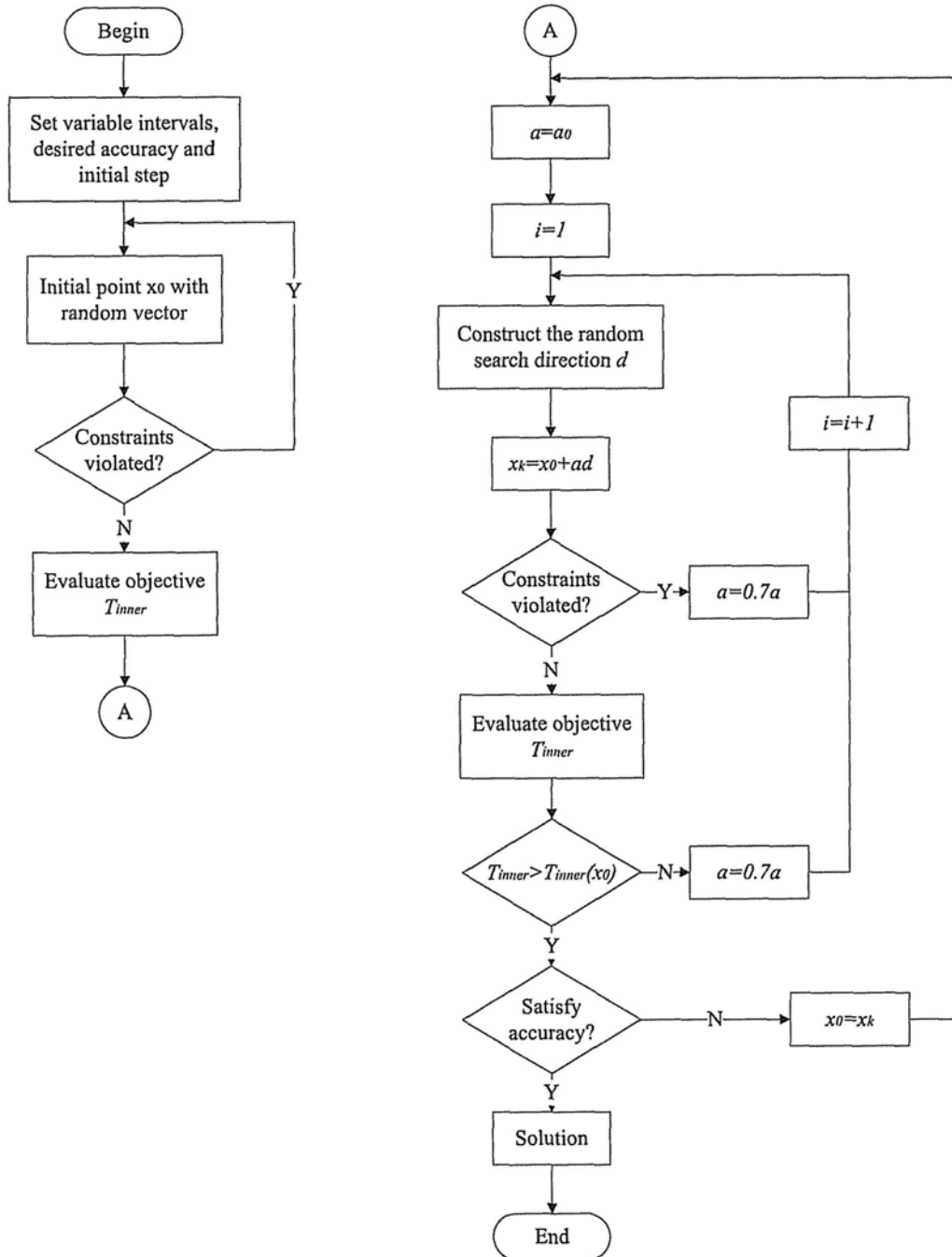
Figure 4.2-2 Random search process for the design optimization
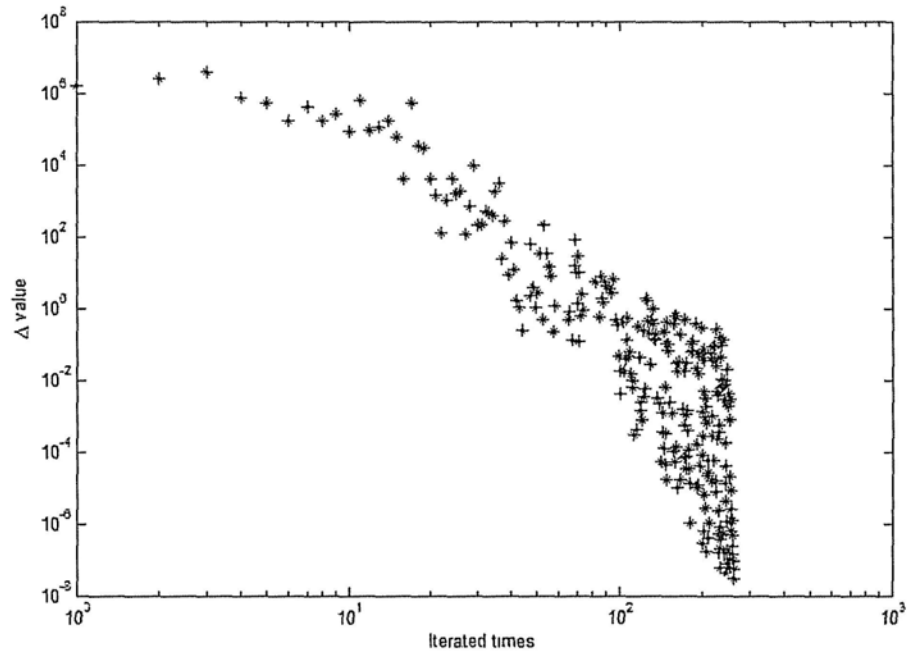
Figure 4.2-3 Convergence of the design optimization

Table 4.2-2 Optimized parameter in design of clutch/brake part

Parameter	Description	Optimized value
L	Radius of the inner clutch/brake part	25
W	Width of the inner clutch/brake part	18
T	Thickness of the side plates	2.53
Ins	Thickness of the insulation layer	3
R	Radius of the shaft	8.79
D	Diameter of the wire	0.4
n_1	Turns of the inner coil in axial direction	32
n_2	Turns of the inner coil in radial direction	25

The convergence criterion is that the difference between the values of the objective function in two steps is smaller than 10^{-8}. If the function value is smaller than that in the previous step, and the constraint function is met, meanwhile the convergence criterion is satisfied, the value is then the optimized result. Figure 4.2-3 shows the convergence of the results. It can be found that the difference of the function values converges rapidly. After iterations, the results of the optimization are listed in Table 4.2-2.

In order to verify the optimized design, finite element method is utilized to analyze the model which is built according to the optimal parameters. Figure 4.2-3 shows the magnetic flux in MR fluid. It can be observed that the flux is perpendicular to the input/output plates, which means the yield shear torque therefore reaches the maximum value. Figure 4.2-4 shows the contour of the flux density. From the figure, it can be found the flux density in shaft reaches saturation with around 1.8 T while the flux density in MR fluids is about 1 T, which meets the target in this design.

```
1                                ANSYS 11.0
                                 JUN 14 2010
                                 21:46:13
                                 NODAL SOLUTION
                                 STEP=2
                                 SUB =1
                                 TIME=2
                                 AZ
                                 RSYS=0
                                 SMX =.463E-04
                                      .772E-06
                                      .232E-05
                                      .386E-05
                                      .695E-05
                                      .849E-05
                                      .100E-04
                                      .131E-04
                                      .147E-04
                                      .178E-04
                                      .193E-04
                                      .208E-04
                                      .239E-04
                                      .255E-04
                                      .270E-04
                                      .301E-04
                                      .316E-04
                                      .347E-04
                                      .363E-04
                                      .378E-04
                                      .409E-04
                                      .424E-04
                                      .455E-04
File: OptimizationAnalysis
```
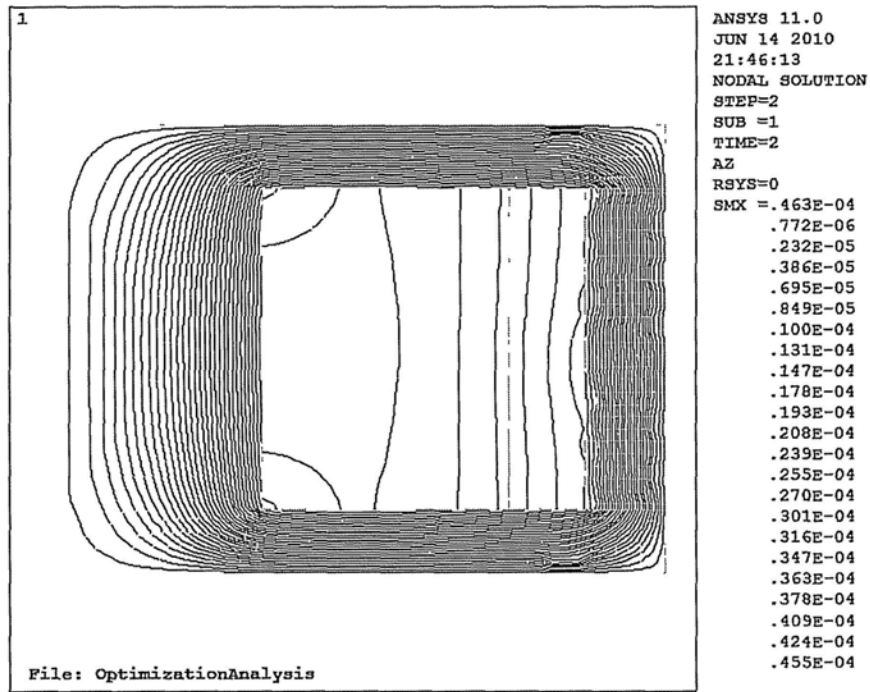
Figure 4.2-4 Magnetic flux distribution in the optimized model


```
1                                ANSYS 11.0
                                 JUN 14 2010
                                 21:47:28
                                 NODAL SOLUTION
                                 STEP=2
                                 SUB =1
                                 TIME=2
                                 BSUM      (AVG)
                                 RSYS=0
                                 PowerGraphics
                                 EFACET=1
                                 AVRES=Mat
                                 SMX =2.003
                                        0
                                        .222535
                                        .445071
                                        .667606
                                        .890142
                                        1.113
                                        1.335
                                        1.558
                                        1.78
                                        2.003
File: OptimizationAnalysis
```
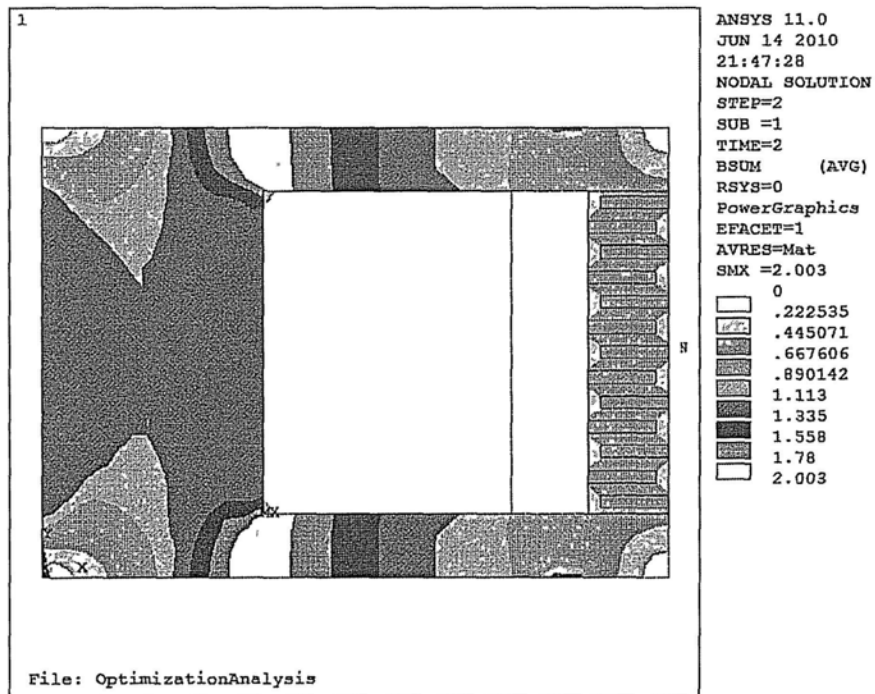
Figure 4.2-5 Flux density in the optimized model

4.3 Prototype of the Optimized Design

A prototype is fabricated according to the optimized design. Experiments are conducted to investigate the torque in brake function.
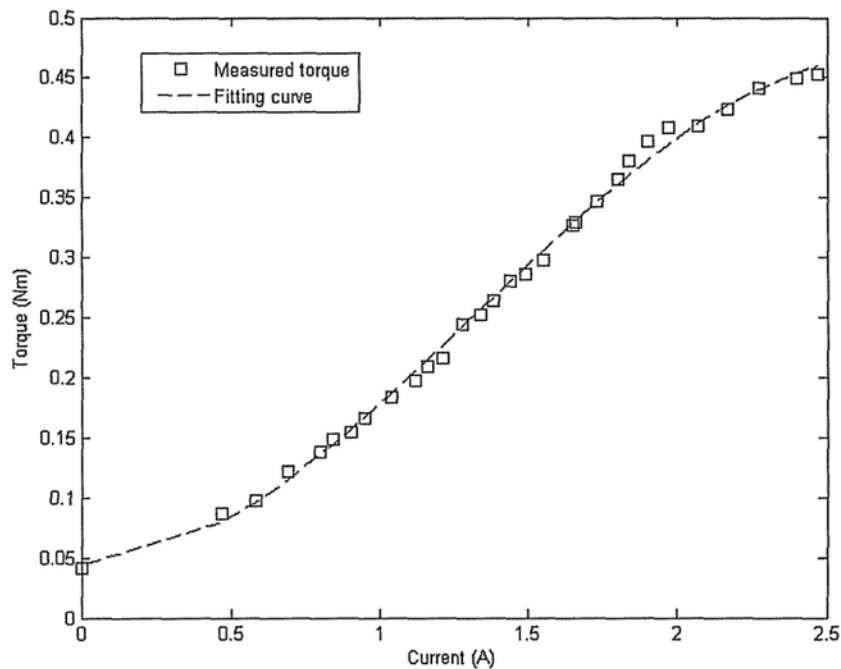
Figure 4.3-1 Measured torque versus applied current in brake function of the optimized prototype

Figure 4.3-1 shows the relationship between the measured torque and applied current. The rotor is rotated at the speed of 600 rpm and step current is applied on the inner coil gradually. With the current augments from 0 A to 2.5 A, the measured torque increases linearly until reach the maximum value 0.48 Nm, when the yield torque produced by clutch/brake part is larger than the interactive magnetic torque between

the stator and permanent magnets. Compared with the result shown in Figure 3.5-8, it can be found that with the same dimension the torque produced by the clutch/brake part with interior inner coil is nearly two times larger than that with exterior inner coil. Although it is not adequate for being applied to human body directly, it is promising to be used in assistive knee braces with transmission mechanism.

From the figure, it can be found in the range of 0.5 A to 2.5 A, the output torque is approximately linear with respect to the applied current. Therefore, the model of the brake function can be expressed as the first order single-input single-output linear plant as follows

$$P(s) = \frac{T(s)}{I(s)} = \frac{K}{Ts+1} \tag{4.42}$$

To verify the linearity, the output torques under currents with different frequency are measured. The applied current is

$$I = 1.5 + \sin(\omega t), \quad \omega = 1, 2, 4, 8, 10, 20, 40, 60, 80, 100 \tag{4.43}$$

Figure 4.3-2 shows the gain between the output torque and applied current, versus frequency. It can be found that the amplitude of torque output decreases with the

increase of the current frequency. With curve fitting, the plant parameters can be

obtained as $K = 0.1789$, $T = 5.5991 \times 10^{-4}$. It can be found that the curve well matches

the equation of the first order linear plant. Therefore, the brake function can be

modeled as a first order linear model in this research.
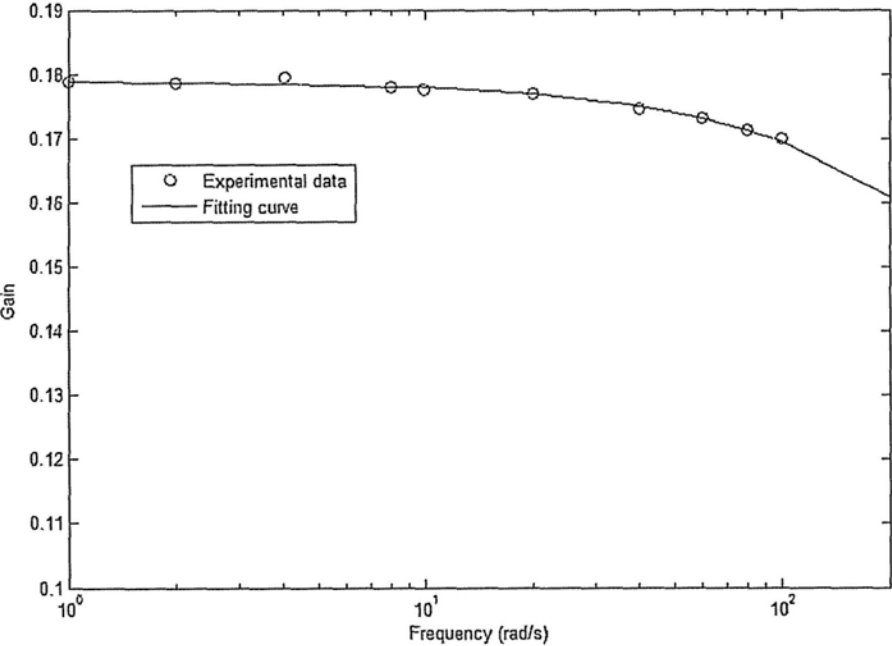
Figure 4.3-2 Curve fitting of gain vs. frequency

4.4 Chapter Summary

This chapter gives the analysis and comparison of three simplified clutch/brake models with different forms of inner coils. According to the simulation, the model with interior inner coil produces the maximal torque and it is the best option for clutch/brake part design. Then, an optimization problem is presented with several design constraints. Random search method is utilized to solve the problem and the optimal values of the design parameters are obtained. Finite element method is used to analyze the optimal model. It is found that the optimization model meets the design constraints and reaches the optimal value of yield torque. The prototype according to the optimization is fabricated and its characteristics are investigated. The measured maximum output torque reaches 0.48 Nm. It is shown that the optimized design almost doubles the torque of the brake function, as compared to that without optimization.

CHAPTER FIVE

MODELING AND CONTROL OF THE ACTUATOR

In this chapter, to control the multifunctional actuator in assistive knee braces, the modeling of the actuator is developed. As the actuator has multiple functions, the models are built for each function. The modeling can be divided into two models, motor function and brake function, while the modeling of the clutch function is the combination of these two models. With the built models of the actuator, experiments on system identification are conducted to determine the values of the parameters in the modeling. Because the coefficients in brake function may vary with time or environmental changes, so the accurate values of these parameters are difficult to determine. Therefore, adaptive control method is used to identify the parameters and control the actuator. From experimental results, it can be found that the control method works well for torque tracking and speed tracking.

5.1 Modeling of the Actuator

As the actuator has multiple functions, the modeling of the actuator would be illustrated in different functions. For motor function, the model is similar to the conventional DC motor. Equation (5.1) to Equation (5.4) are used for the dynamic model of the motor function.

$$V_M = R_M I_M + L_M \frac{dI_M}{dt} + E \tag{5.1}$$

$$E = K_e \omega \tag{5.2}$$

$$T_M = K_t I_M \tag{5.3}$$

$$T_M = J_M \frac{d\omega}{dt} + D\omega + T_L \tag{5.4}$$

where V_M is the supply voltage on outer coil, R_M is the resistance of outer coil, I_M is the current, L_M is the inductance, E is the back-EMF and ω is the angular velocity; T_M is the motor torque, J_M is the moment of inertia, T_L is the load torque including the external load and the friction torque, and D is the viscous damping coefficient; K_e and

K_t are EMF constant and torque constant, respectively. The model of the motor

function then can be expressed in form of state-space as follows

$$\begin{cases} \dot{x} = Ax + Bu \\ y = Cx + Du \end{cases}$$

where
$$A = \begin{bmatrix} -\dfrac{D}{J_M} & \dfrac{K_t}{J_M} \\ -\dfrac{K_e}{L_M} & -\dfrac{R_M}{L_M} \end{bmatrix}; \quad B = \begin{bmatrix} -\dfrac{1}{J_M} & 0 \\ 0 & \dfrac{1}{L_M} \end{bmatrix}; \quad C = \begin{bmatrix} 1 & 0 \end{bmatrix}; \quad D = \begin{bmatrix} 0 \\ 0 \end{bmatrix}$$

$$x = \begin{bmatrix} \omega \\ I_M \end{bmatrix}; \quad y = \omega; \quad u = \begin{bmatrix} T_L \\ V_M \end{bmatrix} \tag{5.5}$$

For brake function where the motor function is off, the model can be derived

according to the properties of MR fluids. According to the properties of MR fluid and

its relationship between the flux density and the yield shear stress, the brake torque

can be represented as

$$T_B = K_H I_{mr} + K_\omega \omega \tag{5.6}$$

where K_H is the coefficient due to the electromagnetic field and K_ω is the coefficient

relating the viscosity. According to the equations illustrated in former chapters, these

two coefficients are non-linear.

The dynamic equation for brake function can be expressed as follows

$$T_L - T_B = J_L \frac{d\omega}{dt} \qquad (5.7)$$

where J_L is the equivalent moment of inertia of the load. The model of the brake

function then can be derived in form of state-space as

$$\begin{cases} \dot{x} = Ax + Bu \\ y = Cx + Du \end{cases}$$

where $\quad A = \begin{bmatrix} -\dfrac{K_\omega}{J_L} & 0 \\ 0 & 0 \end{bmatrix}; \quad B = \begin{bmatrix} \dfrac{1}{J_L} & -\dfrac{K_H}{J_L} \\ 0 & 0 \end{bmatrix}; \quad C = \begin{bmatrix} 0 & -\dfrac{1}{K_\omega} \end{bmatrix}; \quad D = \begin{bmatrix} 0 & -K_H \end{bmatrix};$

$$x = \begin{bmatrix} \omega \\ T_B \end{bmatrix}; \quad y = \omega; \quad u = \begin{bmatrix} T_L \\ I_{mr} \end{bmatrix} \qquad (5.8)$$

For clutch function, there are two cases should be considered. If the current applied on

inner coil is large enough, there is no slipping happened between the actuator and

load. At this state, the clutch will transfer the exact torque and angular velocity from

motor part to load. Therefore, the model in this case is the same as the motor function as Equation (5.5) provided that

$$T_C = T_M \leq K_H I_{mr} \qquad (5.9)$$

In the other case, the current is not large enough and could not transfer synchronous velocity so that slipping happens. The model of the clutch function then is to the same as the brake function as Equation (5.8) and the prerequisite is

$$T_C = K_H I_{mr} + K_\omega \omega < T_M \qquad (5.10)$$

Thus, the control of the multifunctional actuator becomes easy to be implemented. When positive power is needed, the motor function is on; when negative power is required, the brake function is on; the clutch function is worked as a switch to these two functions. By adjusting the current on inner coil, the output torque will be controllable. In order to conduct accurate control, the parameters of the system should be identified first.

5.2 System Identification

5.2.1 Parameters in Motor Function

The parameters in motor function can be determined through experiment, where the steady-state and dynamic characteristics are measured. The torque constant K_t can be obtained from the testing, which is 0.25. Therefore, in steady-state, Equation (5.1) to Equation (5.4) are rewritten as

$$\omega = -\frac{R_M}{K_e}I_M + \frac{V_M}{K_e} \tag{5.11}$$

$$0.25I_M = D\omega + T_L \tag{5.12}$$

For different voltage constant values ranging from 5 V-24 V, the load is adjusted as well as the current. The speed-torque characteristics drawn for the motor function using the data acquired from the test. Hence, the values of K_e and R_M can be calculated.

The viscous damping coefficient D is determined by running the motor under no load condition. For different voltages, the values of speed and current are recorded and the damping coefficient D is then calculated.

From the dynamic characteristics of motor function, the inductance and moment of inertia can be determined regarding Equation (5.1) and Equation (5.4).

If keeping the rotor in standstill, where $\omega=0$, Equation (5.1) can be rewritten as

$$V_M = R_M I_M + L_M \frac{dI_M}{dt} \tag{5.13}$$

It can be solved with respect to the obtained current

$$I_M = \frac{V_M}{R_M}\left(1 - e^{-\frac{R_M}{L_M}t}\right) \tag{5.14}$$

The value of inductance L_M and is given as

$$\left.\frac{dI_M}{dt}\right|_{t=0} = \frac{V_M}{L_M} \tag{5.15}$$

By knowing the slope at a given voltage, inductance can be determined as follows

$$L_M = \frac{V_M}{I_M}\Delta t \tag{5.16}$$

Therefore, the parameters in the modeling of the motor function are achieved and listed in Table 5.2-1.

Table 5.2-1 Parameters in the modeling of motor function

Parameter	Description	Value
K_t	Torque constant	0.25
K_e	Back EMF constant	24.5
T	Velocity constant	40.8
D	Damping coefficient	10.2 (Nm/rpm)
R_M	Resistance of the outer coil	1.0 (Ω)
L_M	Reluctance of the outer coil	0.02 (H)
J_M	Moment of inertia	6.44 (kg·cm^2)

5.2.2 Parameters in Brake Function

As illustrated in Equation (3.16), the torque produced by clutch/brake part in brake function is comprised of two components, one is due to the applied magnetic field and the other is related to the viscosity. Compared with Equation (5.6), the coefficient K_ω can be represented as

$$K_\omega = \eta \frac{n_{CB}\pi}{2g_{CB}}(r_o^4 - r_i^4) \tag{5.17}$$

where the viscosity of MR fluids η is a kind of non-linear parameter, which can be figured out from properties of MRF-132DG [Susan-Resiga, 2009]. The parameter is not only determined by the shear rate, but also affected by the applied field.

As discussed in the previous chapter, the brake function can be modeled as a first order single-input single-output linear time invariant plant. The plant parameters may change slowly as time and environment change (such as temperature variation, abrasion of iron particles in the MR fluid, etc.). Therefore, other approach is proposed for controlling the actuator instead of determining the accurate value of the parameters.

5.3 Control of the Actuator

Adaptive control is a control algorithm of applying some system identification technique to obtain a model of the process from input-output experiments. The parameters of the controller are adjusted during the operation of the plant as the data available for plant identification change. In practice, the adaptive techniques are applied to slowly time-varying unknown plants.

For brake function, the system is described as

$$y_{k+1}^B = a^B y_k^B + b^B u_k^B \qquad (5.18)$$

where y^B denotes the brake torque output, u^B is the control voltage, subscript (k) is the sample index, a^B and b^B are unknown gain parameters.

$$y_{r,k+1}^B = r_k^B \qquad (5.19)$$

where y_r^B is the target output, r^B is the reference input, and the control voltage be given by

$$u_k^B = c_k^B r_k^B + d_k^B y_k^B \qquad (5.20)$$

where c^B and d^B are control gain parameters, and there exist nominal parameter values

that make the output matches the target output

$$c^{B}* = \frac{1}{b^B} \quad d^{B}* = -\frac{a^B}{b^B} \tag{5.21}$$

Define the output error

$$e_k^B = y_k^B - y_{r,k+1}^B \tag{5.22}$$

and the parameter errors

$$\Phi_{r,k}^B = c_k^B - c^{B}*, \quad \Phi_{y,k}^B = d_k^B - d^{B}* \tag{5.23}$$

Choose the following parameter update laws

$$c_{k+1}^B = c_k^B - g^B e_k^B r_k^B, \quad d_{k+1}^B = d_k^B - g^B e_k^B y_k^B \tag{5.24}$$

where g^B is a positive real number as update parameter.

Consider the Lyapunov function

$$v_{k+1}^B = \frac{(e_k^B)^2}{2} + \frac{b^B}{2g^B}[(\Phi_{r,k}^B)^2 + (\Phi_{y,k}^B)^2] \qquad (5.25)$$

$$\delta v_{k+1}^B = v_{k+1}^B - v_k^B = -(e_k^B)^2 \leq 0 \qquad (5.26)$$

Hence, δv_{k+1}^B is negative semi-definite, and the parameter and output errors are upper bounded. It is demonstrated that, in the sense of Lyapunov, the adaptive system is stable.

Experiment on torque tracking of brake function with adaptive controller is conducted and shown in Figure 5.3-1. It can be seen that the actuator can track the reference very well in brake function.

In motor function, speed control can also utilize such an adaptive controller for tracking the reference input. Similar to conventional DC motors, the speed of the motor is driven by pulse width modulation (PWM) signal with respect to the speed reference input. The adaptive algorithm for the speed control in motor function then can be described as

$$v_{k+1}^M = a^M v_k^M + b^M n_k^M \qquad (5.27)$$

where v^M denotes the speed output and n^M is the augmentation.

$$v_{r,k+1}^M = r_k^M \qquad (5.28)$$

where v_r^M is the target speed output, r^M is the reference speed input. And the augmentation can be defined as

$$n_k^M = c_k^M r_k^M + d_k^M v_k^M \qquad (5.29)$$

The speed output error is described as

$$e_k^M = v_k^M - v_{r,k+1}^M \qquad (5.30)$$

And the parameter update laws are

$$\Phi_{r,k}^M = c_k^M - c_\bullet^M, \qquad \Phi_{v,k}^M = d_k^M - d_\bullet^M \qquad (5.31)$$

Using the same parameter update laws as Equation (5.27), the speed control of motor function can also be proved to be stable in the sense of Lyapunov.

Speed control experiment of motor function is conducted to track a desired speed signal in bi-direction using such an adaptive algorithm. Figure 5.3-2 shows that the actuator can track the reference speed well while working in motor function.
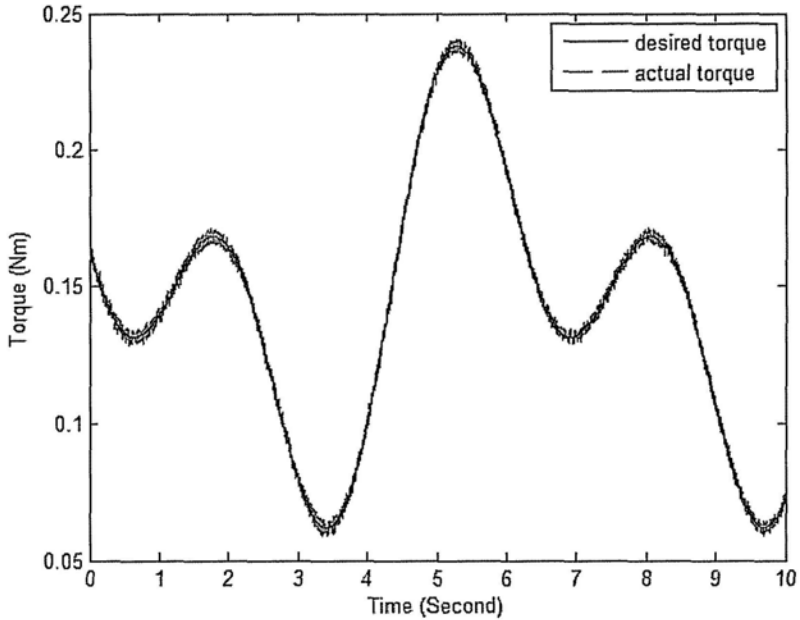
Figure 5.3-1 Torque tracking in brake function
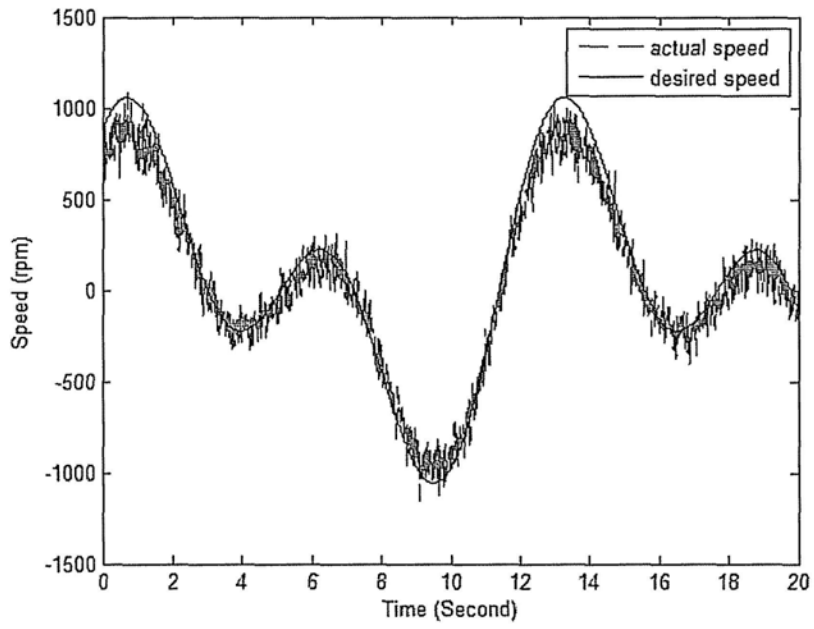
Figure 5.3-2 Speed tracking in motor function

5.4 Chapter Summary

In this chapter, the modeling of the multifunctional actuator is developed. As the actuator has multiple functions, the models are built for motor function and brake function, respectively. For the modeling of the clutch function, if there is no slipping happened between the actuator and load, the model is the same as the motor function. In the other case when slipping happens, the model of the clutch function then is the same as the brake function. Based on the derived models, experiments on system identification are conducted to determine the values of the modeling parameters. The modeling parameters in motor function are obtained by series of experiments. However, because the parameters in brake function are non-linear and may vary with time or environmental changes, the accurate values of these parameters are difficult to determine. Therefore, adaptive control method is used to identify the parameters and control the actuator. Torque tracking and speed tracking are evaluated using the adaptive control.

CHAPTER SIX

SMART JOINT USING MULTIFUNCTIONAL ACTUATOR

As presented in Chapter Four, the torque produced by the multifunctional actuator in motor function and brake function is not large enough to be used into the assistive knee braces. In this chapter, transmission devices, like harmonic drives and planetary gearboxes with movable teeth are introduced first. The later one is the mechanism to be utilized in this research to increase the output torque while reducing the speed. Then, a smart joint integrating the actuator and gearbox is designed and a corresponding prototype is fabricated and tested.

Experiments of the smart joint using the multifunctional actuator and gearbox are carried out to evaluate the performances for assistive knee braces. Power consumption of the knee brace using the smart joint is investigated and compared to that using an electric motor. Based on testing results on bending and extending stages, power consumptions of knee braces during normal walking cycle are analyzed and compared.

6.1 Transmission Mechanisms in the Smart Joint

6.1.1 Selection of the Transmission Mechanism

As shown in Chapter Four, the torque produced by the brake function is around 0.48 Nm, and the rated speed is about 700 rpm, which maybe not sufficient for assisting human motion. Therefore, transmission mechanism should be added up to enlarge the torque while reducing the speed to be used in assistive knee braces.

The harmonic drive is a unique gear system used in robotic engineering, which gives no backlash, and large gear ratio. Illustrated in Figure 6.1-1, the harmonic drive looks like a cup with the input shaft going through the center. The rigid cup has an internal set of teeth all the way around known as the rigid circular spline. What is inside the rigid cup is a slightly smaller flexible cup called the flex spline. The flex spline typically has two teeth less than the outer cup. A rotating device called the wave generator pushes out on the flex spline so that the teeth mesh only on opposite sides. The input shaft is connected to the wave generator, and as it rotates, the two splines mesh with each other. Because they have a different number of teeth, the outer cup, which is connected to the output shaft, will advance a little for each revolution of the flex spline. The actual gear ratio can be calculated from the following equation:

$$N_{ratio} = \frac{N_{rigid}}{D_{splines}} \qquad\qquad (6.1)$$

Where N_{rigid} is the number of teeth on outer rigid cup and $D_{splines}$ is the difference in number of teeth on splines.

However, the value of backdrivability of harmonic drive is comparatively high. Because, the friction resistance is generated between the teeth surface of the flux spline and the inner teethes around the circular spline. There also need additional force and rotational torque to bend the flex spline and the wave generator. Furthermore, harmonic drive usually possesses lower efficiency, whose maximal efficiency is around 80%. Hence, this kind of transmission mechanism is not suitable to be used in assistive knee braces, as during swing states, the joint needs to be rotated smoothly and have good backdrivability.
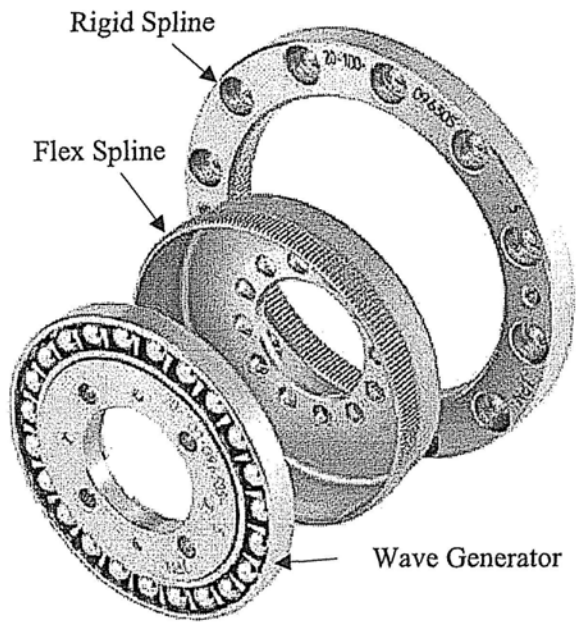
Figure 6.1-1 Components of harmonic drive
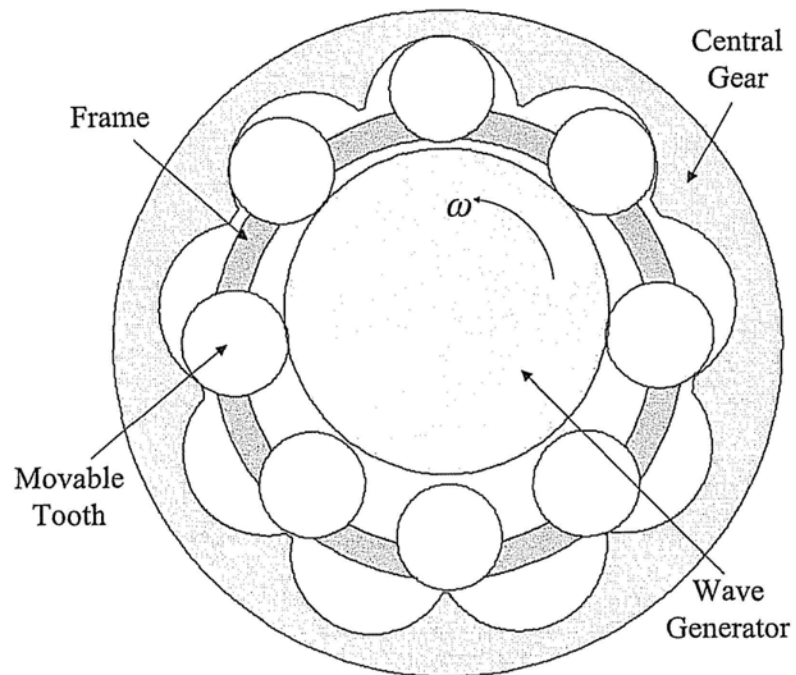
Figure 6.1-2 Scheme of planetary gearbox with movable teeth

Another alternative transmission mechanism is a kind of planetary gearbox with movable teeth. In the device, the gear teeth and body are fabricated separately, forming revolute or translation pairs between these two parts. Therefore, the teeth are called movable teeth and the body is called frame. The teeth can move or rotate around the frame while meshing with the central gear. Meanwhile, the frame rotates around a fixed axis.

Figure 6.1-2 shows the scheme of the planetary gearbox with movable teeth. The wave generator rotates at a given speed. Because of its eccentricity, the wave generator pushes a part of movable teeth to mesh with the central gear. The teeth profile of the central gear in the meantime push the other movable teeth move back. As the movable teeth have one tooth fewer than that of central gear. The central gear will rotate forward or reversely with reduced speed. This kind of planetary gearbox usually has large gear ratio, compact dimensions and smaller size, which is an appropriate choice for be implemented into assistive knee braces. In this research, the gearbox is utilized and specially designed to meet the requirement of compactness.

6.1.2   Testing of the Gearbox

Figure 6.1-3 shows the gearbox utilized in this research. The specifications of the gearbox are listed in Table 6.1-1.

Table 6.1-1 Specifications of the planetary gearbox

Parameter	Value
Width	30 (mm)
Diameter	80 (mm)
Weight	0.76 (kg)
Gear ratio	63:1
Efficiency	94.3 (%)
Maximum input torque	1.67 (Nm)
Maximum input speed	2500 (rpm)
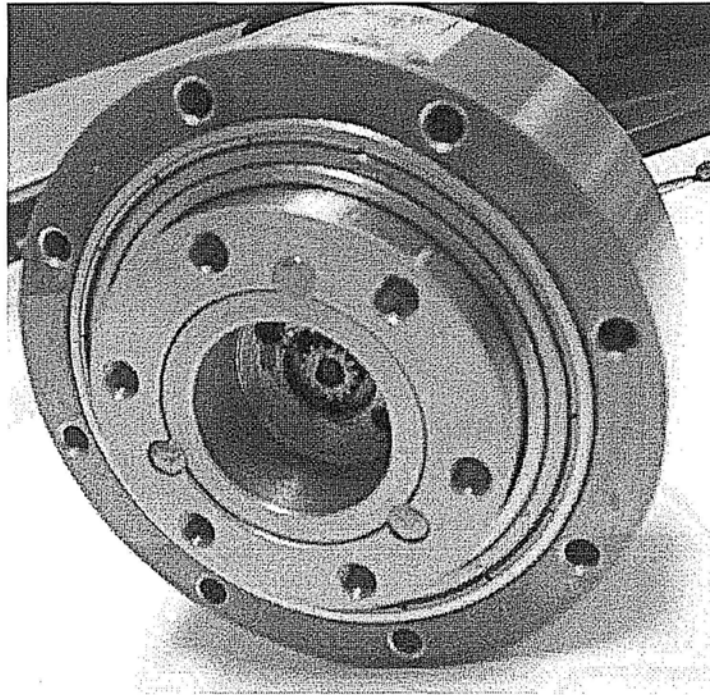
Figure 6.1-3 Prototype of the planetary gearbox
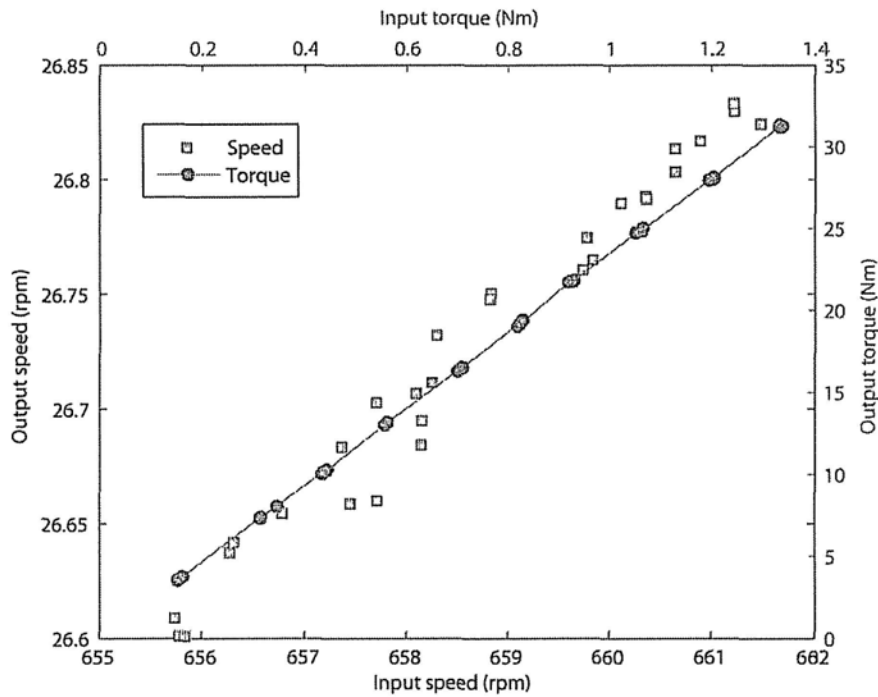
Figure 6.1-4 Measured input/output speed and input/output torque of the gearbox

As the desired speed of the knee joint for normal walking is around 8.5 to 12 rpm, in this research the in the performance of the gearbox is tested with the input speed at 660 rpm. Figure 6.1-4 shows the experimental results representing the relationship between the input speed and output speed, the input torque and output torque.

Therefore, the input power and output power can be calculated according to the following equation

$$P_{gear} = \frac{speed \times torque}{9550} \qquad (6.2)$$
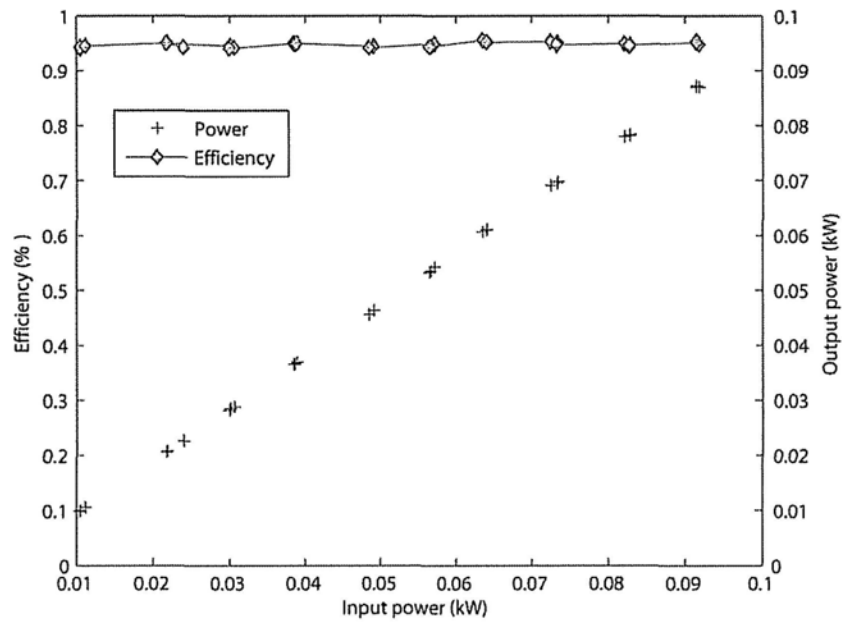
Figure 6.1-5 Measured input/output power and efficiency of the gearbox

Thus, the efficiency of the gearbox can be obtained with the obtained input and output power. Figure 6.1-5 shows the relationship of the input power and output power, and the corresponding efficiency. From the figure, it can be found that the average efficiency is about 94.3%, which is larger than the harmonic drive.

6.2 Configuration of the Smart Joint

As discussed in previous chapters, the original purpose of designing the multifunctional actuator is to fulfill tasks of human knee joint to produce sufficient torque while providing smooth motion. A smart joint integrating actuator and gearbox is designed in this research. Figure 6.2-1 describes the connection approach of the multifunctional actuator and gearbox. The actuator is tightly connected with the gearbox by the shaft placed into the input end of the gearbox. Eight screws are used to fasten the gearbox to the housing of the multifunctional actuator. Hence, the two main parts can be integrated into a mechanical structure of the smart joint.
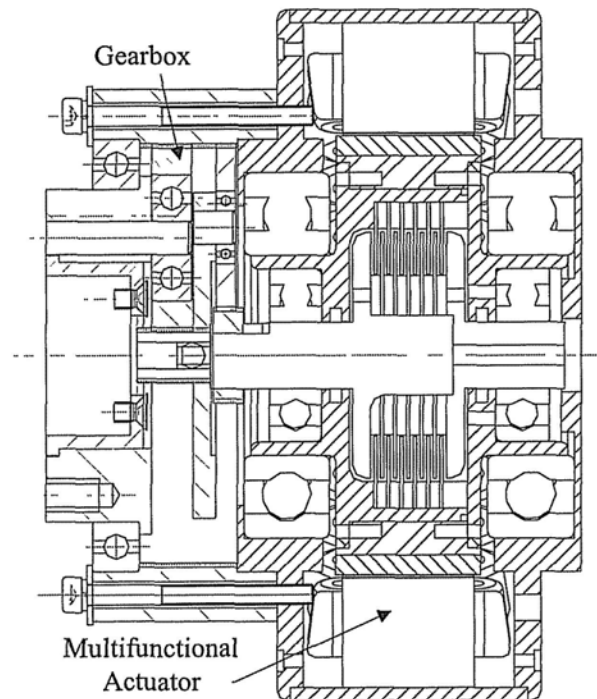
Figure 6.2-1 Connection of the gearbox and the multifunctional actuator

Figure 6.2-2 shows the configuration of the smart joint. To incorporate the joint angle measurement, without significantly affecting the overall joint width, a small rotary optical encoder is placed inside the gearbox to measure the actuator shaft angle. To support all the rotating components of the smart joint, there are some groups of bearings. A kind of roller bearing is placed on the periphery of the gearbox to provide the relative significant off-axis moments, and operate at very low speeds. In addition to sizing and placing all of the bearings, significant effort was involved in properly constraining the bearings and ensuring that they, along with their retaining rings, were assemble-able.
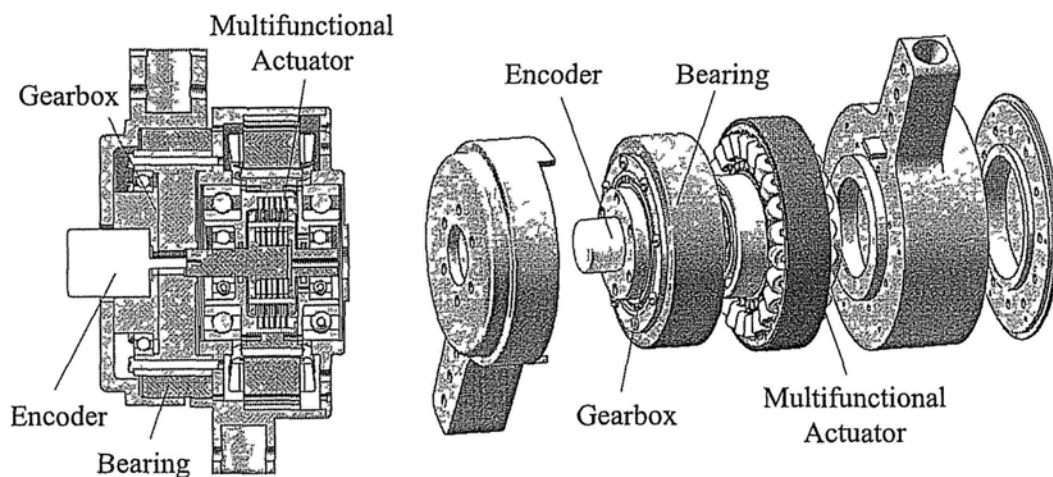
Figure 6.2-2 Configuration of the smart joint

The prototype of the smart joint is fabricated and shown in Figure 6.2-3. The smart joint has a 110 mm outer diameter and its width is 81 mm. Overall, the smart joint weights 2.86 kg.
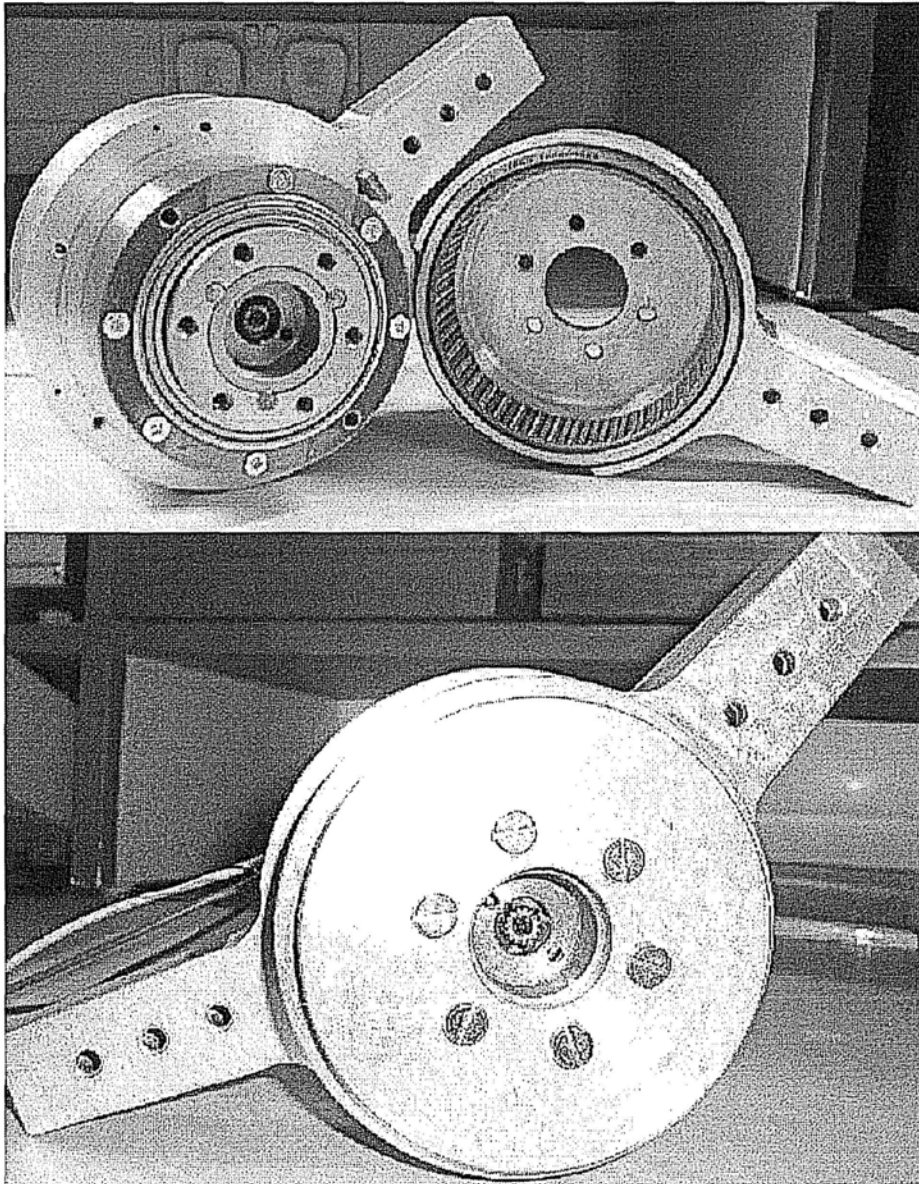
Figure 6.2-3 Prototype of the smart joint

The specifications of the prototype of smart joint are listed in Table 6.2-1. Form the table, it can be found that the geometric dimension meets the desired constraints, and the output speed and torque is adequate for assistive knee braces.

Table 6.2-1 Specifications of the prototype of smart joint

Parameter	Value
Width	81 (mm)
Diameter	110 (mm)
Weight	2.86 (kg)
Gear ratio	63:1
Maximal efficiency	73 (%)
On load efficiency	72.6 (%)
Rated voltage on inner coil	10 (V)
Rated voltage on outer coil	24 (V)
Rated speed in motor function	10.3 (rpm)
Maximal output power in motor function	100 (W)
Maximal output torque in brake function	32.6 (Nm)

6.3 Testing of the Smart Joint

Similar to testing for the multifunctional actuator, each function of the smart joint is investigated by several experiments. The smart joint is connected with a load and the torque is measured by the torque sensor (Model RST-C4A-30-1-A from RSTSensor Inc.), and encoder is fixed on the center to measure angle and speed. Figure 6.3-1 shows the two experimental setups.
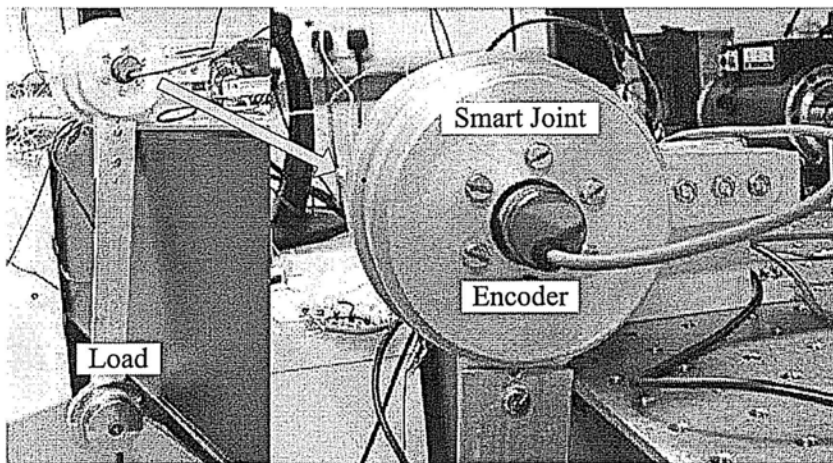
(a) Setup for testing the motor function
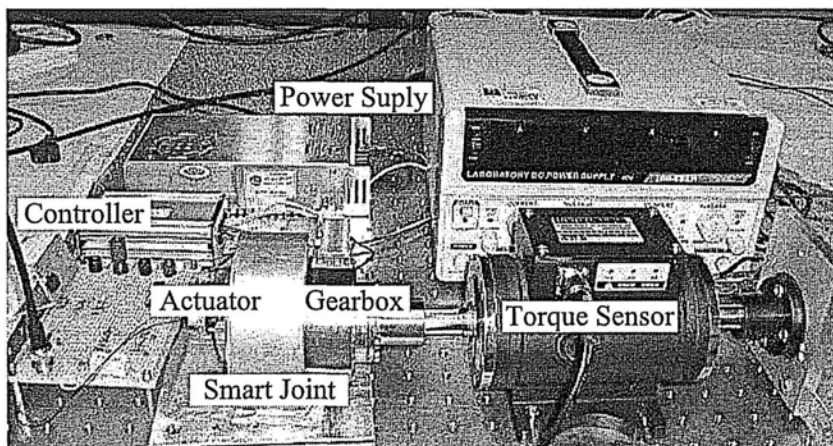
(b) Setup for testing the brake function and clutch function

Figure 6.3-1 Experimental setups to investigate each function of the smart joint
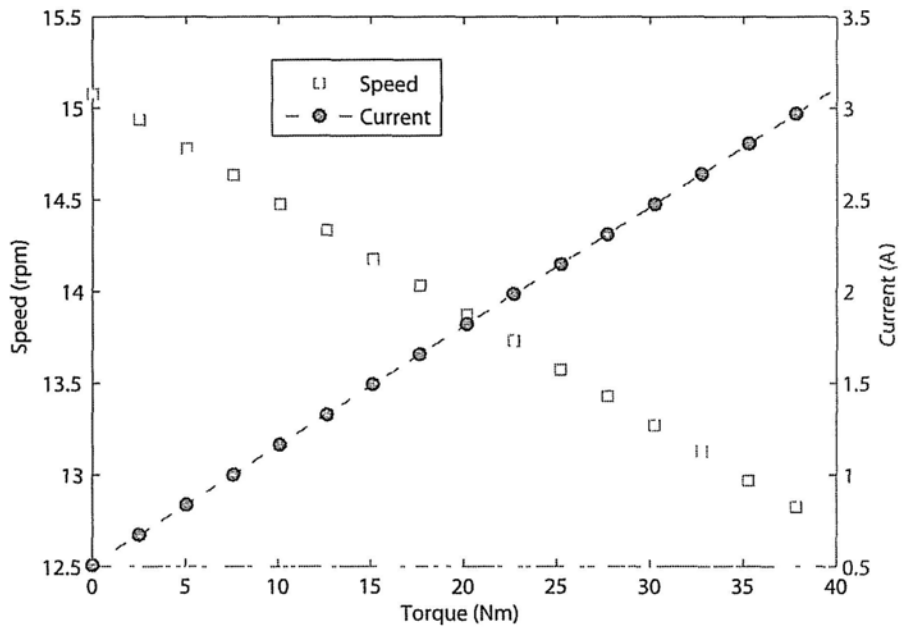
Figure 6.3-2 Torque vs. current and torque vs. speed in motor function of the smart joint
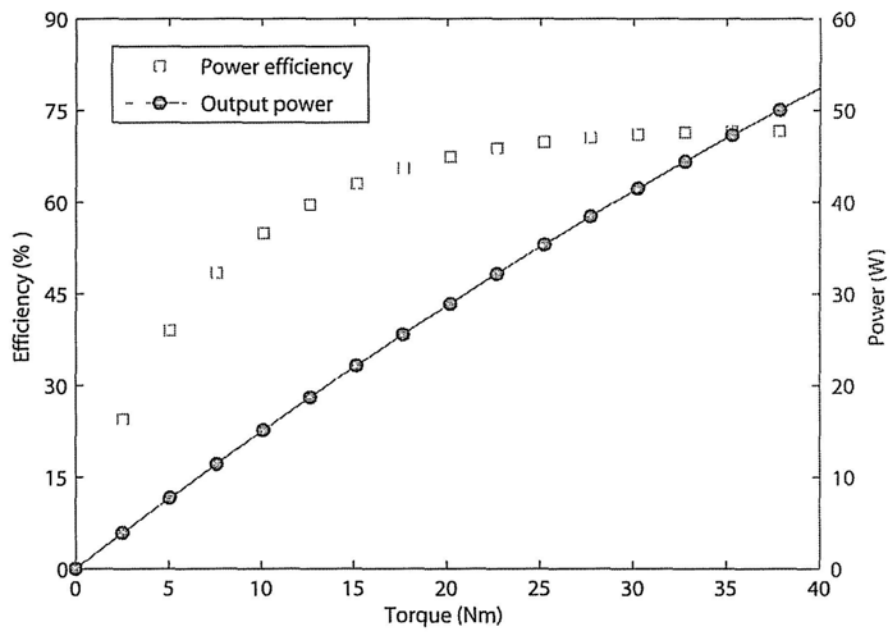
Figure 6.3-3 Input/output power and power efficiency in motor function of the smart joint

By testing the output torque, input and output power, the relationship of the input current and speed, and the relationship between the current and output torque, the performance of the knee braces in motor function can be acquired as shown in Figure 6.3-2 and Figure 6.3-3. The output torque reaches 40 Nm, where is limited by the maximum output torque of the gearbox, and the maximum efficiency is around 73%.
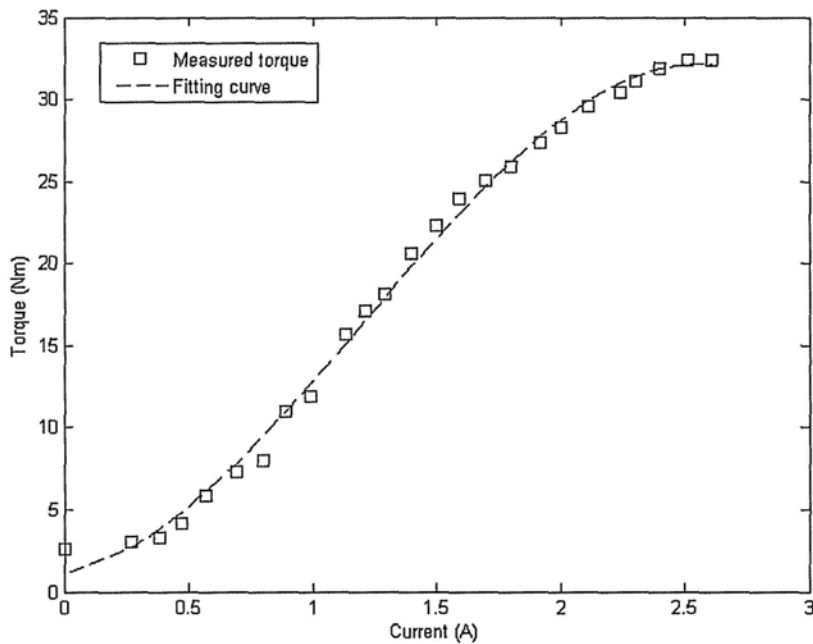
Figure 6.3-4 Measured torque in brake function of the smart joint

When the current is applied to the inner coil of the multifunctional actuator from 0A to 2.5A gradually, the torque in brake function is measured by the dynamic torque sensor. Figure 6.3-4 shows the relationship between the measured torque and applied

current. It can be found that the output torque increases linearly from 2.63 Nm to 32.4 Nm, which is sufficient for providing assistive torque.
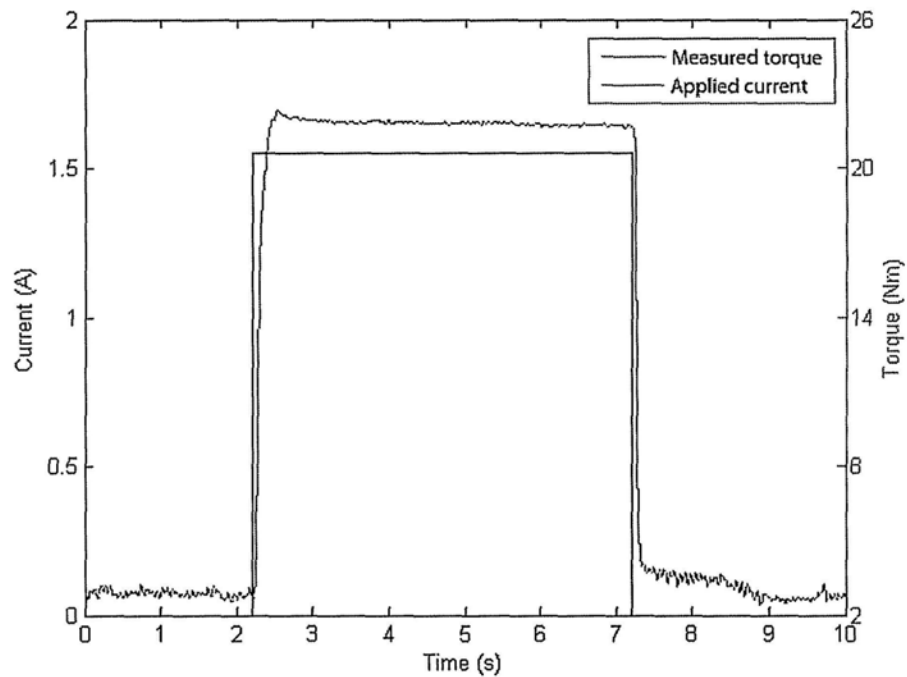
Figure 6.3-5 Testing of the clutch function for smart joint

The clutch function of the smart joint is also tested. Figure 6.3-5 shows the response time of the smart joint under step signal. It can be discovered that the response time is measured as 0.21 seconds, which is a bit larger than the result obtained in Section 4.3. However, as the response time for human is around 0.15 to 0.4 second. That is to say, it is capable of providing safety for stopping the torque transfer from the motor to the assistive knee brace in case of emergency.

6.4 Power Consumption of the Smart Joint

The power consumption of a knee brace using the smart joint is investigated. The experimental setup is built as shown in Figure 6.4-1. The load representing the weight of human body moves up and down along the guide poles under the torque provided by the smart joint and gravity force. The weight of the load (which combined with a pair of linear bearings to minimize the friction force between the load and the guiding poles) is about 6 kg. Currents applied on both inner and outer coils are measured through the current transducer (LTSR 6-NP, LEM).
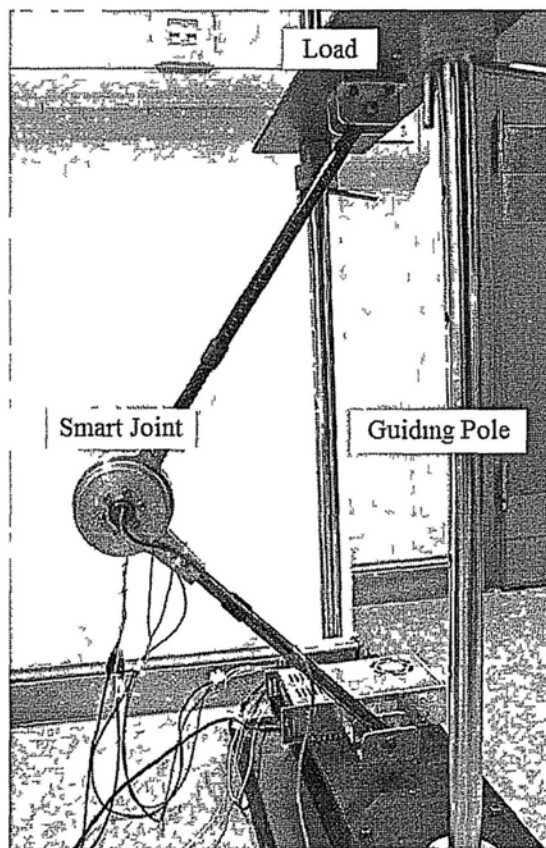
Figure 6.4-1 Experimental setup for evaluating power consumption of the smart joint

When current is applied to both inner and outer coils of the multifunctional actuator, the smart joint provides active torque to lift up the load, which represents the extending motion of knee brace. Turning off the motor function, the knee brace will move down under the gravity force, which represents the bending motion. By adjusting the current on inner coil, the smart joint then functions as controllable brake. The extending speed is 0.166 rad/sec, and the bending speed is 0.158 rad/sec.

To compare the power consumption between the smart joint and an electric motor under the same condition, corresponding currents and voltages are measured accordingly. For example, to investigate power consumption for the knee brace using the smart joint, the voltage and current on inner coil are measured during bending motion. While during extending, currents on inner and outer coil are both measured, as motor function and clutch function cooperated in this case. To investigate power consumption for the knee brace using an electric motor, during both bending and extending motions, only the current on outer coil is measured, although there is current also applied on inner coil. Because in this case, the power consumed on the motor function of the smart joint is approximated to an electric motor with the same specification.

Figure 6.4-2 shows the power consumption in two cases. During bending motion, the average power consumption for the knee brace using the smart joint is about 4.08 W, which is power consumption in brake function; while for knee brace using the electric motor (i.e., motor function in smart joint) is around 16.78 W, which is much larger than that using that smart joint. In this case, the smart joint saves nearly 75.69% power. During extending motion, the average power consumption for the knee brace using the electric motor is about 18.15 W, whereas for the one using the smart joint, it is the summation of power consumed in both motor and clutch functions. In this case, the knee brace using the smart joint consumes 26.15 W (44.08% more power). For the whole cycle, the knee brace using the smart joint saves 13.82% power than that using the electric motor. The comparison is listed in Table 6.4-1.
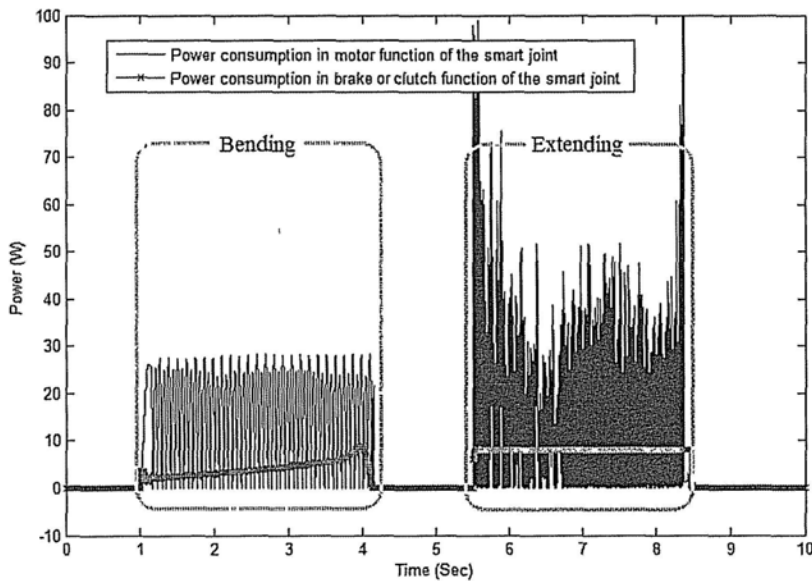
Figure 6.4-2 Power consumed by the knee brace using motor and smart joint

Table 6.4-1 Power consumed by knee brace using motor and smart joint during bending and extending motions

	Bending	Extending	Whole cycle
Using electric motor	16.78 (W)	18.15 (W)	17.44 (W)
Using smart joint	4.08 (W)	26.15 (W)	15.03 (W)
Power saved	75.69%	- 44.08%	13.82%
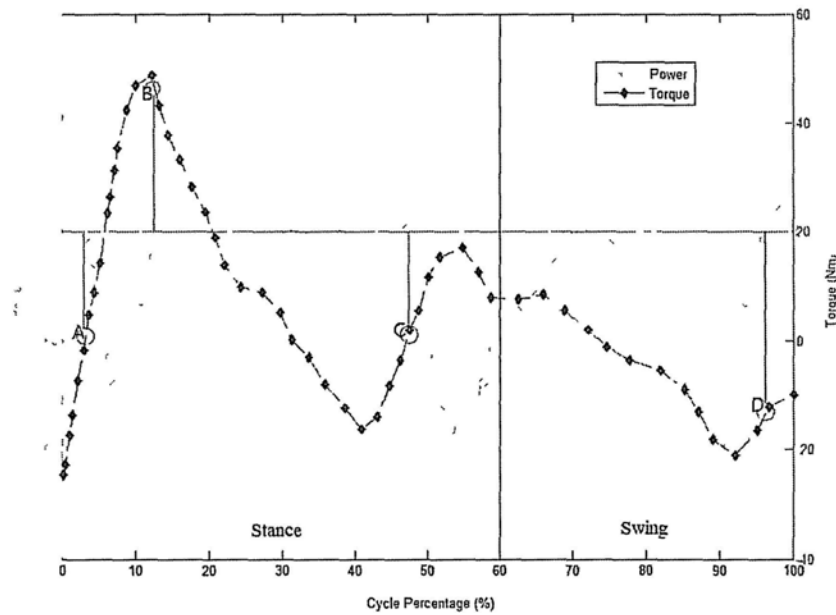
Figure 6.4-3 Power and torque produced from human knee joint during normal walking (adopted from [Zoss and Kazerooni, 2006])

As discussed in chapter one, for normal walking, the average power provided by the knee joint is negative. Figure 6.4-3 shows the power and torque adopted from the Winter CGA data shown in Figure 1.1-2. As shown in the figure, the walking cycle is separated into two stages, stance and swing. There are four key points, A, B, C and D. Powers at stages from the beginning to A, B to C, and D to the end, are positive.

Powers at stages from A to B and C to D, are negative, which means at this state the knee joint is dissipating power instead of providing power. However, torques at each stage can be positive or negative. Positive torque means the direction is the same as the leg's locomotion, whereas negative torque means the direction is opposite to that motion.
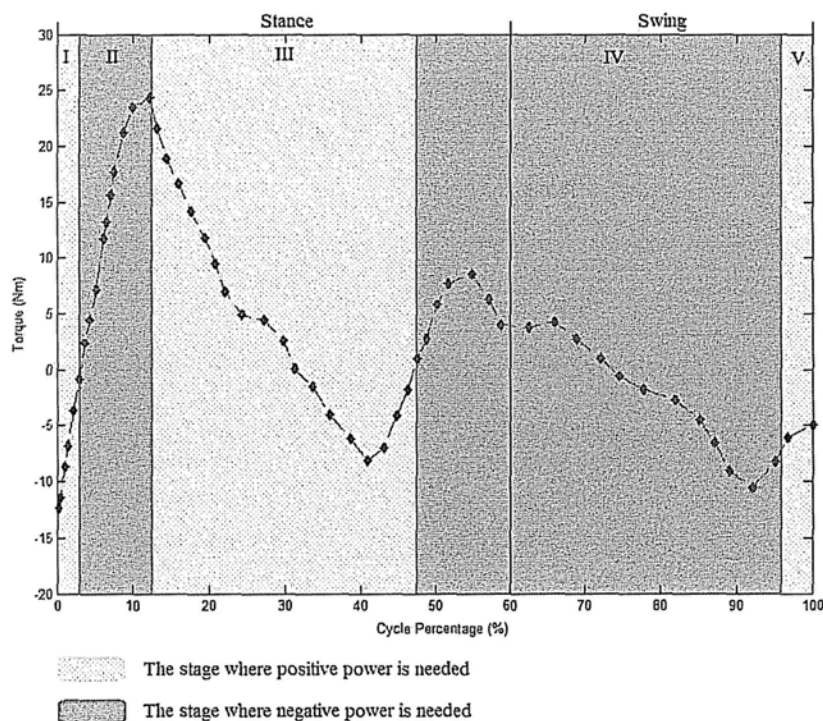
Figure 6.4-4 Torque provide by the knee brace using motor or smart joint during normal walking

Given the output torque, the power in motor function and brake function of the smart joint can be obtained from Figure 6.3-3 and Figure 6.3-4, respectively. Assuming the knee brace provides 50% of the torque provided by the knee joint as shown in Figure

6.4-3, the torque produced from the knee brace is shown in Figure 6.4-4. There are five stages (stage I to stage V) depicting positive and negative powers produced from the actuators. For the knee brace using electric motor, the motor works all the time to provide positive and negative powers. For the knee brace using smart joint, the motor function and clutch function cooperate to provide positive power, while the brake function is utilized to provide negative power. The power consumption in these two cases are estimated and shown in Figure 6.4-5, and corresponding results at different stages are listed in Table 6.4-2. It can be found that the knee brace using smart joint could save 22.99% power than that using electric motor during normal walking.
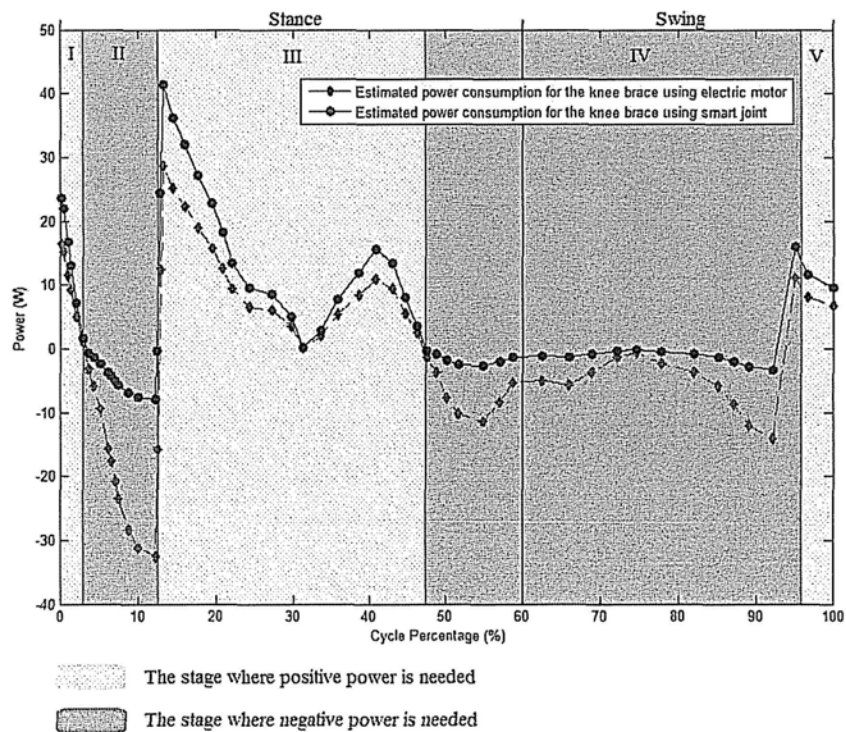
Figure 6.4-5 Estimated power consumption for knee braces using electric motor or smart joint during normal walking

Table 6.4-2 Power consumed by knee braces using motor and smart joint during normal walking

Stages	Using electric motor	Using smart joint	Power saved
Stage I	12.74 (W)	14.02 (W)	-10.05%
Stage II	18.81 (W)	4.07 (W)	78.36%
Stage III	11.69 (W)	15.39 (W)	-31.65%
Stage IV	6.21 (W)	1.51 (W)	75.68%
Stage V	8.58 (W)	12.05 (W)	-40.44%
Whole cycle	9.62 (W)	7.41 (W)	22.99%

6.5 Chapter Summary

To increase the output torque while decreasing the rotation speed, transmission mechanisms like harmonic drives and planetary gearboxes with movable teeth are introduced. The later one is chosen to be the mechanism used in this research. A smart joint is designed to integrate the multifunctional actuator and the selected gearbox. The configuration of the smart joint is then described and a prototype is fabricated. Experiments are conducted to investigate the gearbox and each function of the smart joint. For motor function, the output torque provided by the smart joint ranges from 2.63 Nm to 40 Nm. The rated output speed is about 10.3 rpm. The maximum efficiency of the smart joint is around 73%. The gear ratio and efficiency of the gearbox are 63 and 94.3%, respectively. For motor function, the maximum output torque is limited by the maximum output torque of the gearbox. For brake function, the output torque is increased with the applied current until reaching the limitation due to the maximum value of the interaction magnetic torque between the stator and permanent magnets. Even though, the output torque produced by motor function and brake function are adequate for providing assistive torque. The measured off-state torque is 2.63 Nm. The response time of the smart joint in clutch function is tested and it shows that the designed smart joint can provide safety to be used in assistive knee braces. Power consumption of knee braces using the smart joint during bending and extending stages is investigated, and compared with that using an electric motor.

During one extending and bending cycle, the knee brace using smart joint could save 13.82% power than that using an electric motor. Based on the experimental results and gait analysis, power consumptions of knee braces using the smart joint and electric motor during normal walking cycle are estimated and compared. In this case, as the brake function plays a main role, the knee brace using the smart joint could save 22.99% power than that using an electric motor.

CHAPTER SEVEN

CONCLUSION AND FUTURE WORK

7.1 Conclusion

Assistive knee braces are a type of wearable equipment that can enhance people's strength and provide desired locomotion. It is possible to use knee braces to assist elderly or disabled people for improving their mobility so as to solve many daily life problems. In designing assistive knee braces, a well designed actuator that has properties such as multiple functions, compactness and low power consumption, would be the key component.

In this research, magnetorheological (MR) fluids based multifunctional actuators for assistive knee braces are designed. To decrease the dimension of the actuation device while enhancing its performances, a motor and MR fluids are integrated into a single device. The actuator consists of two parts, motor part and clutch/brake part, while each part is associated with corresponding coils. Multiple functions can be achieved by applying current on different coils.

In this thesis, design details of the motor part and clutch/brake part are discussed. There are various configurations of motor part and clutch/brake part. The motor part

is designed based on interior-rotor BLPM DC motors. For clutch/brake part, two main configurations, inner armature and input/output plates, are presented. Considering different forms of inner coils, possible combinations of these two parts are then discussed. Finite element method is used to analyze the electromagnetic circuits, the influence of permanent magnet on MR fluids, magnetic flux distribution, and sealing as well. Prototypes with different clutch/brake parts are fabricated and tested, and characteristics of each function are investigated. The experimental results show that although the measured output torque in both motor and brake function are not high, by adding transmission mechanisms, the torque will be greatly increased. While for clutch function, the response is sufficiently fast to provide safety. Therefore, the multifunctional actuator is promising for assistive knee braces. In order to improve the output torque in brake function, different clutch/brake models with various inner coils are compared, and then the design optimization is carried out to determine the optimum parameters. The optimized prototype is then fabricated. Results from finite element analysis and experiments show the output torque from the optimized design is nearly doubled as compared to that without optimization.

To control the actuator, modeling in different functions is developed. The modeling can be divided into two models, motor function and brake function, while the modeling of the clutch function is the combination of these two models. System

identification is then carried out to determine the parameters in the models. Because the parameters in brake function may vary with time or environmental changes, so the accurate values of these parameters are difficult to determine. Therefore, adaptive control is used to identify the parameters and control the actuator. Adaptive control is also implemented for torque and speed tracking of the actuator. Experimental results show the control output tracks the reference signal well.

As the output torque is not large enough and the output speed is faster than desired motion, transmission mechanisms like harmonic drives and planetary gearboxes with movable teeth are considered in the design. To integrate the multifunctional actuator with gearbox, a smart joint using the multifunctional actuator is designed, fabricated and tested. Experimental results show that the smart joint can function as motor, clutch and brake. Meanwhile, it can provide sufficient torque and the response time is also acceptable for application to human body. Power consumption of knee braces using the smart joint during bending and extending stages is investigated, and compared with that using an electric motor. During one extending and bending cycle, the knee brace using smart joint could save 13.82% power than that using an electric motor. For normal walking cycle, the power consumptions of knee braces using the smart joint and electric motor are estimated and compared. It is found that the knee brace using the smart joint could save 22.99% power.

The major contributions of this thesis include:

1. A novel actuator that integrates MR fluids with motor to provide multiple functions as motor, clutch and brake is designed. Prototypes are fabricated and tested, and characteristics of each function are investigated.

2. Various configurations of motor part and clutch/brake part are considered and possible combinations of these two parts are discussed. Among them, the clutch/brake part with configurations of inner armature and axial-inner inner coils are selected as new designs in MR fluids based devices.

3. Finite element method is utilized to analyze the magnetic circuit, magnetic flux distribution, interference of permanent magnets on the MR fluids, and dynamic sealing of the actuator.

4. Different clutch/brake models with various inner coils are built, analyzed and compared. The influence of the configuration of inner coil on output torque is studied.

5. A smart joint using the multifunctional actuator is developed and the corresponding prototype is fabricated and tested. The power consumption of the smart joint is evaluated and compared to that using an electric motor.

7.2 Future Work

The smart joint using the multifunctional actuator has not yet been applied to human body. Since the ultimate goal is to provide assistance torque for the wearer, the next step is to develop a knee brace using the developed smart joint, and then apply the knee brace for assisting human walking. Therefore, to build a knee brace of lightweight and low power consumption, mechanical design of the knee braces including linkage, ergonomics and appearance should be considered. Finite element method could be used to optimize the stiffness and stress for the structure.

While applied to the wearer, the knee brace should provide proper assistance torque as human body required. Therefore, how to detect the motion intention in time and how to provide appropriate assistive torque will also be the future research issues.

BIBLIOGRAPHY

Ahmadkhanlou F., Zite J. and Washington G., "A Magnetorheological Fluid-based Controllable Active Knee Brace," *Proceedings of SPIE on Industrial and Commercial Applications of Smart Structures Technologies*, Vol. 6527, pp. 65270O-1 – 65270O-10, 2007

An J. and Kwon D. S., "Five-bar Linkage Haptic Device with DC Motors and MR Brakes," *Journal of Intelligent Material Systems and Structures*, Vol. 20, pp. 97-107, 2009

Andrews A. W. and Bohannon R. W., "Short-term Recovery of Limb Muscle Strength After Acute Stroke," *Archives of Physical Medicine and Rehabilitation*, Vol. 84 (1), pp. 125-130, 2003

Bogue R, "Exoskeletons and Robotic Prosthetics: a Review of Recent Development," *Industrial Robotic*, Vol. 36 (5), pp. 421-427, 2009

Carlson J. D., and Jolly M. R., "MR Fluid, Foam and Elastomer Devices," *Mechatronics*, Vol. 10 (4-5), pp. 555-569, 2000

Chen F., Yu Y., Ge Y., Sun J., and Deng X., "WPAL for Enhancing Human Strength and Endurance During Walking," *International Conference on Information Acquisition*, pp. 487-491, 2007

Chen J. Z. and Liao W. H., "Design, Testing and Control of a Magnetorheological Actuator for Assistive Knee Braces," *Smart Materials and Structures*, Vol. 19, pp. 035029, 2010, doi:10.1088/0964-1726/19/3/035029

Chinese National Committee of Aging, "A predictive research report on development trend of aging in China," 2007, from http://www.cnca.org.cn/default/iroot1000610000

Damiano D. L., Martellotta T. L., Sullivan D. J., Granata K. P. and Abel M. F., "Muscle Force Production and Functional Performance in Spastic Cerebral Palsy: Relationship of Cocontraction," *Archives of Physical Medicine and Rehabilitation*, Vol. 81 (7), pp. 895-900, 2000

Deffenbaugh B., Herr H., Pratt G. and Wittig M., "Electronically Controlled Prosthetic Knee," *U. S. Patent*, No.6764520, 2004

Dodd K. J., Taylor N. F. and Damiano D. L., "A Systematic Review of the Effectiveness of Strength-training Programs for People with Cerebral Palsy," *Archives of Physical Medicine and Rehabilitation*, Vol. 83 (8), pp. 1157-1164, 2002

Dong S. F., Lu K. Q., Sun J. Q. and Rudolph K., "A Prototype Rehabilitation Device with Variable Resistance and Joint Motion Control," *Medical Engineering & Physics*, Vol. 28 (4), pp. 348-355, 2006

Dong S. F., Lu K. Q., Sun J. Q. and Rudolph K., "Adaptive Force Regulation of Muscle Strengthening Rehabilitation Device with Magnetorheological fluids," *IEEE Transactions on Neural Systems and Rehabilitation Engineering*, Vol. 14 (1), pp. 55-63, 2006

General Electric Co., "Hardiman | Arm Test," General Electric Rep., S-70-019, Schenectady, 1969

Hendershot J. and Miller T., [Design of Brushless Permanent-Magnet Motors], *Magna Physics Pub.*, 1994

Herr H. and Wilkenfeld A., "User-adaptive Control of a Magnetorheological Prosthetic Knee," *Industrial Robot*, Vol. 30 (1), pp. 42-55, 2003

HONDA, http://world.honda.com/news/2008/c081107Walking-Assist-Device/

Janocha H., [Actuators: Basics and Applications], *Springer*, 2004

Kawamoto H. and Sankai Y., "Comfortable Power Assist Control Method for Walking Aid by HAL-3," *IEEE International Conference on Systems, Man and Cybernetics*, Vol. 4, pp. 6, 2002

Kawamoto H., Lee S., Kanbe S. and Sankai Y., "Power Assist Method for HAL-3 Using EMG-based Feedback Controller," *IEEE International Conference on Systems, Man and Cybernetics*, Vol. 2, pp. 1648-1653, 2003

Kazerooni H. and Steger R., "The Berkeley Lower Extremity Exoskeleton," *Transactions of the ASME, Journal of Dynamic Systems, Measurements, and Control*, Vol. 128, pp. 14-25, 2006

Kordonski W. I. and Golini D., "Fundamentals of Magnetorheological Fluid Utilization in High Precision Finishing," *Journal of Intelligent Material Systems and*

Structures, Vol. 10 (9), pp. 683-689, 1999

Kordonsky V., Shulman Z., Gorodkin S., Prokhorov S., Zaltsgendler E. and Khusid B., "Physical Properties of Magnetizable Structure-Reversible Media," *Journal of Magnetism and Magnetic Materials*, Vol. 85, pp. 1-3, 1990

Lafortune M.A., Cavanagh P.R., Sommer III H.J. and Kalenak A., "Three-Dimensional Kinematics of the Human Knee During Walking," *Journal of Biomechanics*, Vol. 25 (4), pp. 347-357, 1992

Lau Y. K. and Liao W. H., "Design and Analysis of a Magnetorheological Damper for Train Suspension," *Proceedings of the Institution of Mechanical Engineers, Part F: Journal of Rail and Rapid Transit,* Vol. 219 (4), pp. 261-276, 2005

Lee S. and Sankai Y., "Power Assist Control for Leg with HAL-3 Based on Virtual Torque and Impedance Adjustment," *IEEE International Conference on Systems, Man and Cybernetics,* Vol. 4, pp. 6, 2002

Lee S. and Sankai Y., "The Natural Frequency-based Power Assist Control for Lower Body with HAL-3," *IEEE International Conference on Systems, Man and Cybernetics,* Vol. 2, pp. 1642-1647, 2003

Li C. Q., Tokuda M., Furusho J., Koyanagi K., and Hashimoto Y., "Research and Development of the Intelligently-controlled Prosthetic Ankle Joint," *IEEE International Conference on Mechatronics and Automation,* pp. 1114-1119, 2006

Liao W. H. and Wang D. H., "Semiactive Vibration Control of Train Suspension Systems via Magnetorheological Dampers," *Journal of Intelligent Material Systems and Structures*, Vol. 14 (3), pp. 161-172, 2003

Nakamura T., Saito K. and Kosuge K., "Control of Wearable Walking Support System Based on Human-Model and GRF," *Proceedings of International Conference on Robotics and Automation, Barcelona,* pp. 4405-4410, 2005

Neder J. A., Nery L. E., Shinzato G. T., Andrade M. S., Peres C. and Silva A. C., "Reference Values for Concentric Knee Isokinetic Strength and Power in Nonathletic Men and Women from 20 to 80 Years Old," *Journal of Orthopaedic & Sports Physical Therapy*, Vol. 29 (2), pp. 116-126, 1999

Nikitczuk J., Weinberg B. and Mavroidis C., "Rehabilitative Knee Orthosis Driven by Electro-Rheological Fluid based Actuators," *Proceedings of IEEE International*

Conference on Robotics and Automation, pp. 2283-2289, 2005

Oh H. U., "Characteristics of a Magnetorheological Fluid Isolator Obtained by Permanent Magnet Arrangements," *Smart Materials and Structures*, Vol. 13, pp. 29-35, 2004

Phillips R. W., [Engineering Applications of Fluids with a Variable Yield Stress], *Ph.D. Dissertation*, University of California, Berkeley, 1969

Pratt G. A. and Williamson M. M., "Series Elastic Actuators," *Proc. of the IEEE International Conference on Intelligent Robots and Systems*, Vol. 1, pp. 399-406, 1995

Pratt J. E., Krupp B. T., Morse C. J. and Collins S. H., "The RoboKnee: An Exoskeleton for Enhancing Strength and Endurance During Walking," *Proc. of the IEEE International Conference on Robotics & Automation*, pp. 2430-2435, 2004

Shimada K., Akagami Y., Kamiyama S., Fujita Y., Miyazaki T. and Shibayama A., "New Microscopic Polishing with Magnetic Compound Fluid (MCF)," *Journal of Intelligent Material Systems and Structures*, Vol. 13, pp. 9-15, 2002

Swanson D. K. and Book W. J., "Path-following Control for Dissipative Passive Haptic Displays," *International Symposium on Haptic Interfaces for Virtual Environment and Teleoperator Systems*, pp. 101-108, 2003

Takahashi N., Fukum A. and Miyagi D., "Analysis of Iron Loss under Distorted Elliptical Rotating Flux of SPM motor," *COMPEL: The International Journal for Computation and Mathematics in Electrical and Electronic Engineering*, Vol. 24 (2), pp. 385, 2005

Teixeira-Salmela L. F., Olney S. J., Nadeau S. and Brouwer B., "Muscle Strengthening and Physical Conditioning to Reduce Impairment and Disability in Chronic Stroke Survivors," *Archives of Physical Medicine and Rehabilitation*, Vol. 80, pp. 1211-1218, 1999

Walsh C. J., Endo K. and Herr H., "A Quasi-Passive Leg Exoskeleton for Load-Carrying Augmentation," *International Journal of Humanoid Robotics*, Vol. 4 (3), pp. 487-506, 2007

Wang X., Yang Y. and Fu D., "Study of Cogging Torque in Surface-Mounted

Permanent Magnet Motors with Energy Method," *Journal of Magnetism and Magnetic Materials*, Vol. 267 (1), pp. 80-85, 2003

Wikenfeld A. and Herr H., "Usear-adaptive Control of a Magnetorheological Prosthetic Knee," *Industrial Robot: An International Journal*, Vol. 30 (1), pp. 42-55, 2003

Winter D. A., "Biomechanics and Motor Control of Human Movement," *John Wiley & Sons*, Third Edition, 2005

Yamamoto K., Lee S., Kanbe S. and Matsuo T., "Development of Power Assisting Suit for Assisting Nurse Labor," *JSME International Journal Series C*, Vol. 45 (3), pp. 703-711, 2002

Yoo J. H. and Wereley N. M., "Design of a High-efficiency Magnetorheological Valve," *Journal of Intelligent Material Systems and Structures*, Vol. 13, pp. 679-685, 2002

Yoo J. H. and Wereley N. M., "Performance of a Magnetorheological Hydraulic Power Actuation System," *Journal of Intelligent Material Systems and Structures*, Vol. 15, pp. 847-658, 2004

Zhu Z. Q. and Howe D., "Influence of Design Parameters on Cogging Torque in Permanent Magnet Machines," *IEEE Transactions on Energy Conversion*, Vol. 15 (4), pp. 407-412, 2000

Zoss A. and Kazerooni H., "Design of an Electrically Actuated Lower Extremity Exoskeleton," *Advanced Robotics*, Vol. 20 (9), pp. 967-988, 2006

APPENDIX

A. Designs of the Multifunctional Actuator
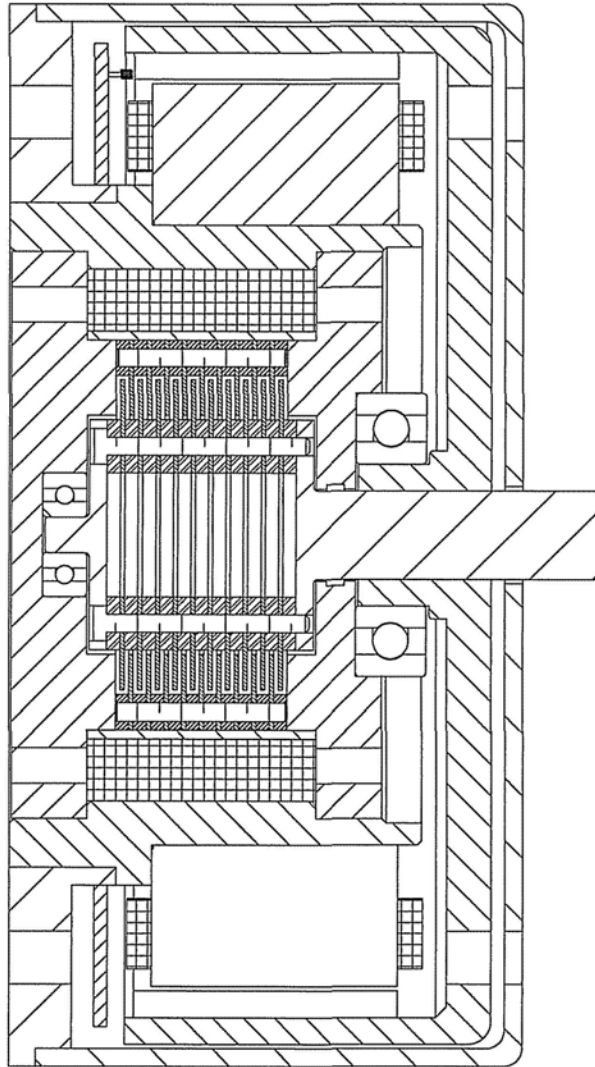
(a) The multifunctional actuator with configurations of interior-rotor plus input/output plates using exterior-inner coil
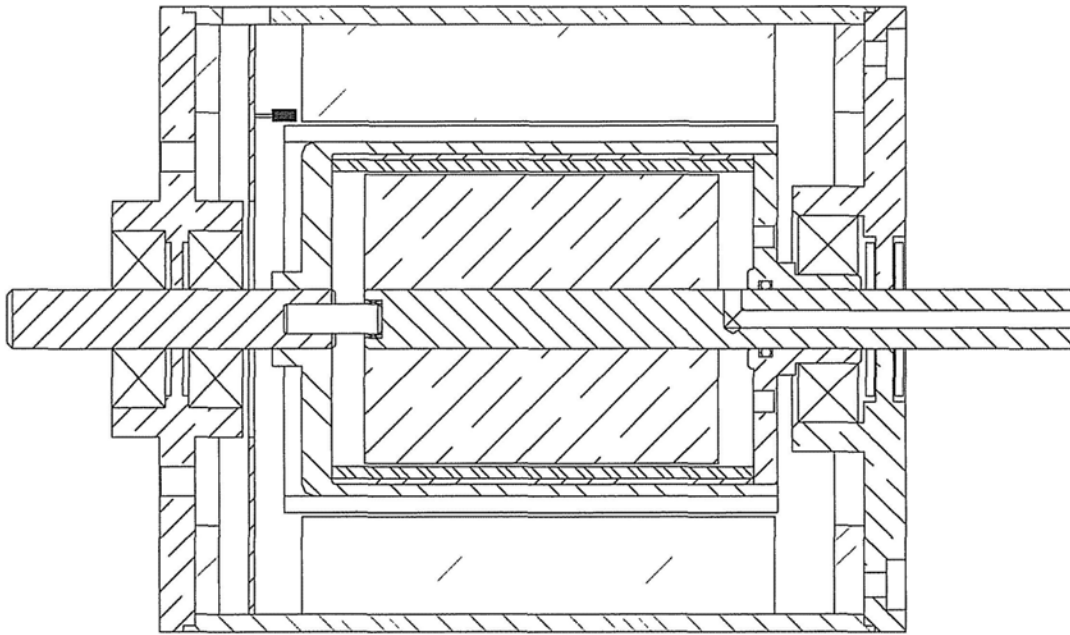
(b) The multifunctional actuator with configurations of interior-rotor plus inner armature
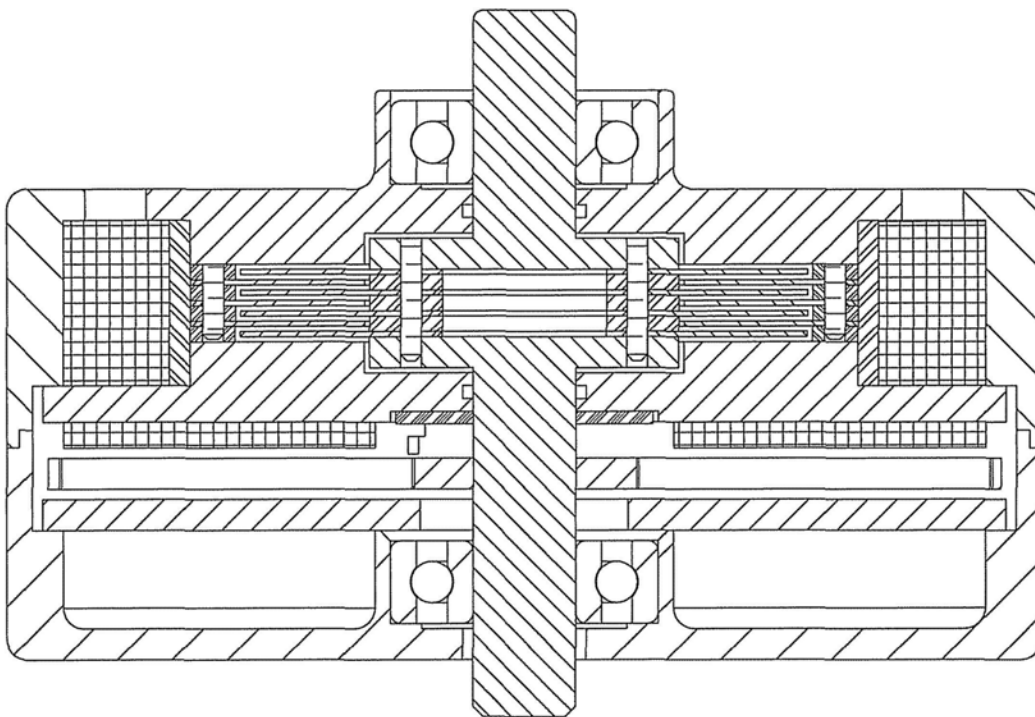
(c) The multifunctional actuator with configurations of axial-rotor plus input/output plates using exterior-inner coil